The Static Testing of a Lockheed P-3 Orion Wing Leading Edge Centre Section

Albert K. Wong and Glenn Luke

DEPARTMENT OF DEFENCE
DEFENCE SCIENCE AND TECHNOLOGY ORGANISATION

DISCLAIMER NOTICE

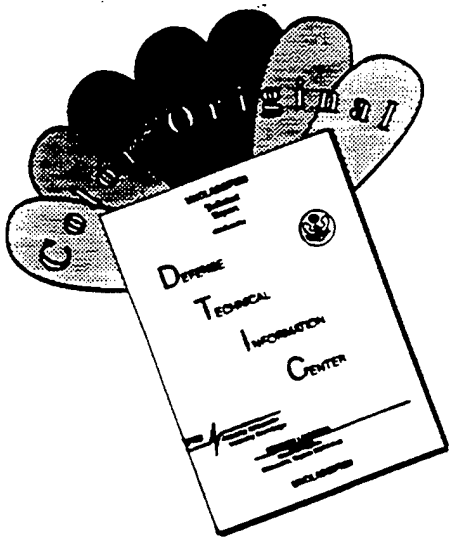

THIS DOCUMENT IS BEST QUALITY AVAILABLE. THE COPY FURNISHED TO DTIC CONTAINED A SIGNIFICANT NUMBER OF COLOR PAGES WHICH DO NOT REPRODUCE LEGIBLY ON BLACK AND WHITE MICROFICHE.

The Static Testing of a Lockheed P-3 Orion Wing Leading Edge Centre Section

Albert K. Wong and Glenn Luke

Airframes and Engines Division
Aeronautical and Maritime Research Laboratory

DSTO-TR-0423

ABSTRACT

This report documents the design of the test rig and the results of the static test of the Lockheed P-3 Orion Wing Leading Edge centre section structure. The test comprised of two parts, viz., the validation of the structural integrity of the structure under design load conditions, and the determination of the static strength of the structure for the local transonic flight regime within which the RAAF Orion A9-754 had evidently failed. The test clearly showed that the structure meets its design specifications and had an adequate margin of safety even for the high speed regime. However, it is pointed out that this margin can be quickly eroded if the material thickness is below specification, as was reported for the case of Orion A9-754, and it is recommended that this aspect be investigated for the RAAF Orion fleet.

RELEASE LIMITATION

Approved for public release

DEPARTMENT OF DEFENCE

DEFENCE SCIENCE AND TECHNOLOGY ORGANISATION

Published by

DSTO Aeronautical and Maritime Research Laboratory
PO Box 4331
Melbourne Victoria 3001

Telephone: (03) 9626 8111
Fax: (03) 9626 8999

AR No. AR-009-899
November 1996

APPROVED FOR PUBLIC RELEASE

The Static Testing of a Lockheed P-3 Orion Wing Leading Edge Centre Section

Executive Summary

The inflight failure of the wing leading edge (WLE) sections of RAAF Orion A9-754 in 1991, and the separate but similar incident with the US Navy Orion 160284, have led to a collaborative investigative program involving Lockheed Aeronautical Systems Company (LASC), the US Naval Air Command (NAVAIR) and AMRL. LASC has undertaken detailed computational air flow calculations and has provided this test program with the appropriate pressure loading profiles. NAVAIR has contributed significantly in the area of structural analysis through detailed finite element models. Part of AMRL's role was to undertake a static test on a WLE section to determine the static strength of such a structure. This report presents the design of the test rig and, more importantly, documents the results of the test. Post failure analysis on the test article showed that the test successfully replicated the nature of failure as experienced by Orion A9-754, indicating that this test was representative of the inflight conditions of interest. The major findings of this test may be summarised as follow:

i) The test structure met its design strength specifications.
ii) At the local transonic regime, where RAAF Orion A9-754 had evidently ventured, the test article would have survived a manoeuvre load of approximately 4.3g. This represents a significant margin of safety over the prescribed 3g operational limit.
iii) The material thickness of the test article was within the manufacturer's specification.
iv) When the failure load obtained in this test is translated to the Orion A9-754 case, where the material thickness was reported to be some 8% below that of the test article, it inferred that Orion A9-754 would have failed during a high speed pull-up manoeuvre of approx. 3.4g, consistent with that found in an earlier investigation.

Based on these findings, it is concluded that the reduction in material thickness of the order of that found for Orion A9-754 can quickly erode much of the safety margin away. As a result, it is recommended that:

i) A survey on the WLE rib and clad thicknesses of the entire RAAF P-3C Orion fleet be undertaken.
ii) Allow the test results to be computationally translated (currently being performed by NAVAIR) to the inboard WLE so that this section can be assessed for its structural strength.
iii) Maintain the present placard limit of 2g (for speeds of 300 knots and above) pending on the outcomes of i) and ii) above.

Authors

Albert K. Wong
Airframes and Engines Division

Albert Wong holds a Bachelor of Engineering (Hon 1) and a PhD in Mechanical Engineering from the University of New South Wales. Since joining DSTO in 1985, he has worked in a number of research areas including fracture mechanics, Finite Element modelling and experimental stress analysis. He has published numerous research papers in these areas, and in particular, in the area of thermoelastic stress analysis. He is the co-developer of the world's first thermoelastic stress analysis system based on an infra-red focal plane array imager. Dr Wong is currently a Principal Research Scientist in AMRL's Airframes and Engines Division and heads the Machine Dynamics area which is primarily concerned with research into Health Monitoring of rotating machineries using vibration analysis techniques.

Glenn Luke

Glenn Luke was the contract engineer chiefly responsible for the design and management of the construction of the test rig. He is currently a senior engineer in AWA Defence Industries.

Contents

1. Introduction

A structural test on the P-3 Orion Wing Leading Edge (WLE) was performed at AMRL on March 21, 1995. This test formed part of a collaborative project involving RAAF/AMRL, the US Navy (NAVAIR) and Lockheed Aeronautical Systems Company (LASC), which arose from the lost of the RAAF Orion A9-754 over the Cocos Island in 1991. The conduct of this test was to fulfil two primary objectives. The first was to validate the structural integrity of the structure under the design condition whilst the second aim was to establish the static strength of the structure within a local transonic flight regime. The latter part is particularly important in that it corresponds to conditions associated with the A9-754 accident. During the course of the investigation, it was shown that the handling characteristics of this aircraft are such that this aircraft can well venture into this transonic regime inadvertently under certain load configurations at high speed. Because of the non-linearities involved, the operational margin of safety[1] in this regime is hitherto uncertain and the conduct of this test would provide information to resolve this.

This report briefly describes the design of a static test rig and details the test results for a centre section wing leading edge (WLE) structure of the Lockheed P-3 Orion aircraft. The test rig incorporated the use of adhesively bonded rubber pads and conventional whiffle tree systems to simulate the aerodynamic loads to the test article for 2 critical load cases mentioned above, namely, i) the Design Limit and Ultimate Load (DLL & DUL) cases under a low speed and positive high angle of attack (PHAA) condition, and ii) the high speed (Mach 0.56) and positive low angle of attack (PLAA) condition.

2. Applied Test Loads

This section describes the loads which were applied to the test article, and were therefore used as the design loads for the test rig structure. For the purpose of rig stressing, the design loads were multiplied by a rig design factor of 1.8 to provide adequate overload capability and margin of error.

2.1 Pressure Distributions

The pressure profiles for this test were provided by Lockheed Aeronautical Systems Company (LASC), (see Molent[1]). The test cases were represented by 3 pressure profiles, viz., the PHAA design case, and the 2 pressure profiles corresponding respectively to 3g and 4.5g pull-ups under the PLAA conditions. However, because the PLAA profiles were derived from a 3 dimensional computational fluid dynamics model, some degree of simplification was necessary in order for the whiffle tree design (which had to be applicable to both the PHAA and PLAA load cases) to be kept manageable. Fortunately, the variations of the pressure profile over the span of the

[1] "operational margin of safety" is defined in this document as the amount of vertical accelerations (g's) that can be sustained by a component above and beyond the operational limits without the failure of that component.

centre section WLE are relatively small such that a good approximation could be obtained by assuming a fixed pressure profile (corresponding to that at the mid-span) which was scaled by a spanwise correction factor as presented in Callinan *et al* [2]. The three different pressure profiles are shown in Fig. 1 and listed in Table A1, and the spanwise correction factors applied are listed in Table A2 (see Appendix).

2.1.1 PHAA Design Load Case

The design loads, under the PHAA configuration, were provided by LASC as a pressure (psi) distribution over the WLE chord position (x/c). For convenience, the LASC distribution was linearly interpolated for a set of chord positions which corresponded to nodes of a Finite Elements Model developed earlier in AMRL (see Molent [3]) and which was also used in this current work to validate the discretisation of loading (see Section 2.2). These values were converted to metric units and are shown in Table A1.

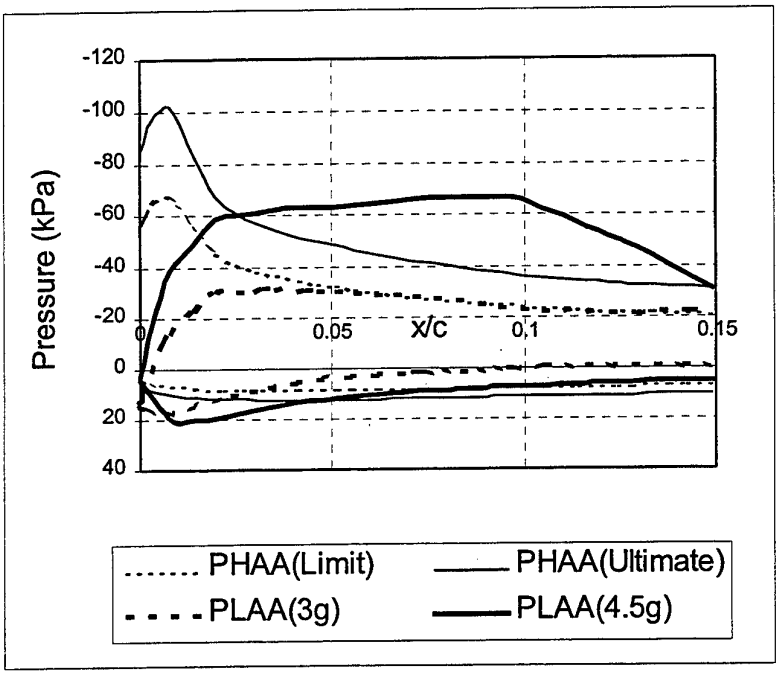

Figure 1. Pressure profiles over the WLE (1st 15% of chord) for the different test conditions.

2.1.2 PLAA Load Case (3g)

The 3g pressure distribution under the PLAA condition, corresponding to a *fuselage reference line* angle of attack (AoA) of 1.3°, was computed by LASC using a 3-D Euler computational fluid dynamics code. This was provided to AMRL as values of coefficient of pressure (C_p) over the WLE chord length (for both upper and lower surfaces) and for various span positions. As mentioned in Section 2.1, it was decided that the mid-span distribution be used throughout, but with the application of a spanwise correction factor for each of the other wing stations. The coefficients of pressure were converted to pressures using the following expression:

$$P = 0.5\, C_p\, P_{sl}\, M^2\, H \qquad (1)$$

where P_{sl} = 101.3 kPa is the pressure at sea level, M = 0.56 is the Mach Number, and H = 1.4 is the Specific Heat ratio.

The pressure data, after conversion to metric pressures and linearly interpolated for each leading edge node position, are shown in Table A1.

2.1.3 PLAA Load Case (4.5g)

As for the previous case, this pressure distribution, corresponding to an AoA of 5.0°, was also computed by LASC and was provided to AMRL as a C_p distribution. The values for the mid-span case were similarly transformed and are also shown in Table A1.

2.1.4 PLAA Load Case (Interpolated 4g)

From Fig. 1, it may be seen that the 3g PLAA pressure load is less severe than that for the DLL case. Since the WLE is expected to survive the design load case, it would be superfluous to test the 3g PLAA case. Furthermore, it may be noted that the 3g PLAA case consists of a significant degree of positive pressure near the nose on the upper surface and would therefore not be amenable to the proposed loading system. Consequently, linear interpolation between the 3g and 4.5g PLAA cases was performed to determine a lower bound pressure profile for which a suction load for the pad nearest the nose could firstly be applied. This point occurred at an interpolated AoA of 3.8°, and corresponds to an interpolated vertical acceleration of approximately 4g. This interpolated load case was applied as the first load case for the PLAA test.

2.2 Load Discretisation

The lift loading was achieved via the application of adhesively bonded rubber tension pads on the upper surface, and similar rubber compression pads (which were not necessarily bonded to the test article) at the lower surface. In order to establish the number of pads required to adequately represent the continuous pressure profiles, a 2-D finite element model (FEM) of the WLE was constructed and a number of discrete loads as well as the continuous pressure load case were applied and studied. It was found that 4 discrete loads on the upper surface and 2 discrete loads on the lower surface were adequate in producing equivalent stresses near the critical region to those of the continuous case and was consequently adopted for the tests.

The discrete load locations were selected based on dividing the pressure profiles into sections in which the net lift for each was roughly equal to the others. However, some compromise to this criterion was necessary as the discretisation had to cope with 3 different pressure profiles.

With the chordwise pad positions selected, the actual applied loads were calculated based on equating both forces and moments to those attributable to the continuous pressure distributions. Along the span, it was decided that a set of tension pads be

placed directly over each of the 11 internal rib stations, thus giving a total of 66 loading pads which covered some 70% of the surface area. Figures A1 and A2 show the schematic diagrams of the loading pad locations, and the discrete applied loads for each pad are listed in Tables A3 and A4.

3. Test Article

The test article was a left hand (port-side) centre section WLE of a P-3A Orion supplied by the USN, Part Number: 800061-501; Serial Number: D6-156. This component came from the USN aircraft EP-3E ARIES I Buno 150497 with total flight hours of 20,250 and a Fatigue Life Expenditure of 98.4% when it was retired in December 1992. A detailed inspection, including the application of ultrasonic Non-Destructive Inspection over the critical regions, showed that it was in good general condition and was deemed fit for testing.

The chordwise nodal coordinates of the test section profile were established from geometrical data on the test article and a finite element model (FEM) of the centre WLE was constructed for the purpose of validating the adequacy of the discretised loading arrangement. The normalised coordinates used for the current work can be found in Table A1 in the Appendix.

4. Test Rig Structure

The layout of the test rig structure is detailed in AMRL drawing series SE 5/51/7 /R and titled "Orion Leading Edge Test Rig". A side view of the test rig structure is shown in Figure A3. Some details have been omitted there for clarity. The upper surface rubber pads were loaded in tension with wire cables. Pulley wheels were used in the lower stage of the whiffle tree assembly to enable correct angular orientation of the loads while keeping the majority of the whiffle tree structure in the vertical plane. A system of cables and beams was also used to load the rubber pads in compression for the lower surface.

The following sections give an outline of the design of the major components of the test rig structure. The rig was generally constructed from mild steel, and the rig design loads were taken as 1.8 times the ultimate loads being applied to the structure and the allowable deflections were taken as 0.3% of the length of the structural element.

Figure A4 shows a front view of test rig with the test article mounted prior to the test. The details of the tension pads and cables may be seen in Fig. A5.

4.1 Bonded Loading Pads

The discrete loads representing the aerodynamic loading were applied using bonded rubber pads loaded in tension on the top surface and similar pads in compression on the lower surface. Given that the ultimate bond strength was found experimentally to

be 0.5 MPa [4], the pads were generally sized based on an average adhesive stress in tension of 0.2 MPa at the maximum applied load. However, this target was found to be not possible in all cases, particularly for those pads nearest the nose under the PHAA condition due to the nature of the pressure profile. Nevertheless, the maximum average adhesive stress under this condition was 0.36 MPa (Pads [1,7], [1,8], [1,9] - see Table A3), and meant that there was still a safety factor of 1.4.

Similar pads were used in compression for loading of the leading edge lower surface. Because these pads were loaded in compression, there was no need to bond these to the test article. However, to facilitate the mounting and positioning of the lower loading beams, the front row of the lower pads were bonded to the test article. The rear row was not bonded so as to allow this to be positioned differently for the PHAA and PLAA load cases.

4.2 Upper Surface Whiffle Trees

4.2.1 Layout

The upper surface was loaded using four independently controlled hydraulic actuators connected, respectively, to the four rows of rubber loading pads through a series of whiffle trees. The upper surface whiffle tree details may be found in the AMRL general arrangement drawing SE 5/51/7/R006. The pad loads presented in Table A3 essentially defined the beam ratios for the upper surface whiffle tree beams. The whiffle trees run along the span over the four chordwise discrete locations, in which each tree followed the same method of construction and load point geometry (see Figure A6).

4.2.2 Deviations from Initial Design

The final test rig possessed a number of minor improvements made and thus deviated from the initial design and were consequently not incorporated in the referred drawings. All these were made with the consideration of added rig strength or improved representation of the distributed load. They included:

i) the addition of the sub whiffle tree "G" beam and associated extra links and the extra row of pads (Pads [1,11] to [4,11]),
ii) all cable diameters were up-graded to 3/16",
iii) all pulleys were up-graded to 2" diameter solid brass hub type and all pulleys and cables were grease lubricated,
iv) the lower beams were replaced by higher strength (stiffer) channel sections.

4.3 Lower Surface Whiffle Tree

The lower surface whiffle tree system is detailed in AMRL general arrangement drawing SE 5/51/7/R006. The pad loads presented in Table A4 defined the beam ratios for the lower surface whiffle trees and were applied by a single hydraulic actuator situated above the actuators used for the upper surface. The whiffle tree was connected by cables to a set of beams ('LB' beams - see Fig. A7) below the lower

surface which transferred the compression loads to the pads. The methods of design and construction were similar to those for the upper whiffle trees.

4.4 Leading Edge Support Frame

The support frame consisted of the ladder frame (drawing SE 5/51/7/R010) and three "A" frames (drawing SE 5/51/7/R001). The test article was attached to the ladder frame via the screw holes at the trailing edges (including the piano hinge on the lower surface). The WLE was supported at a nose down angle of 20° so as to allow the resultant applied up-load to the lower surface to be essentially vertical and thus simplified the layout of the loading system. The tubular steel ladder frame was attached horizontally across the "A" frames. The "A" frames, in turn, transferred the applied loads to the anchorage points on the laboratory floor.

4.5 Upper Surface Pulley Guide Frame

The pulleys for providing the correct orientation of the applied load to the upper surface tension pads were all supported on a welded steel guide frame which was bolted to the 4 main supporting columns (refer to Drawing SE 5/51/7/R021). There were 5 guide rails on this frame situated between the "B" and "C" beams on the whiffle tree (see Fig. A6). Each rail was designed to house four pulleys whose positions may be adjusted along a series of slots. After adjustment, the pulley hub bolts were fixed in place by plates welded across the slots. Clearance between the pulley guide frame and the whiffle tree beams and load links was adjusted by sliding the pulley frame along the main supporting columns.

4.6 Actuator Support Structure

The four upper surface actuators were supported by three spanwise mounted I-beams. The forward I-beam was positioned to carry loading from the two front actuators and the remaining two I-beams each supported one of the rear actuators. These I-beams were supported at their ends by a tapered flange channel beam straddling the front and rear main support columns.

The lower surface actuator was supported on a single I-beam in the same manner as the above arrangement.

4.7 Actuator Mounting

The mounting details of the actuators are detailed in AMRL drawings SE 5/51/7/R024 to 028. The actuators were mounted to the lower extruded channel (with tapped holes) by using threaded rod ends. Below each actuator (at full stroke), a threaded adaptor was used to connect the load cell. The load cell was then connected to the top whiffle tree beam with a threaded link.

The lower surface actuator was mounted in a similar fashion to that for the upper surface.

4.8 Test Rig Columns

Four steel columns were used as overall main support for the test rig. These columns were recycled from a previous test rig and whose details are described in AMRL drawing SE 5/51/7/R002. The columns were capable of transferring all applied loads to the existing anchorage points on the laboratory floor.

5. Instrumentations

5.1 Data Acquisition

Two data acquisition systems were used to accommodate 84 channels of data. The first system, designated as the AMRL "HP 75000", which consisted of a HP75000B mainframe incorporating a HPE1326B voltmeter and HPE1358A 350Ω strain relay multiplexers, was used to monitor the 5 load cells and the first 45 channels of strain data. The 4 LVDTs and the remaining strain gauge channels were sampled and recorded by the second system designated as AMRL "HP LQA" which consisted of two 20 channel in-house designed strain gauge conditioner connected to a HP 3497A relay multiplexer and a HP3458A voltmeter.

Data acquisition was manually initiated at the beginning of each test and during the load-hold at the end of each load increment. The loading schedules are later described in Sections 6.2.1 and 6.3.1.

5.2 Strain Measurements

All strains were measured using 350Ω resistance strain gauges. Gauges used were 5mm uni-axial gauges with the exception of the 5 × 1 mm strip gauges used at the critical flange section near the tension (lower) leg tangency point. The strain gauge locations were selected largely by the NAVAIR engineers who had a good knowledge of the general stress distributions through their experience with detailed FE models (see Molent [3]). Figures A8 to A13 illustrate the locations where strain gauges were attached. A summary of the strain gauge locations is also presented in Table A5.

5.3 Deflection Measurements

Two vertical and two horizontal displacement transducers (LVDT) were used for the test. The vertical displacement transducers were attached to the nose at each end of the WLE (WS228 and WS321). A horizontal displacement transducer was attached on the upper leg of the mid-span rib (WS273) and of the inboard closure rib (WS228). These horizontal transducers were attached at mid-depth of the web near the tangency

point of the upper leg to record the amount of lateral movement of these webs as they buckled under compressive stresses.

5.4 Load Links

For the front and rear upper whiffle trees, a set of load links was used for the purpose of monitoring the loads actually applied to the cables between the tension pads and the pulleys (see Fig. A6). These links were implemented so that the effects of the pulley friction could be taken into account.

The load links were machined from aluminium Al2024 stock to have a rectangular shank of nominally 6 mm × 10 mm in cross section. Swivel bearings were used as end fittings and were press-fitted to the ends. A single 6mm uniaxial strain gauge was bonded on the in-plane side of the shank to provide strain measurements which could then be translated to applied load. However, at the calibration stage before the test, and also during the test, the strain data from the majority of these load links showed high degree of non-linearity with respect to the applied load. The load links were subsequently removed from the test rig and tested separately in a specially constructed rig to see whether pulley friction could have been the cause of the anomaly.

The load link calibration rig consisted of a single cable placed around a pulley to the same wrap-angle as the most severe case in the actual test (Row-1). One end of the cable was attached to a fixed load cell and the other was attached to another load cell which was in turn attached to a hand operated hydraulic actuator. Incremental loads were manually applied via the hydraulic actuator, and readings on both load cells (before and after the pulley) as well as the strain gauge readings from the load links were recorded for each load increment. Figure 2a shows the 2 load cell readings plotted against each other for all of the links. The results show that there were only small losses (approx. 3%) due to pulley friction. However, the strain readings showed large variations from link to link, and that many of the links showed high degree of non-linearity as can been seen in Fig. 2b. It was thought that this non-linear behaviour might have come about due to the fact that non-linear bending of the shank was possible as the strain gauge was bonded on the in-plane side of the shank, and that the swivel bearing had only a small degree of play before the load link could be levered against the cross members. In retrospect, it would have been better for a gauge to be bonded on each of the opposing sides of the shank which were perpendicular to the plane of the link. Undertaking such modification would have delayed the testing, and was therefore not pursued in view of the fact that little loss was present over the pulley assemblies as shown by the calibration test.

In fact, the total error in the overall loading would be much less than 3% as the cable wrap-angle over the pulley progressively diminished from the first to the fourth row (see Fig. A3).

It was also hoped that the results from the calibration tests (Fig. 2b) could be used as calibration curves to convert strain readings to load readings. From test results, however, it is clear that this was not possible as it was found that most of the load links behaved quite differently for the different load cases. As an illustration, the

results for Link-2 for the 2 load cases under the PLAA conditions are shown in Fig. 3, where it may be seen that the load link readings deviated from the expected value quite inconsistently. In particular, it may be noted that in both cases, and especially for the 4g case, the strain reading on this link registered negative values over a significant portion of the test range during load up. This clearly indicated the readings to be erroneous as the applied load cannot possibly be negative in such a cable-pull system. Consequently, it must be concluded that the load link results should not be used to infer cable loads. Fortunately, this should not degrade the outcome of the test significantly in that little losses were encountered through the pulley assemblies.

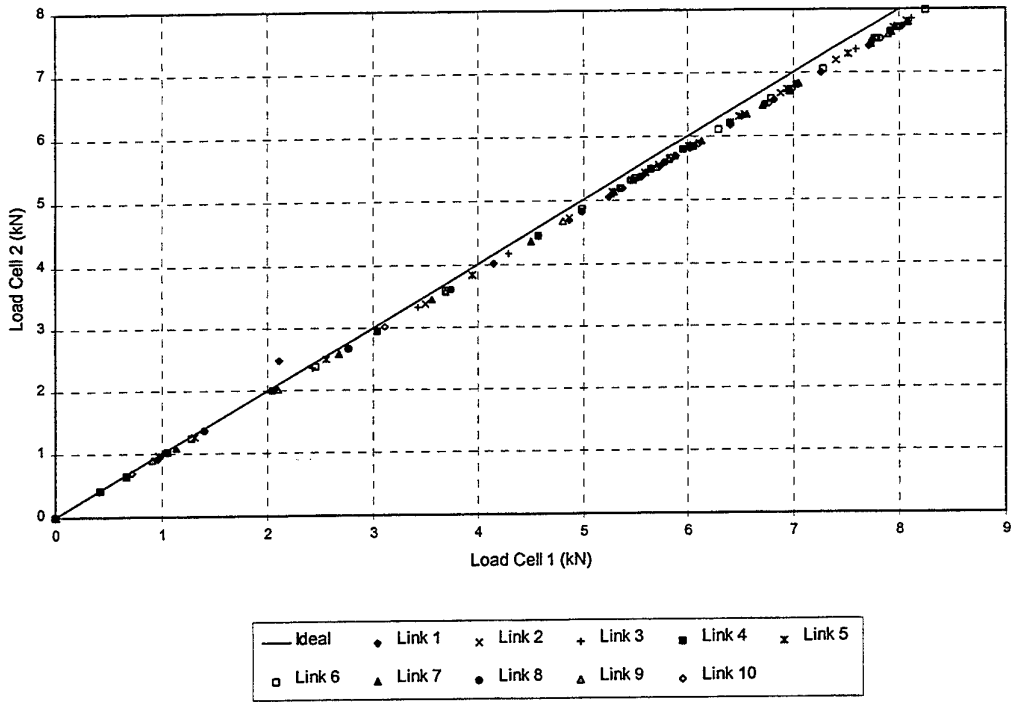

(a)

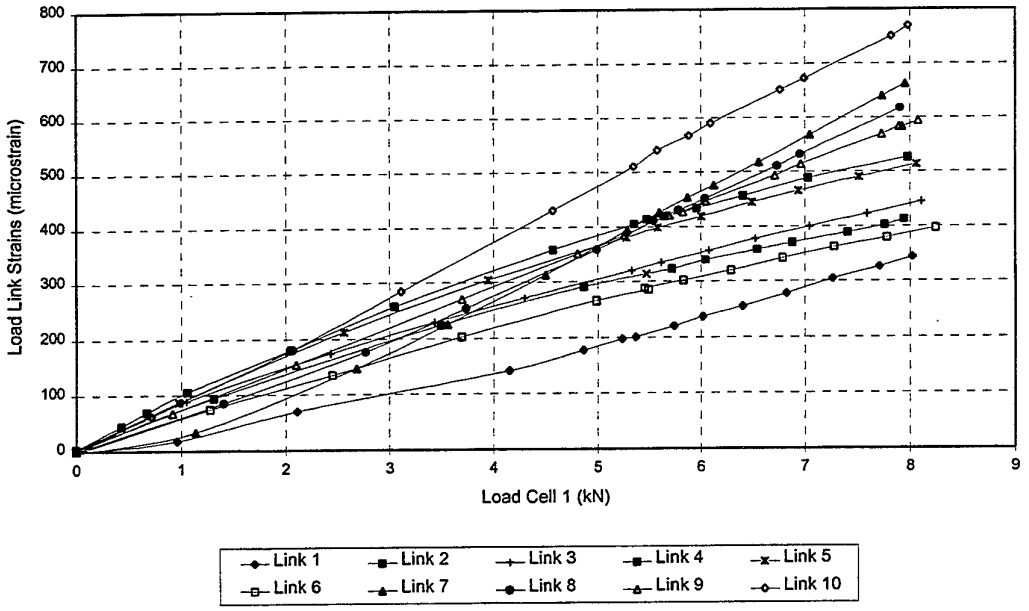

(b)

Figure 2. Load link calibration results: a) Load cell readings (before vs after pulley), b) load link strain readings.

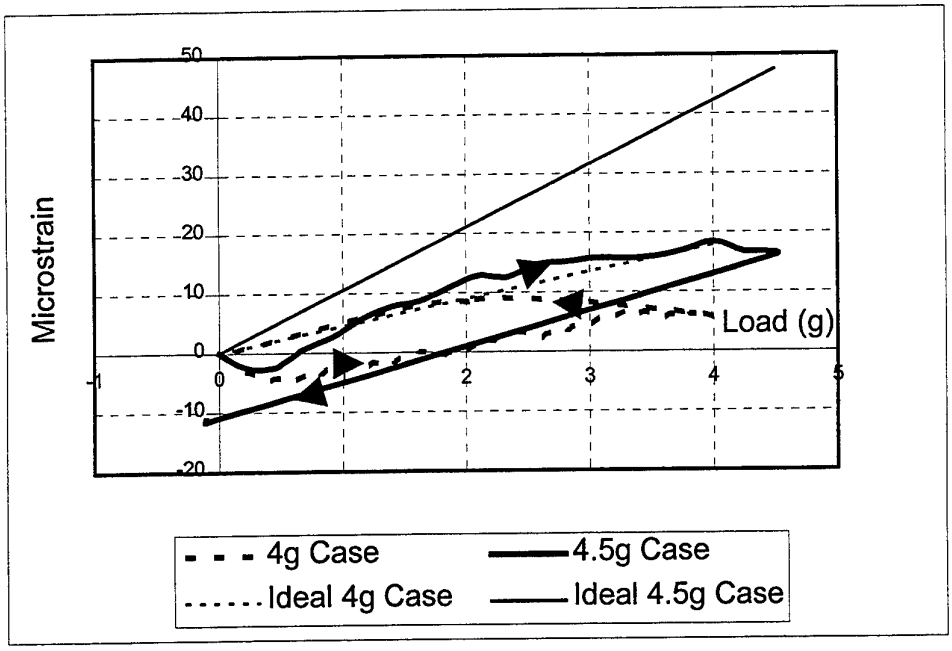

Figure 3. Strain readings on Load Link-2 for both the 4g and 4.5g PLAA cases.

5.5 Other Recordings

In addition to the digital recordings specified above, 3 video cameras were utilised to record the entire test proceedings, covering, respectively, a side view of the inboard closure rib WS228, a close up rear view near WS239 and a side view of outboard closure rib WS322. Still photographs of the deformed ribs were also taken during the various load-holds.

6. Test Results

The test was carried out on March 23, 1995 in AMRL's Building 3 Wingbay under nominal ambient conditions. The test schedule and setup were inspected and approved in advance by RAAF MPLM Squadron Chief Engineer (Mr C.J. Wetherall), Senior Structural Engineers from NAVAIR (Mr N. Phan) and LASC (Mr J.O. Wilson), who were also all present to witness the test proceedings.

6.1 Test Sequence

As mentioned in Section 2.1, the test program was devised to cover both the PHAA and PLAA cases. The first relates to the design requirements whilst the latter corresponds to the conditions within the local transonic affected flight regime. It was planned that the test article would be firstly tested under the PHAA condition up to the Design Ultimate Load (DUL). If the test article survived this first test, as it turned

out to be the case, then the test rig would be re-configured and testing would proceed under the PLAA conditions until failure of the test article was detected.

A complete record of all the data acquisition channels are presented in Tables A6 to A8 in the Appendix.

6.2 PHAA Case

6.2.1 Loading Schedule

For this load case, the following schedule was followed:

i) Under the PHAA loading condition, load was applied in 10% increments from the unloaded condition up to 100% DLL.
ii) Load was held at 100% DLL for approximately 1 minute.
iii) Load was decreased to 20% DLL and held for approximately 1 minute to determine whether any part of the test article had suffered significant permanent deformation.
iv) 100% DLL was re-applied quasi-statically, and loading resumed from this point at 5% increments to DUL (150% DLL).
v) DUL was held for approximately 3 minutes over which photographs and visual inspection of the test article were again taken.
vi) The test article was totally unloaded quasi-statically in 4 steps (100%, 50%, 20% and 0%DLL) and the lower loading beam and pressure pads were re-configured for the PLAA Test.

6.2.2 Measured Strains

a) Spanwise Distributions (Section EE)

All internal ribs, from WS239 to WS317, of the test article were strain gauged at the mid-height of the lower web near the hinge line (see Section EE in Figs A8 to A13). The strains recorded for these ribs give an idea about the distribution of load along the span of the test article. Figure 4 shows the entire Section EE strain histories throughout this test. It may be seen that during the first parts of the loading sequence (i-iii of the schedule listed in Section 6.2.1), Section EE strains responded relatively linearly with respect to the applied load. The exceptions for this occurred at WS239 and WS248, where the non-linearities shown were most probably due to geometric effects (e.g., these webs might have been initially bowed) as they occurred at relatively low strains (approx. 20% of DLL) and disappeared in the later parts of their excursions.

For the second part of the loading schedule (iv and v of Section 6.2.1), all Section EE strains began to depart from linearity at approximately 130%DLL. Because strains experienced were relatively low (below 1400 microstrains), the non-linearities seen here were not attributable to local yielding at these locations.

Figure 4 also shows a table of Section EE strains at various critical stages during the test, viz., at a) load-up to 20%DLL; b) 100%DLL; c) load-down to 20%DLL; d) load-up

to 150%DLL; and e) complete load removal. It may be noted that the residual strains at this location after unloading from both DLL and DUL (c and e) were only of the order of 5%, and may be considered acceptably small for such a fabricated structure.

b) Lower Leg

As shown in Figs A8 to A10, 3 selected ribs (WS228, WS273 and WS317) were equipped with extra strain gauges to provide more detailed strain data. The lower leg strains for these ribs are shown in Figs 5-8. As expected, the lower leg strains under the applied load were predominantly in tension and progressively increased from Section EE through to Section FF as the sections approach the tangency point (near Section KK, see Fig. A9 for example). The recorded strains across these sections (EE, GG, FF) were all below 4000 microstrains, although they generally began to respond non-linearly with respect to the applied load at around the 120%DLL mark. For WS228, it is interesting to note that the strain at the vertical lip of the flange at Section FF (Gauge-9 in Fig. 5) initially became negative. This was due to the section being near the tangency point where there could be a large variation across the flange as a result of the curvature of the flanged (see [3,5]).

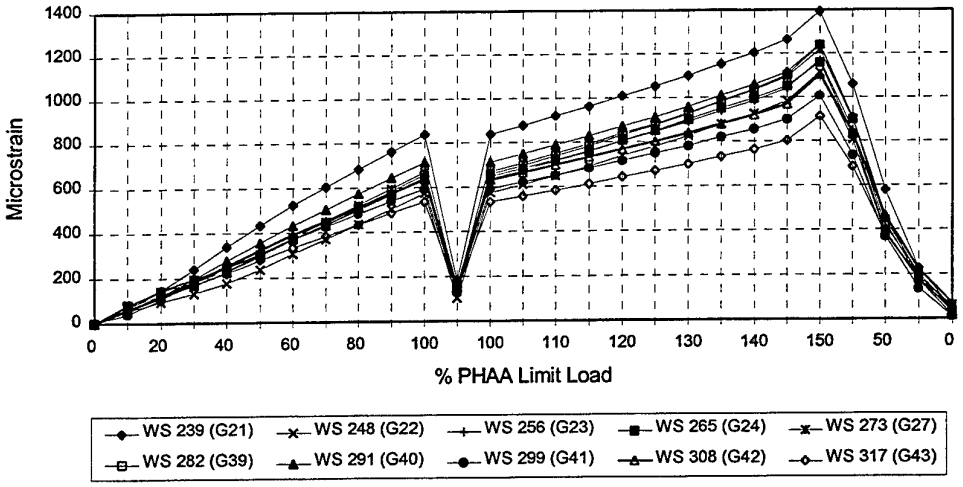

Load Stage		WS 239 G21	WS 248 G22	WS 256 G23	WS 265 G24	WS 273 G27	WS 282 G39	WS 291 G40	WS 299 G41	WS 308 G42	WS 317 G43
a	20%DLL	144	93	148	142	141	124	121	104	116	113
b	100%DLL	837	573	645	638	667	657	713	594	635	534
c	unld 20%	181	102	166	155	148	143	146	131	149	136
d	150%DLL	1392	1113	1168	1157	1218	1238	1241	1004	1104	912
e	unld 0%	39	61	36	14	49	36	30	11	68	45
RESIDUAL STRAINS											
c	unld 20%	37	9	19	13	7	19	24	27	32	23
e	unld 0%	39	61	36	14	49	36	30	11	68	45

Figure 4. Section EE strains for the PHAA Test.

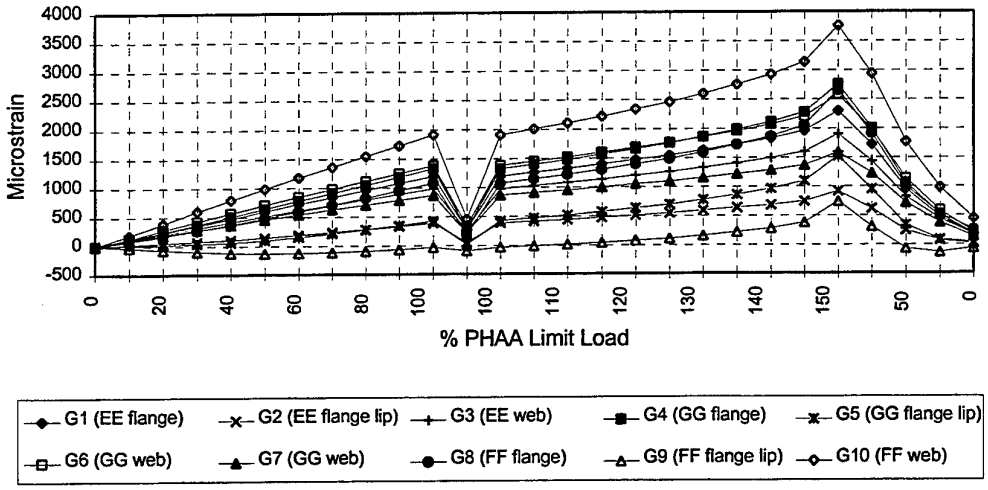

	G1	G2	G3	G4	G5	G6	G7	G8	G9	G10
20%DLL	228	51	202	239	17	275	180	172	-71	388
100%DLL	1196	385	979	1326	424	1381	865	1076	-36	1910
unld 20%	266	50	240	270	10	332	219	195	-98	457
150%DLL	2299	918	1900	2760	1523	2582	1587	2664	743	3765
RESIDUAL STRAINS										
unld 20%	38	-1	38	31	-7	57	39	23	-27	69
unld 0%	174	11	165	184	34	210	135	258	-64	444

Figure 5. WS228 Lower leg strains for the PHAA Test.

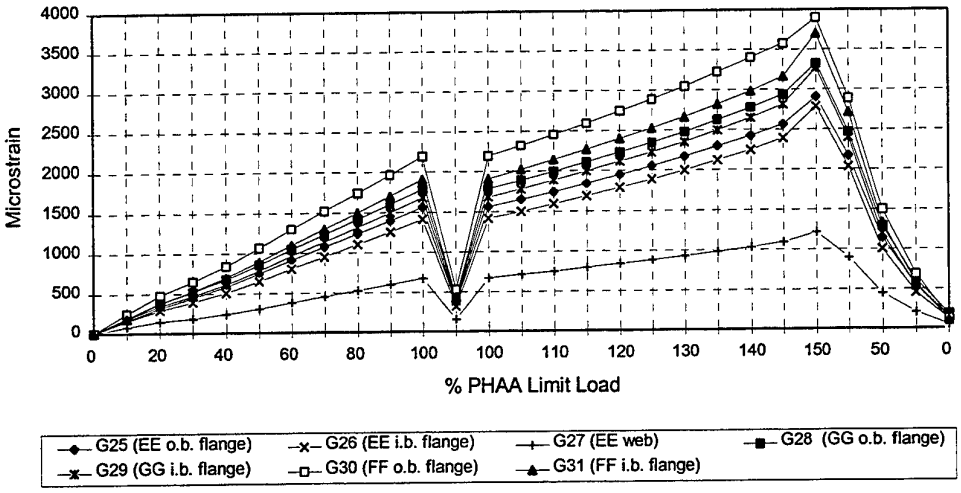

	G25	G26	G27	G28	G29	G30	G31
20%DLL	312	284	141	373	337	471	374
100%DLL	1558	1411	667	1783	1678	2190	1906
unld 20%	355	318	148	417	380	531	429
150%DLL	2899	2785	1218	3319	3266	3899	3698
RESIDUAL STRAINS							
unld 20%	43	34	7	44	43	60	56
unld 0%	155	116	49	181	141	125	105

Figure 6. WS273 lower leg strains for the PHAA Test.

The ribs at WS273 and WS317 were also equipped with a 5x1mm strip gauge at the expected critical location (Section KK), and their recorded strains are shown in Figs 7 and 8. As expected the strains here were much higher than those at the other sections (EE, GG, FF). It is interesting to note that, at DUL, the highest recorded strains reached at WS273 (midspan rib) were approx. 10,000 microstrains compared to approx. 3,750 microstrains reached at WS317 (furthermost outboard internal rib). The lower strains exhibited by this outboard rib were due mainly to the fact that the rib spacing between this rib and the adjacent outboard closure rib is approximately half of the normal spacing. This evidence does not support the earlier conclusion that the WS317 rib might have been the critical rib (see Callinan *et al* [2]).

Beyond 120%DLL, the Section KK strains at WS273 rapidly increased such that the yield strain of approx. 5,000 microstrains was reached at 135%DLL and proceeded exponentially to approx. 10,000 at DUL. It may also be noted from the table shown in Figs 7 that whilst the residual strain introduced by the DLL loading were insignificant, they were extremely high (approx. 3900 microstrains) as a result of the DUL loads.

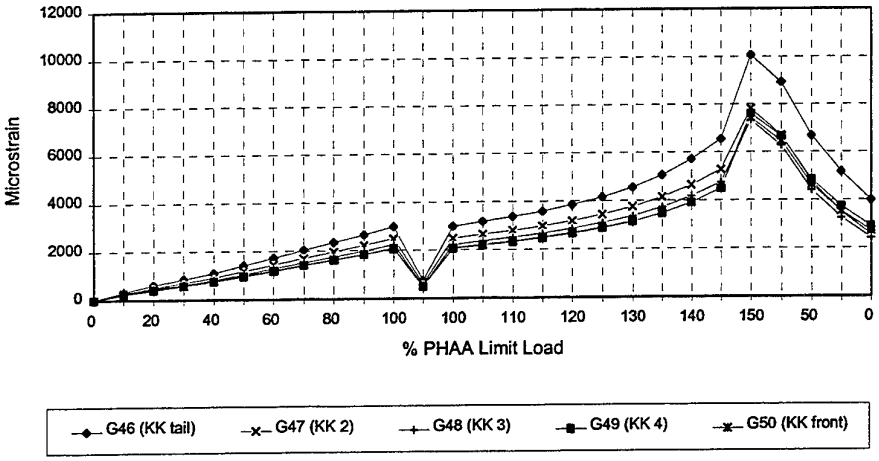

STRAINS	G46	G47	G48	G49	G50
20%DLL	610	505	449	414	419
100%DLL	2996	2490	2231	2066	2081
unld 20%	740	580	520	478	485
150%DLL	10064	7804	7334	7607	7427
RESIDUAL STRAINS					
unld 20%	131	75	72	64	65
unld 0%	3924	2512	2384	2875	2671

Figure 7. WS273 lower leg strains at critical region for PHAA Test.

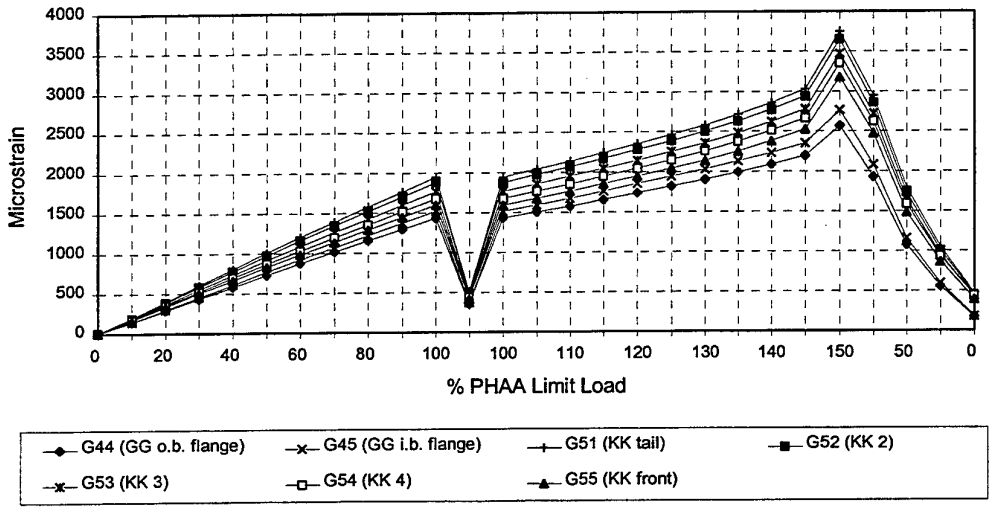

	G44	G45	G51	G52	G53	G54	G55
20%DLL	285	295	396	384	362	346	332
100%DLL	1434	1519	1944	1878	1765	1677	1596
unld 20%	351	369	504	486	457	434	417
150%DLL	2566	2767	3751	3653	3477	3359	3179
RESIDUAL STRAINS							
unld 20%	67	75	107	101	94	89	85
unld 0%	168	178	460	439	424	429	385

Figure 8. WS317 lower leg strains for the PHAA Test.

c) Upper Leg

The upper leg strains for the WS228 and WS273 ribs are shown in Figs 9 and 10. In contrast to the lower leg, this part of the structure supported the compressive loads under the applied lifting forces. Consequently, the recorded strains here (Sections BB, CC, DD) were generally comparable in magnitude, but opposite in sign, to those of their tensile counterparts (Sections EE, GG, FF). Under compression, however, the vertical part of the flange lip would have an increased tendency to buckle, and thus lost most of its effectiveness beyond 100%DLL (compare Gauges 12, 15 and 19, Fig 9 with Gauges 9, 5 and 2, Fig 5 respectively). The low levels of residual strains upon unloading tend to suggest that such behaviour was due to elastic buckling.

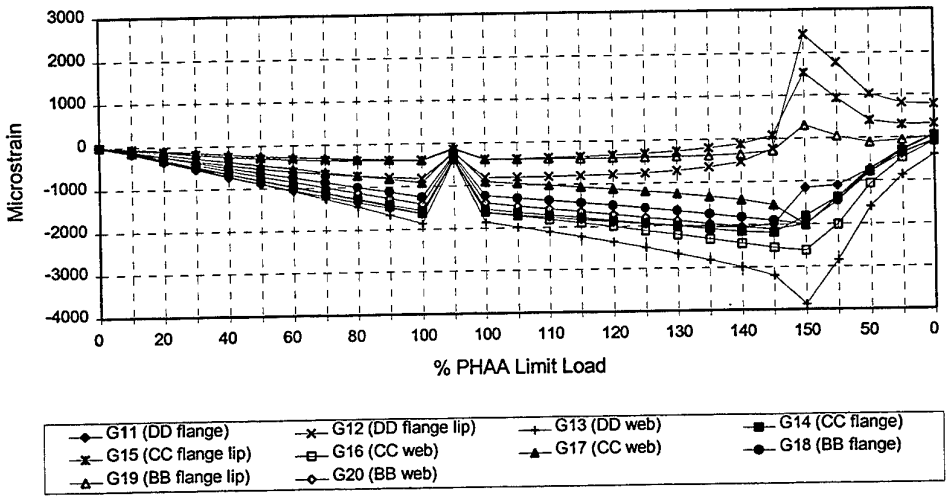

	G11	G12	G13	G14	G15	G16	G17	G18	G19	G20
20%DLL	-348	-223	-326	-311	-125	-301	-171	-237	-96	-272
100%DLL	-1643	-814	-1873	-1571	-391	-1632	-919	-1245	-388	-1418
unld 20%	-389	-237	-393	-362	-140	-351	-200	-274	-116	-309
150%DLL	-1157	2422	-3881	-1810	1535	-2620	-2020	-2000	303	-2008
RESIDUAL STRAINS										
unld 20%	-41	-13	-67	-51	-15	-51	-29	-37	-21	-37
unld 0%	56	768	-399	47	318	-81	-86	-72	34	46

Figure 9. WS228 upper leg strains for the PHAA Test

d) Skin

Figure 11 shows the skin strain readings throughout the PHAA test. As expected, the skin strains were low, in which the maximum recorded strains did not exceed 600 microstrains at DUL. For 2 of the 3 rib locations, WS247 and WS273, the strains apparently plateaued over much of the test, suggesting that either the respective ribs were bearing the increasing loads or that there was local geometric effects (such as bowing or buckling of the skin) which happened to produce the opposite effects to those generally due to an increasing load. For WS299, the skin strains appeared to be relatively linear up to the applied load of approx. 130%DLL.

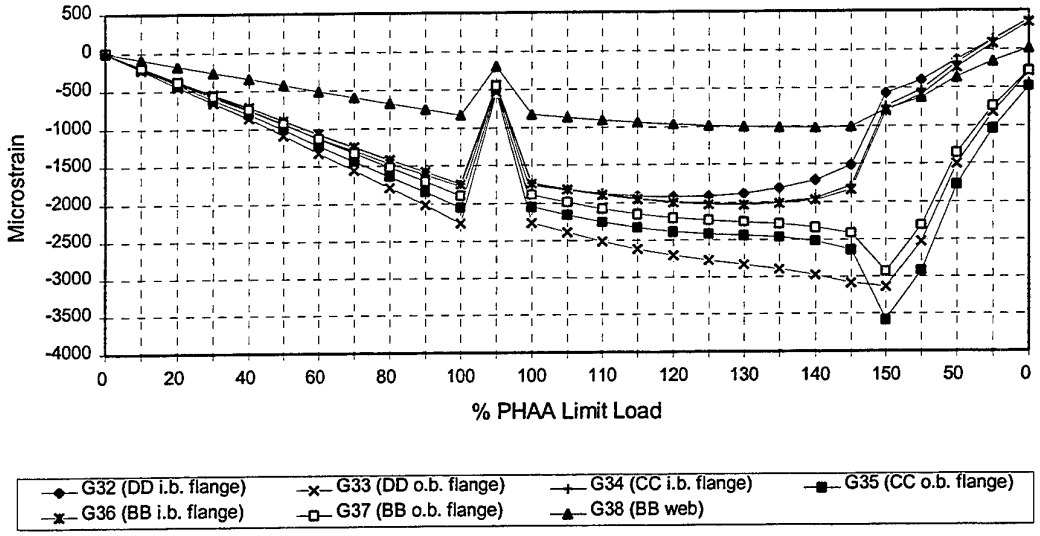

	G32	G33	G34	G35	G36	G37	G38
20%DLL	-401	-450	-377	-419	-373	-386	-182
100%DLL	-1769	-2264	-1742	-2051	-1744	-1896	-832
unld 20%	-465	-530	-433	-496	-435	-451	-196
150%DLL	-567	-3141	-741	-3583	-802	-2929	-783
RESIDUAL STRAINS							
unld 20%	-63	-80	-56	-77	-62	-65	-14
unld 0%	380	-295	379	-482	348	-280	9

Figure 10. WS273 upper leg strains for the PHAA Test

6.2.3 Measured Deflections

The deflection history during the PHAA Test is shown in Fig. 12. It may be seen that the test article deflected relatively linearly with respect to the applied load up to 130%DLL. There were also negligible differences between the inboard and outboard rib vertical deflections up to approximately 130%DLL. Rapid loss of overall stiffness was evident between 140%DLL to 150%DLL. In particular, it is noted that relatively small lateral deflections (less than 1mm) were experienced by the ribs up to 145%DLL, but the last load increment saw these jumped to over 2mm, indicating a rapid loss of stability of the upper leg near DUL.

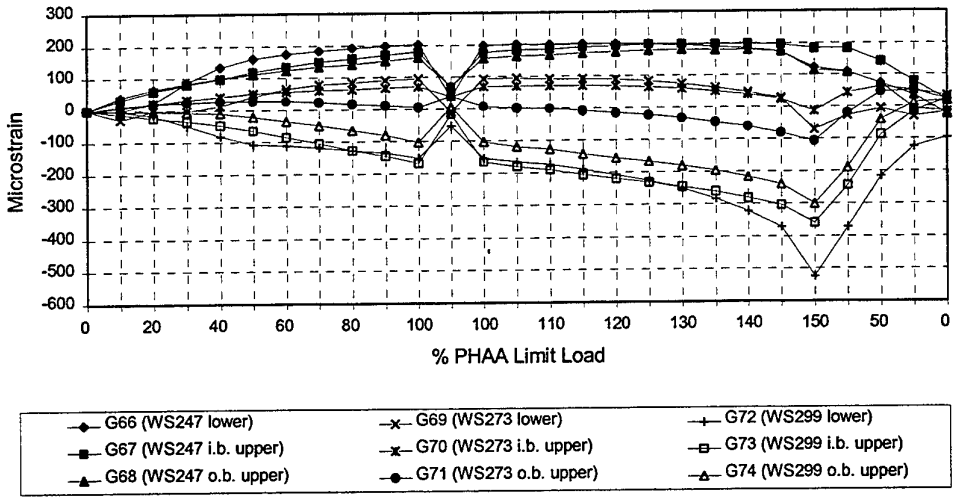

	G66	G67	G68	G69	G70	G71	G72	G73	G74
20%DLL	21	58	65	-3	21	18	-19	-24	-5
100%DLL	202	179	162	95	69	4	-152	-168	-103
unld 20%	36	67	69	-11	38	39	-54	-17	7
150%DLL	122	183	114	-72	-15	-108	-523	-359	-301
RESIDUAL STRAINS									
unld 20%	15	10	5	-8	17	21	-36	8	11
unld 0%	-16	19	-25	-17	31	19	-97	21	15

Figure 11. Skin strains for the PHAA Test

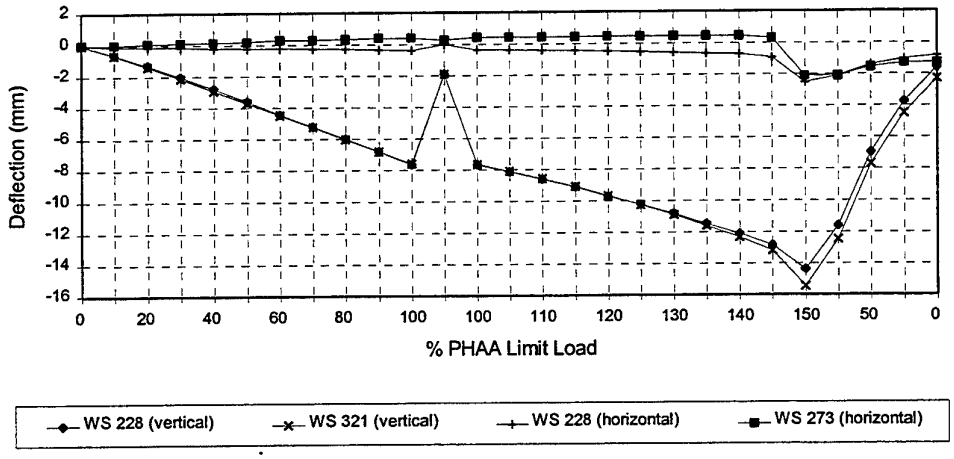

	WS 228 (vert)	WS 321 (vert)	WS 228 (hor)	WS 273 (hor)
20%DLL	-1.3	-1.4	-0.1	0.1
100%DLL	-7.6	-7.6	-0.4	0.4
unld 20%	-1.9	-1.9	0.0	0.2
150%DLL	-14.4	-15.5	-2.5	-2.1
RESIDUAL DEFLECTIONS				
unld 20%	-0.6	-0.5	0.1	0.2
unld 0%	-1.6	-2.3	-0.8	-1.3

Figure 12. Deflections for the PHAA Test.

6.3 PLAA Case

6.3.1 Loading Schedule

As mentioned in Sections 2.1.3 and 2.1.4, the PLAA Test was represented by the pressure profiles corresponding to the 4g and 4.5g load cases. Ideally, a gradual transition between the 2 pressure profiles as the loading is increased from the 4g case to the 4.5g case would best represent reality. However, the available controller did not have sufficient flexibility to permit such incremental profile variation. Consequently, the PLAA Test was handled by performing the following 2 separate tests:

i) The application of the 4g pressure profile in increments of 5% (from zero load) up to 100% and unloading in 2 equal decrements, and

ii) The application of the 4.5g pressure profile in increments of 5% (from zero load) until failure occurs.

All transducers were zeroed at the commencement of each of the tests and the loads were generally held steady for approx. 20s after each increment during which data were logged. Visual inspection and photographs were also taken when warranted.

6.3.2 Measured Strains

a) Spanwise Distribution (Section EE)

Section EE strains along the span are shown in Fig. 13. The test article survived 100% of the 4g load case and the maximum Section EE strain attained was for WS239 reaching approx. 1,080 microstrains. The strains behaved relatively linearly throughout this test and were lower than those for the PHAA case at DUL. For the 4.5g load case, the strains also behaved surprisingly linearly and the maximum recorded strain at this Section was approx. 1,350 microstrains at 95% of the 4.5g load at WS239. The test article failed during the load excursion between 95% and 100% load. From the audio tracks on the video recordings, it was deduced that catastrophic failure occurred virtually immediately after the load was being increased from 95% level. The mode of failure is discussed later in Section 6.4.2.

b) Lower Leg

The lower leg strains of ribs WS228, WS273 and WS317 for the PLAA Test are shown in Figs 14 to 17. As was seen in the previous Section, the tensile strains for the PLAA 4g case were less severe than those seen at DUL under the PHAA condition, but the maximum strains reached at 95% of the 4.5g case were slightly higher. The maximum recorded strains at the critical region (Section KK) for WS273 was 11,571 microstrains just prior to failure.

Interestingly, the PLAA strains appeared to be more linear compared to the PHAA case with respect to the applied load. This is most probably due to the fact that the PLAA Test was conducted after the PHAA Test during which some degree of strain hardening would have taken place (as mentioned in Section 6.2.2b, yielding at the critical region would have occurred at around 135%DLL during the PHAA Test).

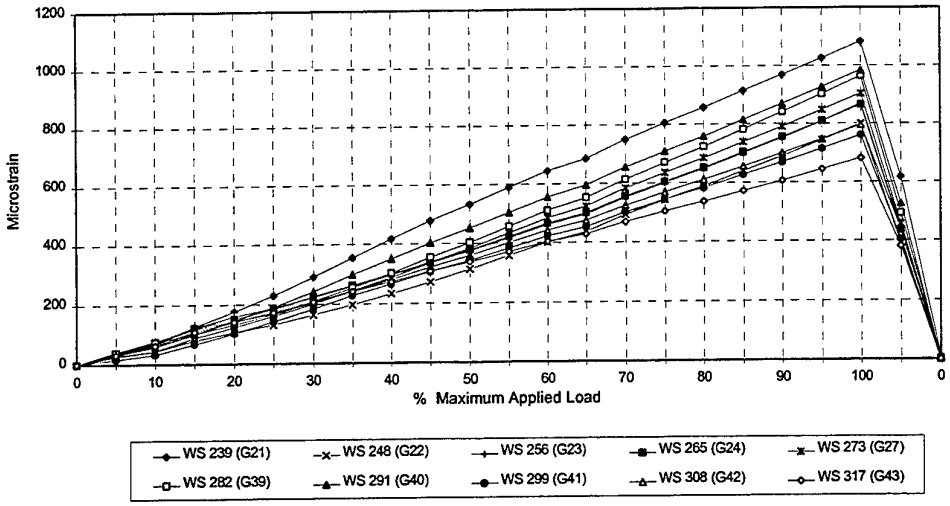

	WS 239 G21	WS 247 G22	WS 256 G23	WS 265 G24	WS 273 G27	WS 282 G39	WS 291 G40	WS 299 G41	WS 308 G42	WS 317 G43
50%MAX	532	313	374	378	383	403	451	343	359	338
100%MAX	1083	799	865	863	902	962	983	760	795	680
unld 50%	616	389	444	434	456	491	525	403	438	381
RESIDUAL STRAINS										
unld 50%	84	77	70	56	73	88	74	61	79	44
unld 0%	8	4	2	1	3	2	-2	-5	-3	-1

(a)

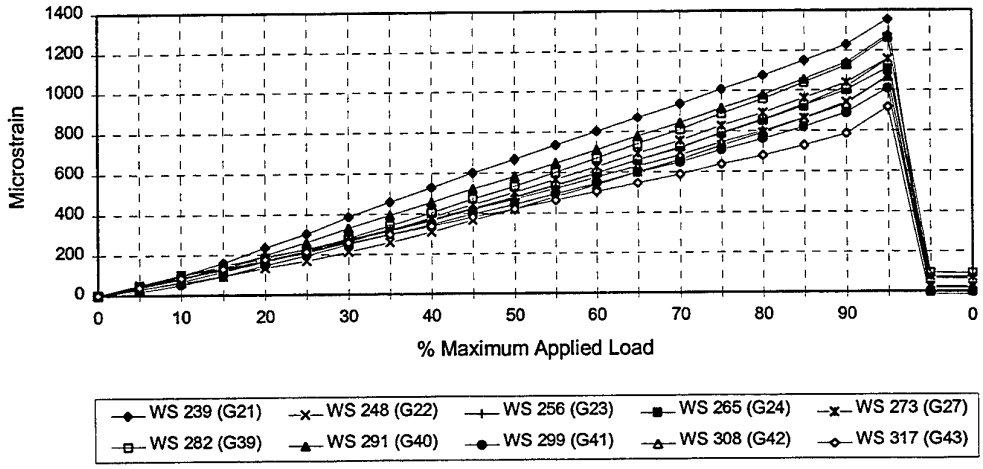

	WS 239 G21	WS 247 G22	WS 256 G23	WS 265 G24	WS 273 G27	WS 282 G39	WS 291 G40	WS 299 G41	WS 308 G42	WS 317 G43
95%MAX	1352	1063	1154	1110	1156	1261	1273	1008	1069	916
RESIDUAL STRAINS										
unld 0%	-66	22	15	63	72	90	22	-9	-20	-45

(b)

Figure 13. Section EE strains for the PLAA Test: a) 4g case, b) 4.5g case.

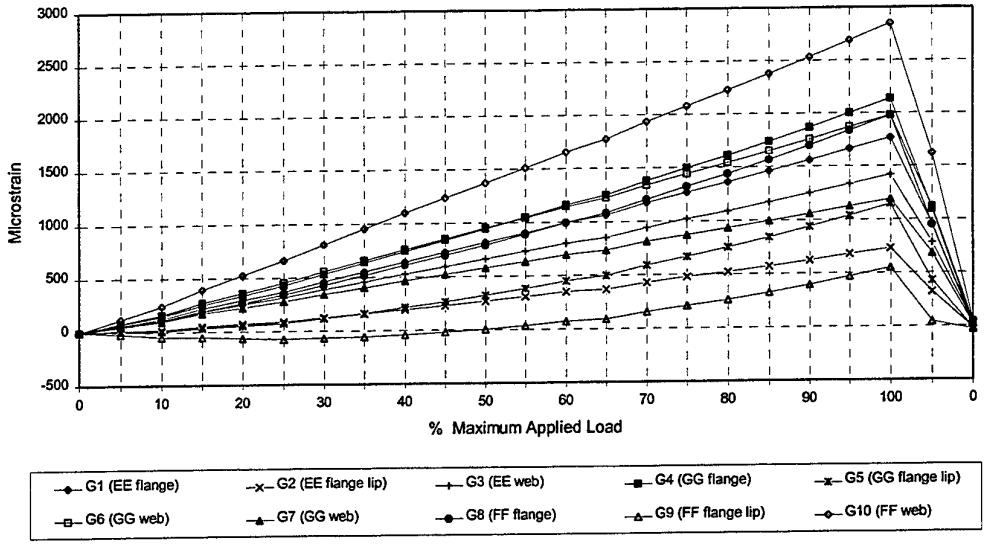

	G1	G2	G3	G4	G5	G6	G7	G8	G9	G10
50%MAX	814	265	660	942	320	947	575	791	4	1372
100%MAX	1768	731	1415	2137	1145	1979	1188	1980	547	2851
unld 50%	950	320	777	1090	422	1113	679	946	44	1618
RESIDUAL STRAINS										
unld 50%	136	55	117	149	103	166	104	155	40	247
unld 0%	24	-12	28	9	-21	38	17	6	-33	42

(a)

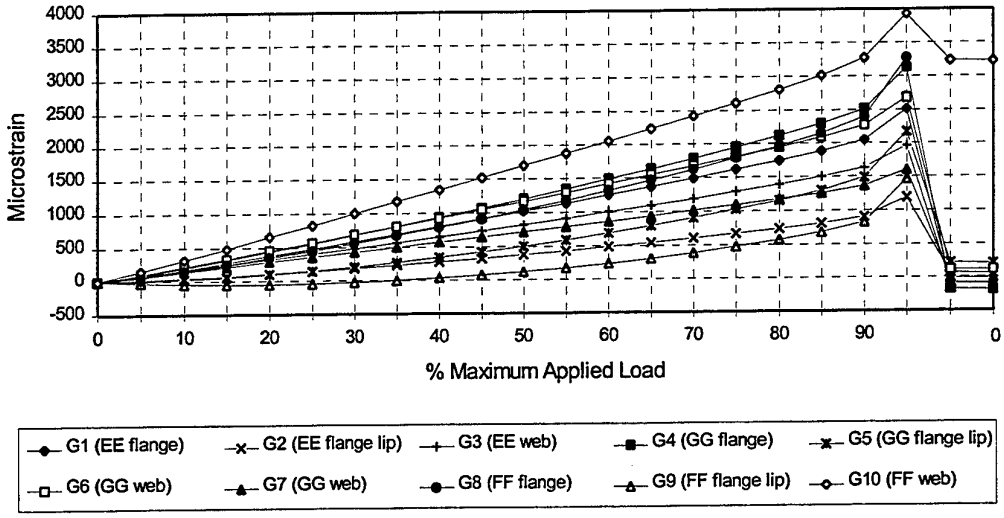

	G1	G2	G3	G4	G5	G6	G7	G8	G9	G10
95%MAX	2508	1192	1957	3128	2171	2679	1601	3275	1470	3927
RESIDUAL STRAINS										
unld 0%	-104	50	-92	-192	204	109	-17	-19E+6	-19E+6	3224

(b)

Figure 14. WS228 lower leg strains for the PLAA Test: a) 4g case, b) 4.5g case.

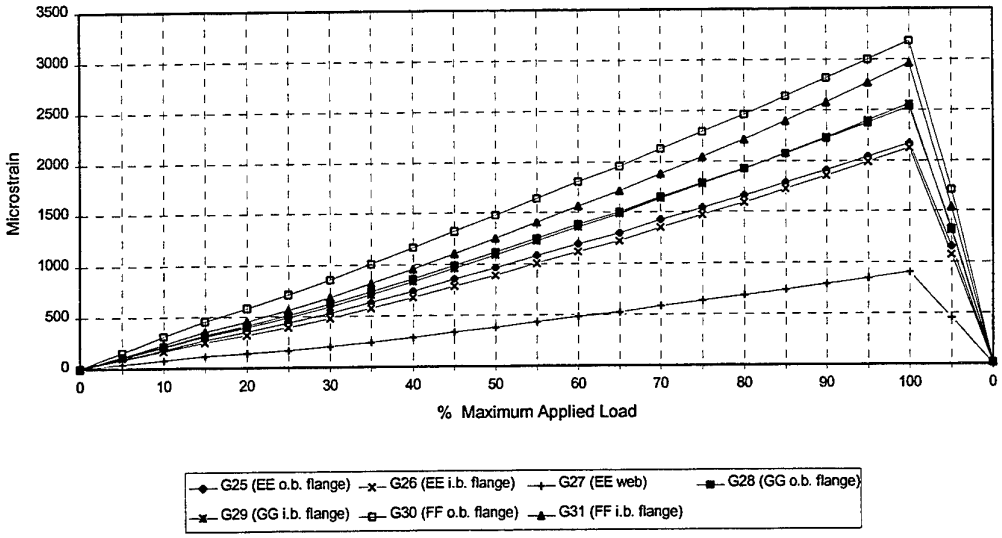

	G25	G26	G27	G28	G29	G30	G31
50%MAX	964	891	383	1115	1087	1478	1250
100%MAX	2169	2126	902	2532	2559	3180	2960
unld 50%	1151	1073	456	1323	1308	1708	1534
RESIDUAL STRAINS							
unld 50%	187	182	73	208	221	230	284
unld 0%	18	14	3	18	14	17	18

(a)

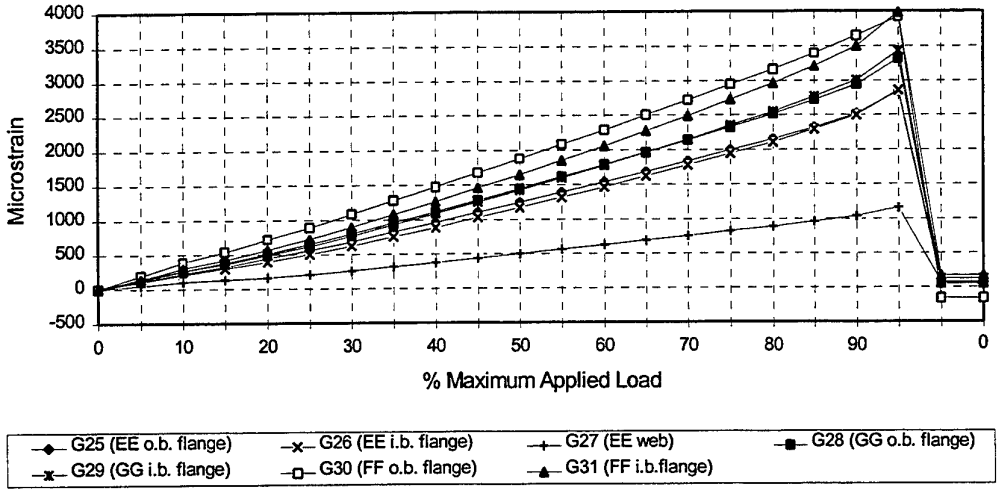

	G25	G26	G27	G28	G29	G30	G31
95%MAX	2840	2851	1156	3313	3428	3919	3982
RESIDUAL STRAINS							
unld 0%	62	125	72	48	123	-163	170

(b)

Figure 15. WS273 lower leg strains for the PLAA Test: a) 4g case, b) 4.5g case.

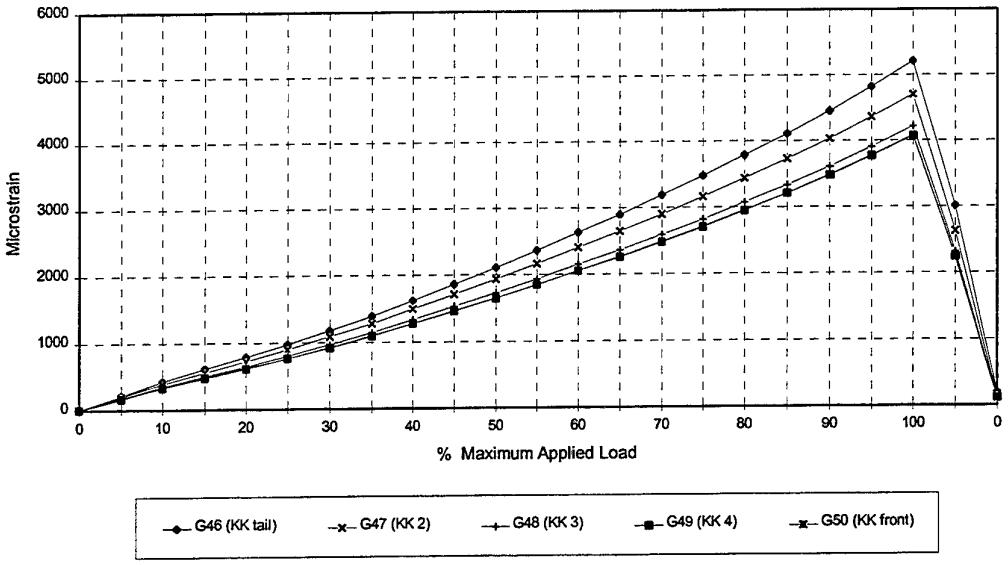

STRAINS	G46	G47	G48	G49	G50
50%MAX	2107	1935	1725	1645	1646
100%MAX	5212	4700	4207	4068	4074
unld 50%	3006	2627	2316	2241	2247
RESIDUAL STRAINS					
unld 50%	899	692	590	596	602
unld 0%	186	130	107	110	106

(a)

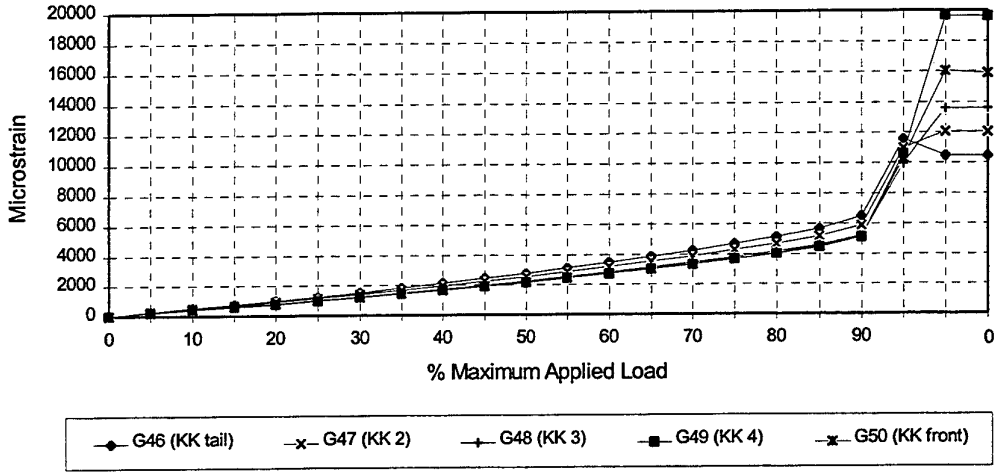

STRAINS	G46	G47	G48	G49	G50
95%MAX	11571	10946	9932	10566	10305
RESIDUAL STRAINS					
unld 0%	10430	12037	13579	19633	15898

(b)

Figure 16. WS273 lower leg strains at critical region for the PLAA Test: a) 4g case, b) 4.5g case.

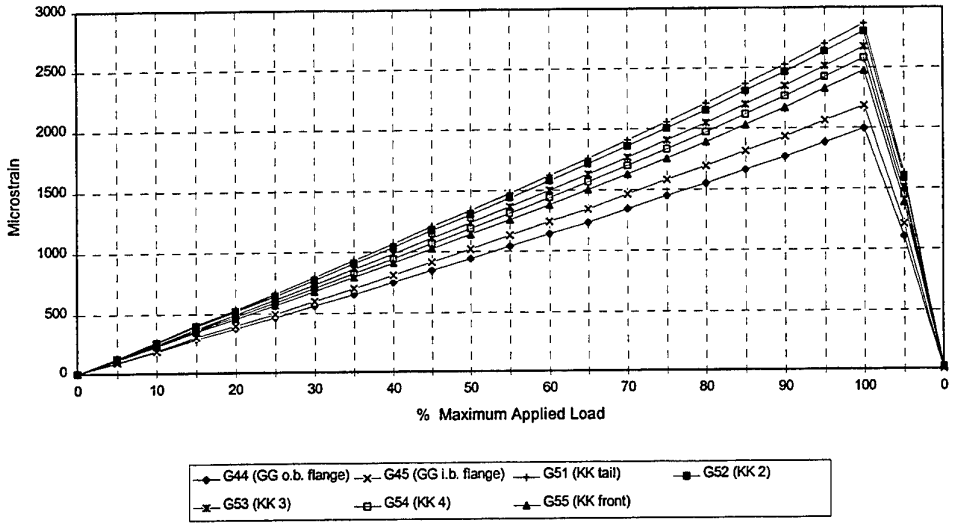

STRAINS	G44	G45	G51	G52	G53	G54	G55
50%MAX	942	1020	1337	1301	1237	1188	1141
100%MAX	1994	2183	2865	2800	2671	2576	2471
unld 50%	1104	1206	1627	1584	1504	1445	1384
RESIDUAL STRAINS							
unld 50%	162	185	290	282	267	257	243
unld 0%	2	2	23	20	18	17	15

(a)

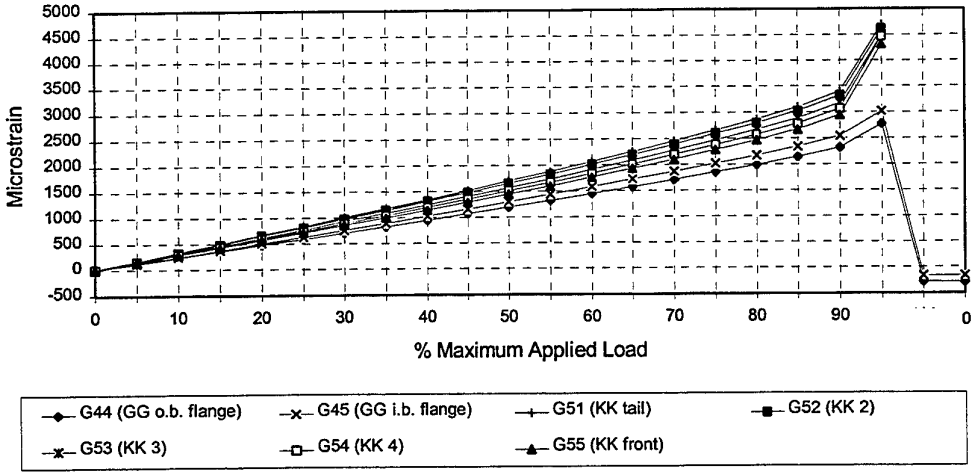

STRAINS	G44	G45	G51	G52	G53	G54	G55
95%MAX	2769	3018	4699	4605	4494	4462	4316
RESIDUAL STRAINS							
unld 0%	-291	-167	7597	10082	16752	31733	8191

(b)

Figure 17. WS317 lower leg strains for the PLAA Test: a) 4g case, b) 4.5g case.

c) Upper Leg

The PLAA upper leg strains for the ribs at WS228 and WS273 are shown in Figs 18 and 19. As mentioned earlier, the upper leg sustained the compressive loads under the applied lifting forces. The strains here behaved much the same as the PHAA Test although it may be seen that the vertical part of the flange lip for the PLAA Test now became even less effective than for the PHAA Test. This, again, may be attributed to the prior permanent deformation which was introduced during the PHAA Test. The evidence of this is much clearer here as, for example, it may be seen from Fig. 9 that Gauges 12 and 15 on WS228 showed noticeable tensile residual strains at the completion of the PHAA Test.

d) Skin

Figure 20 shows the skin strain readings throughout the PLAA Test. The skin gauges showed that similarly low strains were reached compared to those of the PHAA Test. However, the PLAA results showed a noticeably more linear response with respect to the applied load. One exception seen was with Gauge 72 (on the lower skin near WS299) in which little strain was experienced throughout the PLAA Test whereas this gauge recorded the highest skin strains during the PHAA Test. Partial detachment of this gauge is one possible explanation, although this was not likely as the strains reached during the PHAA Test was low (approx. -520 microstrains). A more likely explanation may be the fact that the rear row of lower pads were moved rearwards closer to the skin gauges for the PLAA Test and therefore affected the local skin strains.

6.3.3 Measured Deflections

The deflection measurements for both cases of the PLAA Test are shown in Figs 21. It may be seen that the test article deflected relatively linearly and with little difference between the inboard and outboard ribs throughout the Test. Rapid loss of overall stiffness was evident between 140%DLL to 150%DLL. In particular, the rapid relative increase in lateral deflection in the final stages highlights the buckling of the upper leg at high loads. However, it is to be noted that over the 85%-90% of the 4.5g load range, the deflections for WS273 did not show a disproportionate increase, whereas the strains at the critical region (Section KK) have already begun to increase markedly. This strongly suggests that failure was not preceded by a sudden loss of compressive stiffness of the upper leg, but rather, that the ultimate strain at the critical region was duly reached.

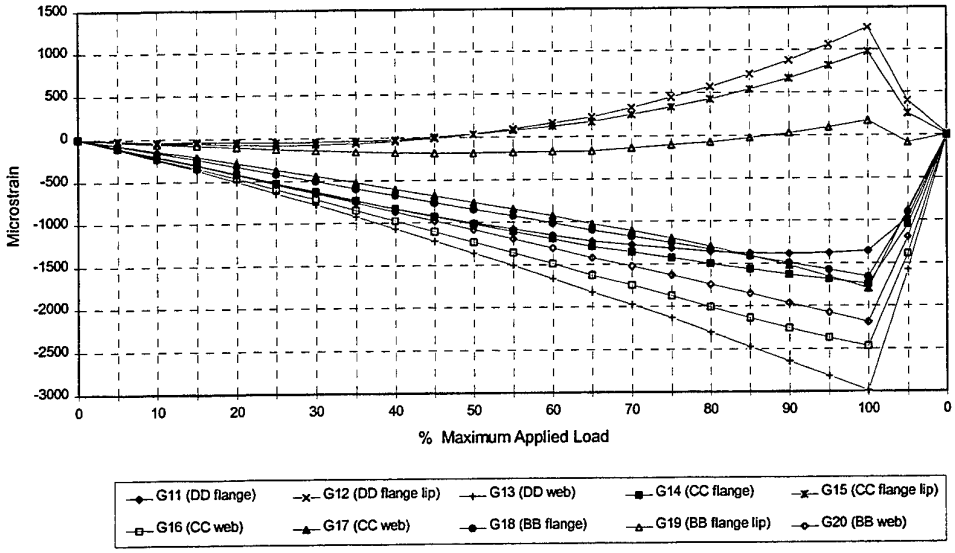

STRAINS	G11	G12	G13	G14	G15	G16	G17	G18	G19	G20
50%MAX	-1005.8	33.5	-1358.7	-1021.7	33.8	-1230.2	-763.6	-847.2	-183.9	-1089.1
100%MAX	-1356.1	1257.9	-2988.6	-1748.6	972.4	-2469.3	-1799.1	-1656.0	168.3	-2189.8
unld 50%	-974.2	398.0	-1577.4	-1052.9	249.7	-1388.9	-883.0	-907.0	-86.9	-1193.9
unld 0%	-6.7	15.8	-11.3	-6.4	5.5	-8.1	-3.9	0.6	-0.3	-6.8
RESIDUAL STRAINS										
unld 50%	31.7	364.5	-218.7	-31.2	215.9	-158.7	-119.4	-59.8	97.0	-104.8
unld 0%	-6.7	15.8	-11.3	-6.4	5.5	-8.1	-3.9	0.6	-0.3	-6.8

(a)

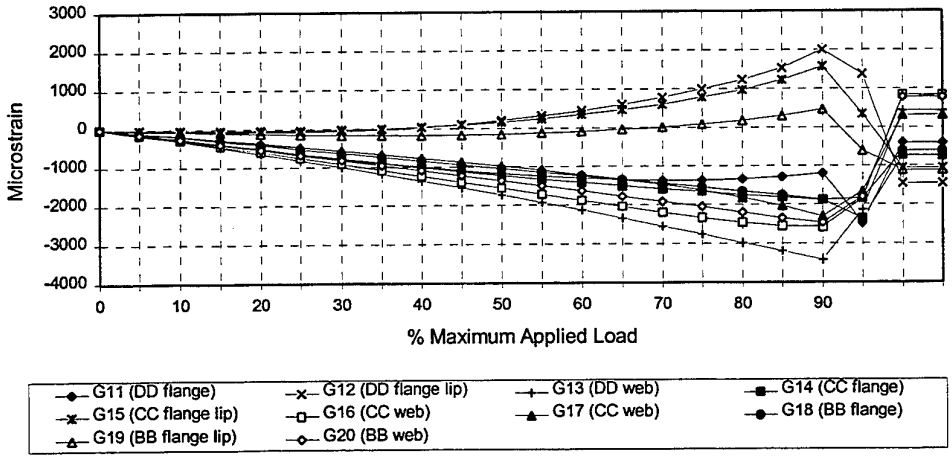

STRAINS	G11	G12	G13	G14	G15	G16	G17	G18	G19	G20
95%MAX	-2488.2	1370.7	-2143.7	-2363.5	335.8	-1861.2	-1671.0	-1855.0	-607.0	-1807.7
unld 0%	-408.6	-1461.1	419.5	-744.1	-1064.6	823.8	314.1	-612.0	-1115.5	768.3
RESIDUAL STRAINS										
unld 0%	-408.6	-1461.1	419.5	-744.1	-1064.6	823.8	314.1	-612.0	-1115.5	768.3

(b)

Figure 18. WS228 upper leg strains for the PLAA Test: a) 4g case, b) 4.5g case.

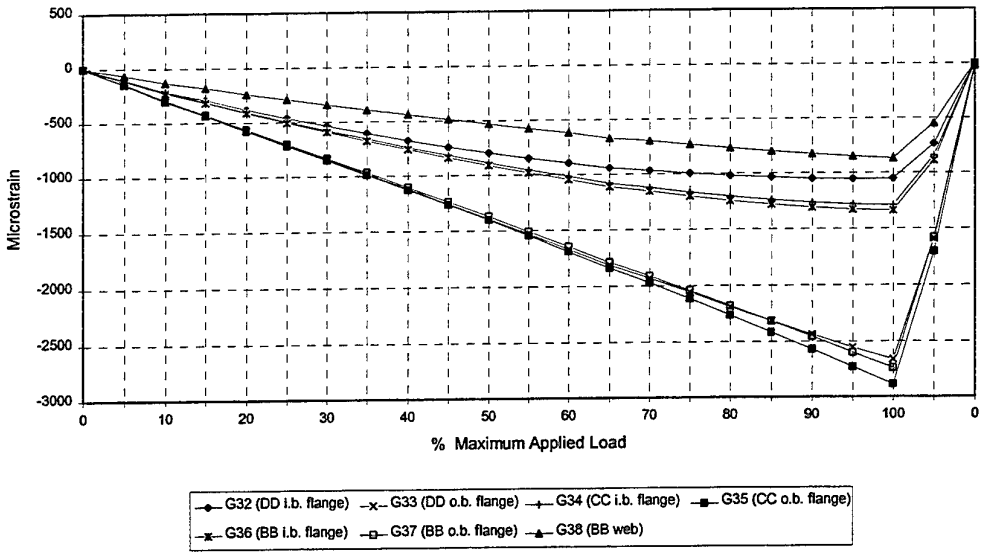

	G32	G33	G34	G35	G36	G37	G38
50%MAX	-794.5	-1393.2	-885.3	-1403.0	-908.3	-1373.3	-531.4
100%MAX	-1054.8	-2662.7	-1295.3	-2887.9	-1342.8	-2739.0	-868.9
unld 50%	-737.2	-1590.6	-844.4	-1703.0	-886.9	-1579.7	-546.7
unld 0%	11.6	-16.7	9.4	-27.9	4.0	-16.6	2.5
RESIDUAL STRAINS							
unld 50%	57.4	-197.4	40.9	-300.0	21.4	-206.4	-15.3
unld 0%	11.6	-16.7	9.4	-27.9	4.0	-16.6	2.5

(a)

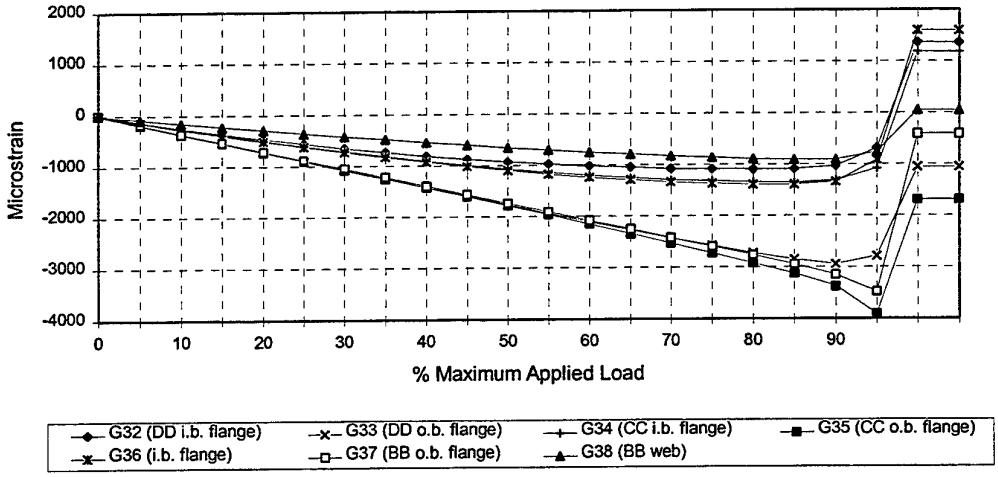

	G32	G33	G34	G35	G36	G37	G38
95%MAX	-684.3	-2790.0	-1074.1	-3904.2	-909.7	-3475.8	-750.2
unld 0%	1347.8	-1050.0	1169.2	-1682.9	1585.2	-411.7	37.2
RESIDUAL STRAINS							
unld 0%	1347.8	-1050.0	1169.2	-1682.9	1585.2	-411.7	37.2

(b)

Figure 19. WS273 upper leg strains for the PLAA Test: a) 4g case, b) 4.5g case.

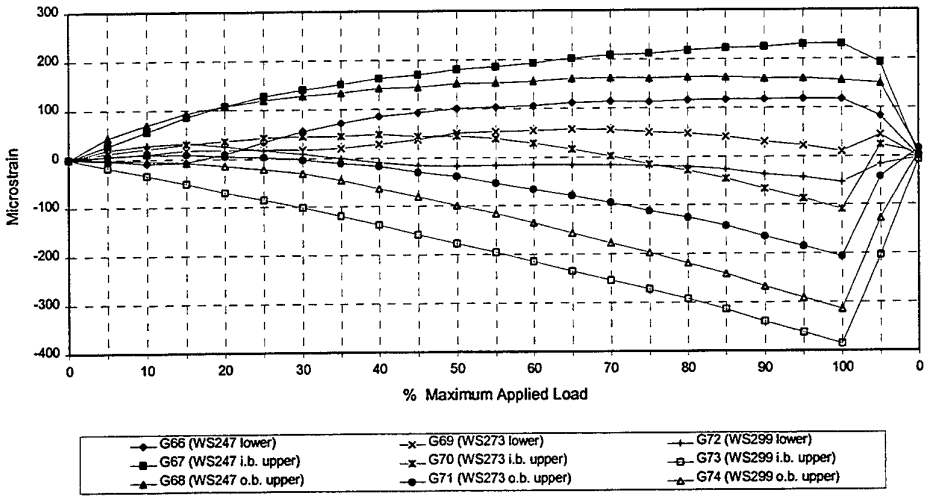

	G66	G67	G68	G69	G70	G71	G72	G73	G74
50%MAX	99.8	180.1	150.9	49.9	44.0	-39.1	-17.7	-177.6	-99.2
100%MAX	117.0	230.7	155.9	10.4	-109.5	-207.0	-53.7	-385.6	-314.5
unld 50%	82.5	191.7	149.3	44.1	23.6	-42.5	-16.5	-204.2	-127.9
unld 0%	-0.1	0.1	10.9	-1.3	7.2	15.4	-2.9	-6.8	7.0
RESIDUAL STRAINS									
unld 50%	-17.2	11.6	-1.6	-5.8	-20.4	-3.5	1.3	-26.6	-28.7
unld 0%	-0.1	0.1	10.9	-1.3	7.2	15.4	-2.9	-6.8	7.0

(a)

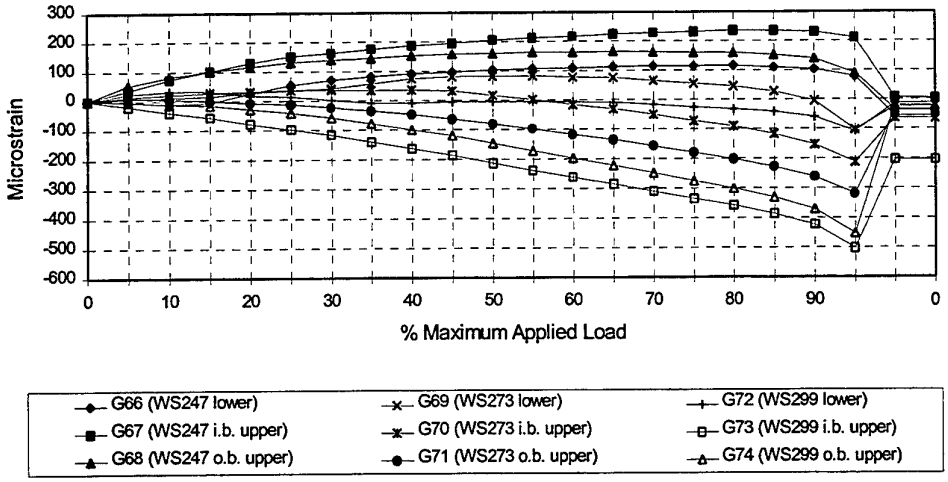

	G66	G67	G68	G69	G70	G71	G72	G73	G74
95%MAX	78.0	210.8	89.4	-103.1	-213.1	-319.9	-108.5	-502.4	-451.8
unld 0%	-56.8	3.5	-36.4	-23.0	-65.3	-38.8	-12.9	-204.2	-22.4
RESIDUAL STRAINS									
unld 0%	-56.8	3.5	-36.4	-23.0	-65.3	-38.8	-12.9	-204.2	-22.4

(b)

Figure 20. Skin strains for the PLAA Test: a) 4g case, b) 4.5g case.

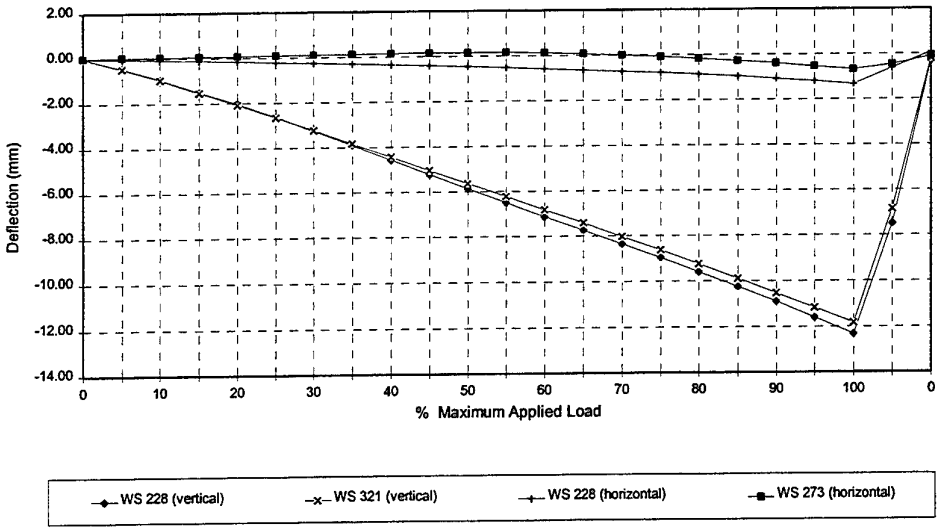

	WS 228 (vert)	WS 321 (vert)	WS 228 (hor)	WS 273 (hor)
50%DLL	-5.86	-5.63	-0.46	0.15
100%DLL	-12.33	-11.84	-1.34	-0.69
unld 50%	-7.50	-6.86	-0.64	-0.47
unld 0%	-0.32	-0.22	0.06	-0.11
RESIDUAL DEFLECTIONS				
unld 50%	-1.63	-1.23	-0.18	-0.62
unld 0%	-0.32	-0.22	0.06	-0.11

(a)

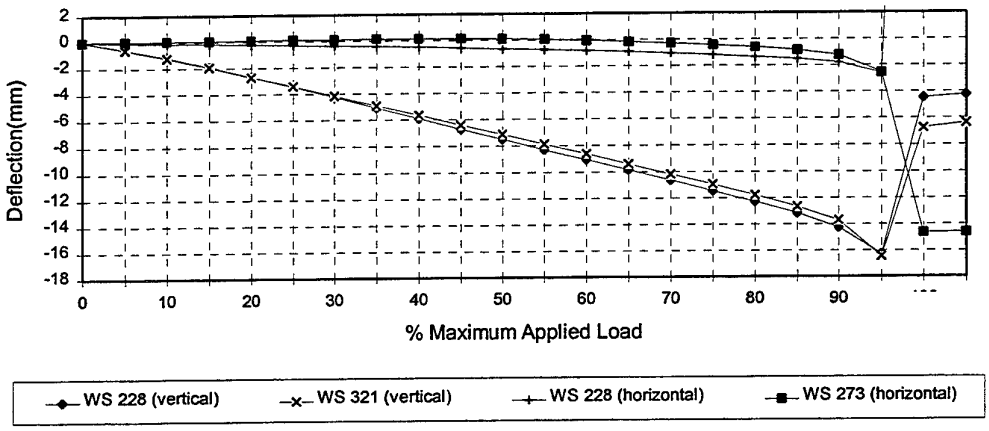

	WS 228 (vert)	WS 321 (vert)	WS 228 (hor)	WS 273 (hor)
95%MAX	-16.26	-16.47	-2.63	-2.56
unld 0%	-4.27	-6.37	60.75	-14.61
RESIDUAL DEFLECTIONS				
unld 0%	-4.27	-6.37	60.75	-14.61

(b)

Figure 21. Deflections for the PLAA Test: a) 4g case, b) 4.5g case.

6.4 Failure Analysis

During the load increment between 95% and 100% of the 4.5g load case, a loud "bang" emanated from the test article signifying the failure of the test article. As mentioned earlier, the video records revealed that the breaking point occurred soon after the 95% level. With the loss of stiffness, the controller shut down the hydraulic system and the test load was effectively removed. Whilst the test article was still mounted in the test rig, an initial inspection of the failure sites were performed and photographs of the deformed ribs were taken. It was found that each of the 13 ribs was fractured at the tangency point on the lower leg (see Fig. 22 for example). For the internal ribs, the line of failure traversed across the lowermost stiffening dimple as found in the accident case. It was not possible to determined from the inspection which of the ribs had failed first, although from the strain data, it would appear that the WS239 was the most likely candidate as it had experienced the highest strains throughout the tests.

The test article was subsequently removed from the test rig for a more detailed analysis, and the following sections described the major findings.

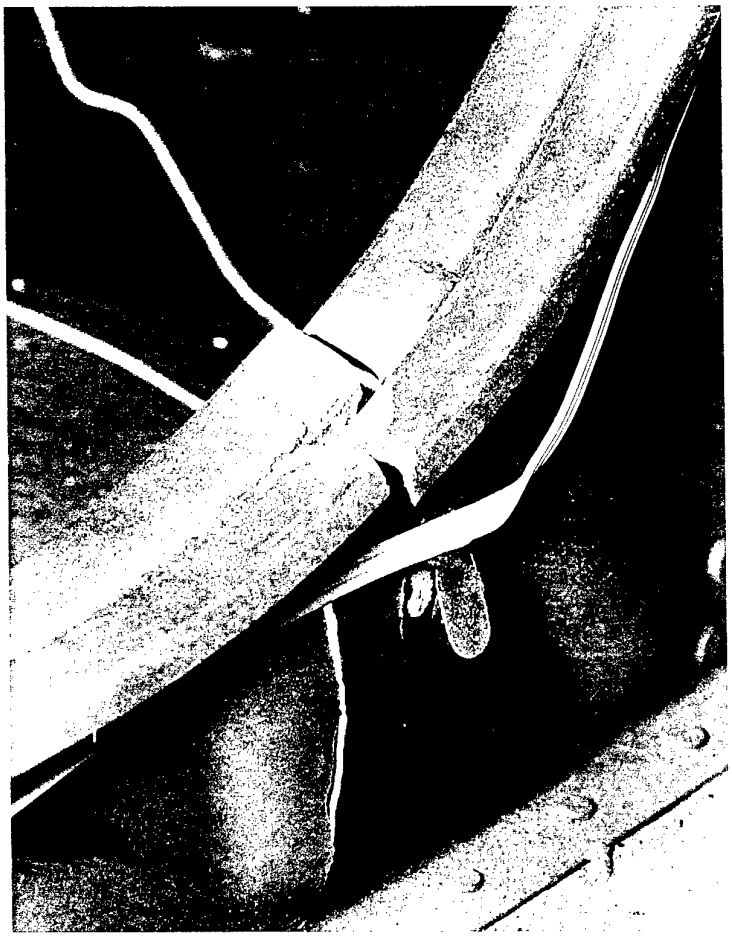

Figure 22. Typical fracture on the lower leg of the rib.

6.4.1 Residual Deformation

From the strain data, it was seen that at least some parts of the test article had undergone plastic deformation prior to failure. This was also reflected most clearly by the permanent deformation of the ribs at the conclusion of the tests. To quantify this, detailed measurement of the deformed shapes of each rib was carried out. This was achieved by dividing the inner perimeter of each rib into 50 evenly spaced locations and a distance was measured from the centre-line of each rib at these locations to a reference plane mounted on the inboard closure rib WS228. Because the inboard rib is canted, there was a linear component of the measurement associated with this inclination which could be effectively removed. Figure 23 shows the results of the measurements after the canted components were removed. Some of the noteworthy locations are as follows:

a) Position 1: First measurement node, approx. 20mm from the hinge line at the bottom surface.
b) Position 19 to 20: enclosing the tangency point on the lower leg, and where fracture was found for all ribs.
c) Position 25: Corresponding to the nose of the inner flange.
d) Position 50: Last measurement node, approx. 20mm from the re-entrant corner where the web meets the under side of the top surface.

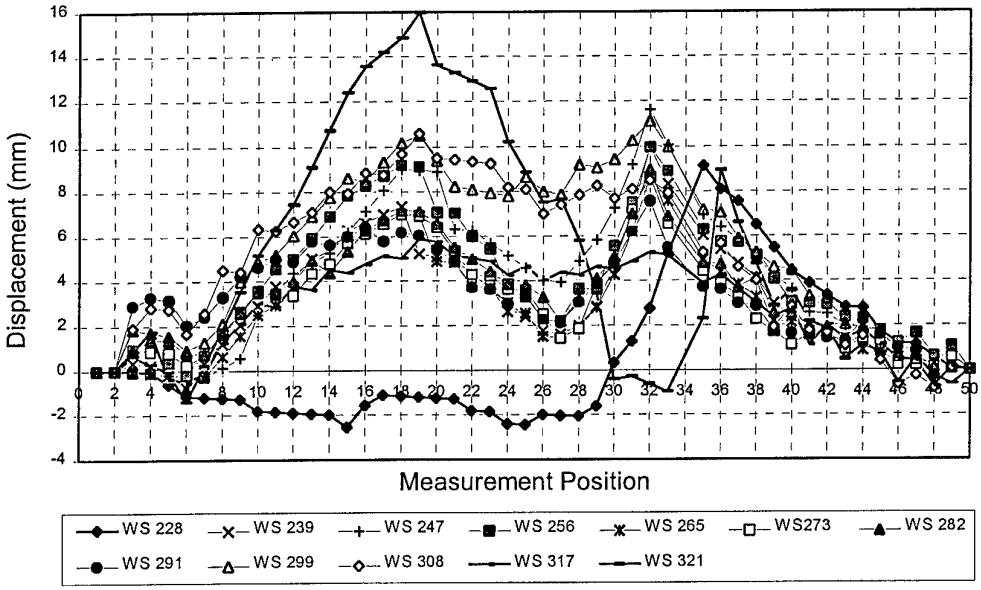

Figure 23. Final rib displacements after failure.

It may be seen from the results that most of the ribs deformed similarly, and predominantly in the positive (outboard) direction. There were 2 dominant peaks, namely, one near Position 19 corresponding to the critical location, and one near Position 32 which was the counterpart of the citical location on the upper leg. Some departure from this general trend was seen for the 2 closure ribs (WS228 and WS321), both of which were structured significantly differently from the internal ribs. For the

inboard closure rib (WS228), it lacked the large deformation at the tensile critical location whereas for the outboard closure rib (WS321), the deformation at this location was the greatest amongst all the ribs. The reason for this may be attributed to the asymmetry of these closure ribs where the web/flange is of a "C" section ("C" for WS228 and an inverted "C" for WS321) compared to the "T" section of the inner ribs.

On the compressive leg, both the closure ribs had the maximum deformation further down stream when compared to the internal ribs (Position 35 for WS228 and Position 36 for WS321), and were of comparable in magnitude. The shift in the critical position was attributable to the stiffening cleats attached near Position 32 on both the closure ribs.

An interesting feature to note is the sharpness of the deformation peaks on the compressive legs for all ribs, which reflect the sharp folds formed by the compressive collapse of this part of the structure when failure occurred.

Some parts of the failed structure from the test also showed remarkable resemblance to the recovered crashed article from the RAAF Orion A9-754. For example, Fig. 24 shows the collapsed intercostal near the midspan for both the test and crashed articles where the good likeness in the collapse of these components can be clearly seen.

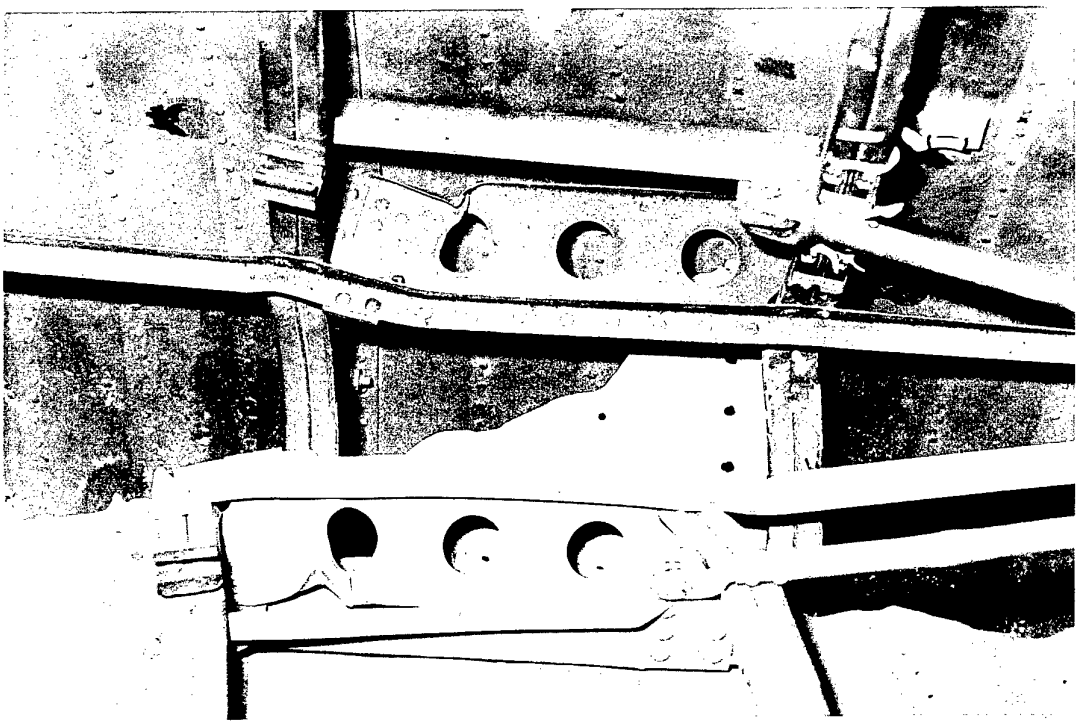

Figure 24. Comparison of the failed parts near the midspan inter-costal between the test article and that from RAAF A9-754 (the lower component is from the A9-754 starboard centre WLE and thus the mirrored image compared to the portside test article).

6.4.2 Mode of Failure

To established the mode of failure of the test article, sections of the failed region were cut out from 3 ribs (WS239, WS291 and WS317, these were selected based on their spread along the span and on the ease of access for the cutting operation) and the fracture surface examined microscopically. Care was taken during the cutting operation to prevent the fracture surfaces from rubbing. Figure 25 shows an optical micrograph of a typical failed surface, revealing the classical cup-and-cone type ductile failure near the top edge of the rivet hole which was nearest the lowermost stiffening dimple. This feature extends for approx. 1 hole diameter before merging into a 45° planar fracture surface (not shown). This feature was also found in the accident report on the RAAF Orion A9-754 (see Fig. 18 of Callinan *et al* [2]), and strongly suggests that failure was initiated from such a hole. This also accords with the findings of Wong *et al* [5] where it was revealed by thermoelastic stress analysis that such a rivet hole would experience the highest stresses under load.

Figure 25. Optical micrograph of the failed surface through a rivet hole. Note the necking on the left hand side of the hole edge indicating a ductile type failure emanating from the hole.

6.4.3 Rib Thickness Measurements

Detailed material thickness measurements were also taken on the 3 selected ribs previously mentioned. A small section (approx. 2cm x 1cm) was cut out on the lower leg away from the stiffening dimples, and edges were then polished and etched so that the structural material and cladding may be determined under an instrumented microscope. For each specimen, ten measurement points were taken to determine the total thickness, whereas twenty measurement points were used to find the clad thicknesses because of a slight increase in uncertainty involved in locating the clad/alloy interface. For these microscopic measurements, there was no need to remove the paint from the specimens. Total thickness measurements were also taken using a standard micrometer on the ribs (close to the cut-out sections) both with the paint attached and with the paint chemically removed. The results of the measurements are summarised in Table 1.

It may be seen that the measured thicknesses show very little variations both from measurement to measurement, and from rib to rib. The microscopic measurements fell between the micrometer measurements for "with" and "without" the paint, although as expected, they are much closer to the latter. The small differences (≤0.0015") between the two measurement techniques can easily be accounted for by the resolution of the micrometer used and the fact that they were taken from different parts of the structure. This result shows that micrometer measurements, assuming a consistent (or even an upper-bound) clad thickness, can provide a useful assessment on the thickness of structural material.

Table 1. Thickness measurements for the 3 selected ribs.

WS	inb. clad[1] (in.)	outb. clad[1] (in.)	total thickness[2] (in)	total clad thickness[3] (%)	alloy thickness[4] (in)	micrometer meas.[5] (in) with paint	micrometer meas.[5] (in) without paint
239	0.00243	0.00209	0.0419	10.8	0.0374	0.0424	0.0413
	(0.0004)	(0.00023)	(0.00077)			(0.00092)	(0.00097)
291	0.00225	0.00181	0.0420	9.6	0.0379	0.0457	0.0412
	(0.00018)	(0.00016)	(0.00048)			(0.00058)	(0.00053)
317	0.00239	0.00188	0.0421	10.1	0.0379	0.0453	0.0406
	(0.00031)	(0.00013)	(0.00050)			(0.00100)	(0.00058)

Notes:
1) mean value of clad thickness over 20 measurements with standard deviation given in parenthesis.
2) mean value of total thickness over 10 measurements with standard deviation given in parenthesis.
3) sum of inboard and outboard clad thicknesses as percentage of the total thickness.
4) total thickness minus the sum of inboard and outboard cladding.
5) mean value of total thickness over 5 measurements with standard deviation given in parenthesis.

For comparison purpose, the microscopic measurements averaged over the 3 selected ribs together with the thickness measurements reported for the recovered centre section WLE of A9-754 are shown in Table 2. It is interesting to note that the mean thickness for test article is slightly higher than the specification requirement of 0.040" whereas it was found that the A9-754 had ribs which were slightly below this value. Whilst the absolute difference is not great, it is significant in a relative sense. For example, both the total thickness and the actual Al2024 alloy thickness for A9-754 are some 8% below those of the test article. Although this figure cannot be directly translated to a reduction in load to failure due to the various non-linearities involved, it would nevertheless be expected to have a significant effect on the structure's overall strength. In fact, in the analysis carried out by LASC (see Appendix L in Molent [1]), the effects of a reduced rib thickness was reported by LASC as "significant" and amounts to some 20% reduction in the load sustainable at the critical section for the A9-754 case.

Table 2. Comparison of thickness measurements between test article and A9-754.

	total thickness (in)	alloy thickness (in)
Test Article	0.0420[1]	0.0377[1]
	(0.00016)	(0.00005)
A9-754	0.0387[2]	0.0346[2]
	(0.0016)	(0.0015)

Notes: 1) mean value over the 3 ribs measured using the microscope, with standard deviation shown in parenthesis.
2) mean value over the 12 ribs studied microscopically in [2] with standard deviation given in parenthesis.

7. Conclusions and Recommendations

A static test rig has been constructed for testing a Lockheed P-3 Orion centre section wing leading edge. The test rig incorporated the use of adhesively bonded rubber pads and conventional whiffle tree systems to simulated the aerodynamic loads to the test article. Two load cases were tested, namely, a) the Design Ultimate Load (DUL) case under a low speed and positive high angle of attack condition, and b) the high speed (Mach No. of 0.56) and positive low angle of attack condition. The following summarise the findings:

1) Under the design load case (a), the test article

i) sustained the Design Limit Load without resulting in any significant permanent deformation,
ii) sustained the Design Ultimate Load (DUL, 150%DLL) without failure. The recorded strain data showed that the strains at the critical region reached the yield strain of approx. 5,000 microstrains at around 135% DLL and rose quickly to 10,000 microstrains at DUL.

2) Under the high speed case (b), the test article

i) responded relatively linearly to the applied load and reached the full 4g load case without failure,
ii) responded relatively linearly up to 90% of the 4.5g load case. The strains and deflections indicated a rapid loss of stiffness between 90%-95% and failed virtually immediately as the load was being increased from the 95% mark. Failure load under the PLAA condition was therefore estimated to be equivalent to a 4.3g pull-up.

3) Under both the PHAA and PLAA Tests, the strain data suggest that the most highly loaded internal rib was that at WS239, where the strain at the tension leg web was some 12% (PHAA) and 7% (PLAA) higher than the next highly stressed rib at WS273 (centre rib) at the respective maximum loads.

4) Post failure analysis revealed the following:

i) All 13 ribs (including the end ribs) were fractured through the tangency point on the lower (tension) leg. For the internal ribs, the fracture extended through the lowermost stiffening dimple similar to that found for the failed RAAF Orion A9-754. Other final deformed parts of the structure, notably the inter-costal near the mid-span, also resembled closely to those of the recovered components from the A9-754 aircraft and show that the test was able to accurately replicate the failure mechanism.

ii) Three ribs spread along the span of test article (WS239, WS291 and WS317) were selected for detailed inspection. It was revealed that fracture was initiated from the rivet hole nearest the critical stiffening dimple and accords with the findings for A9-754.

iii) The thickness measurements taken from the 3 selected ribs showed that the material thickness of the test article to be highly consistent and were within the manufacturer's specification. It was pointed out that the rib material thickness for the A9-754 was, on average, some 8% below that of the current test article. It was also shown that micrometer measurements made on the ribs (after chemical removal of the paint) can provide a useful means for assessing whether the thickness specification has been met.

5) The test results showed that provided the material thickness is within specification, the centre section wing leading edge satisfies the designed strength criterion of being able to sustain 1.5 times the Design Limit Load without failure. Under the high speed conditions, it has been demonstrated that this component is able to sustain loads associated approximately with a 4.3g pull-up and may therefore be considered to have a significant margin of safety. However, it must be cautioned that this margin applies only to the structural strength which may or may not be directly translated to an operational safety margin as the handling characteristics of this aircraft in this regime, and particularly under certain weight configurations, should be taken into consideration. In any case, it should be stressed that the demonstrated safety margin means that this component is demonstrated to be safe up to the operational limits and is NOT to be interpreted as proof of safety for its operation outside the operating flight envelope.

Material thickness for the ribs is also a major issue. In LASC's analysis, it was shown that the reduced thickness reported for A9-754 would have suffered a reduced load carrying capacity of approximately 20% although it was shown that this was still sufficient to survive DUL based on the result of their single rib test [6]. However, if this same factor was applied to the current test results, it appears that A9-754 would have failed at approximately 3.4g (= 0.8 × 4.3g) which, despite some over-sights[2], coincides with the value deduced in Callinan *et al* [2]. In this case, the margin of only 0.4g would not be considered as sufficient.

[2] In the accident investigation reported in Callinan *et al* [2], the effects of the stiffening dimple were neglected. However, this was compensated by the choice of a relatively severe stress concentration factor of 3 and the omission of any plastic analysis.

Further, it should be noted that the test carried out was only on the centre section. The inboard section WLE has relatively taller ribs, although their relative spacings are smaller. The translation of the centre section results to the inboard section, and hence the inference on its structural strength, is not straight forward, and will need the application of detailed numerical modelling. This task is currently being undertaken by NAVAIR as agreed in this collaborative test program.

6) Based on the findings of this investigation, it is recommended that:

i) A complete survey on the rib and clad thicknesses of the RAAF P-3C Orion fleet be undertaken. Whilst performing this task non-destructively and reliably may be difficult to achieve, the present investigation has shown that simple measurements using a standard micrometer on the bare material can serve as a useful first assessment.

ii) Wait for the results of the NAVAIR computational analysis on the inboard WLE.

iii) Maintain the existing placard (2g limit for 300 knots and above) pending on the results of i) and ii).

8. Acknowledgments

The authors wish to thank: T. van Blaricum for his valuable contributions to the design of the test rig and the conduct of test; D. Aker and M. Richmond for working on the initial rig design; R. Bailey, R. Dingley and D. Rowlands for the construction of the test rig; H. Morton for performing the pre-test NDI; B. Ashcroft for the extensive strain gauging of the test article; P. Hayes and L. Sammut for the preparation and operation of the data acquisition and test control systems; P. Mazeika and N. Goldsmith for performing the post-failure metrological analysis and thickness measurements; M. Stimson for his input to the preparation of this manuscript, and many others who contributed to the success of the test.

9. References

1. Molent L., "Visit report to LASC to discuss the analysis of the accident involving Orion A9-754", DSTO-OSR-0004, 1994.

2. Callinan R.J., Kepert J.L., Stimson M.G., "Investigation of the accident to Lockheed P-3C Orion A9-754", ARL-STRUC-TM-554, 1992.

3. Molent L., "Further structural investigation into the collapse of the wing leading edges of Orion A9-754", DSTO-TR-0008, 1994.

4. Luke G., Van Blaricum T.J., "The use of bonded rubber pads for the application of loads for structural testing of the P-3 Orion leading edge", DSTO-TR-0433, 1996.

5. Wong A.K., Ryall T.G. and Richmond M.J., "Structural assessment of the Orion wing leading edge using a state-of-the-art thermal imaging system", Proc. 6th Australian Aeronautical Conference, Melbourne, Australia, Mar. 1995, pp795-800.

6. Williams H.H., "Static test of wing leading edge rib", Temco Aircraft Corp. Report 118.4.1, June 1957.

Appendix

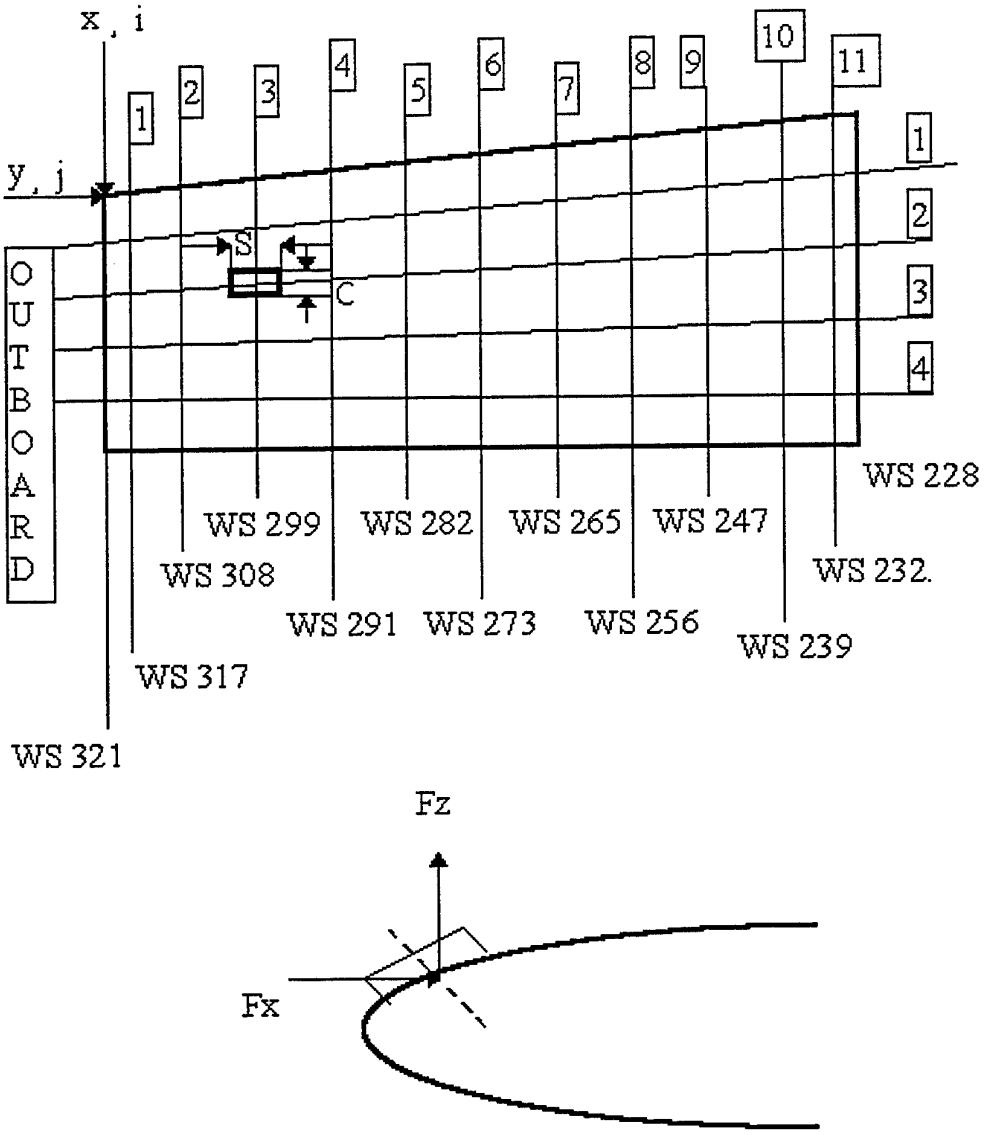

Figure A1. Upper surface load pad locations

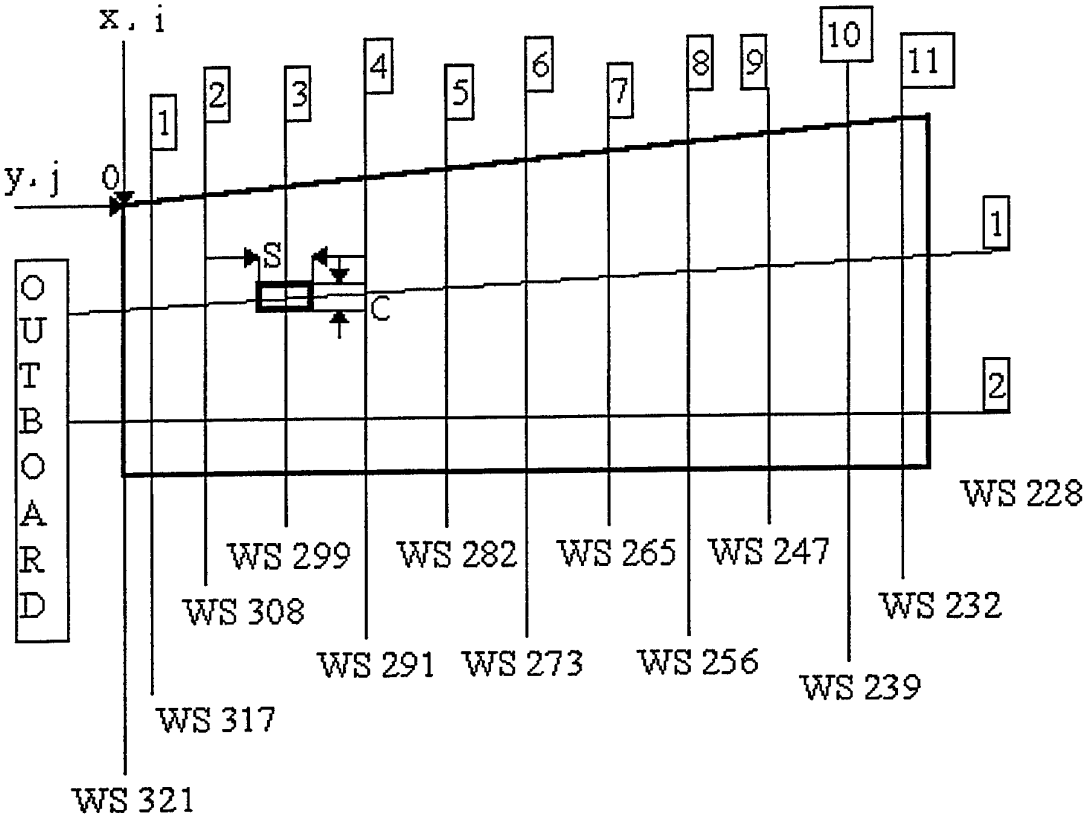

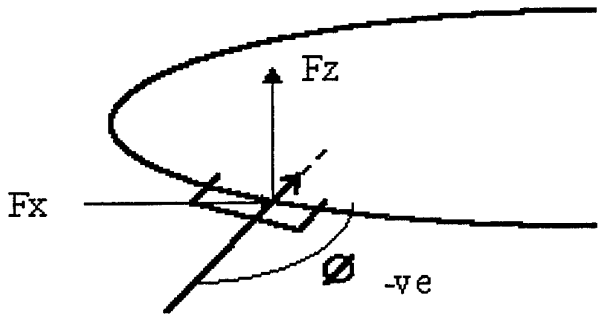

Figure A2. Lower surface load pad locations

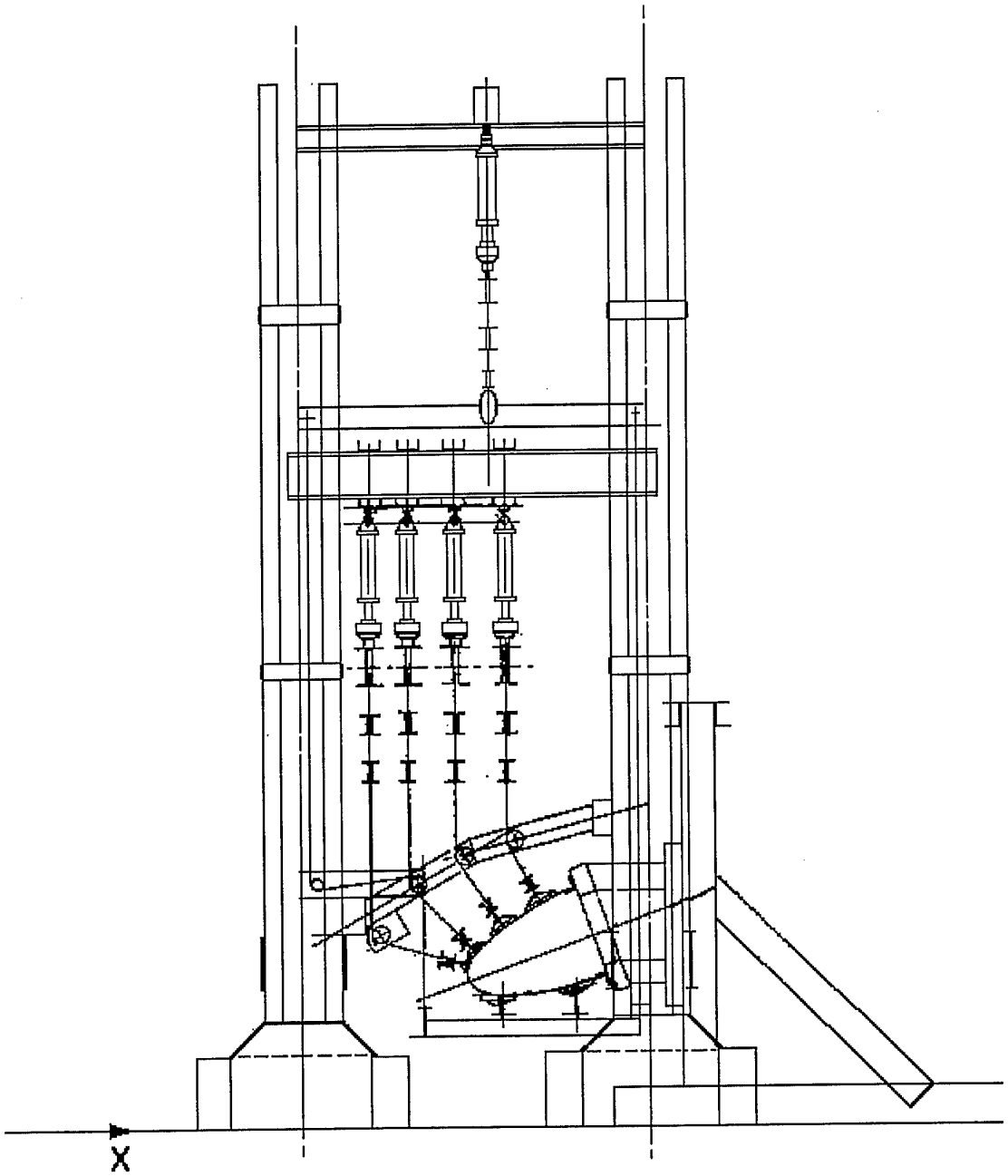

Figure A3. Schematics of test rig (side view)

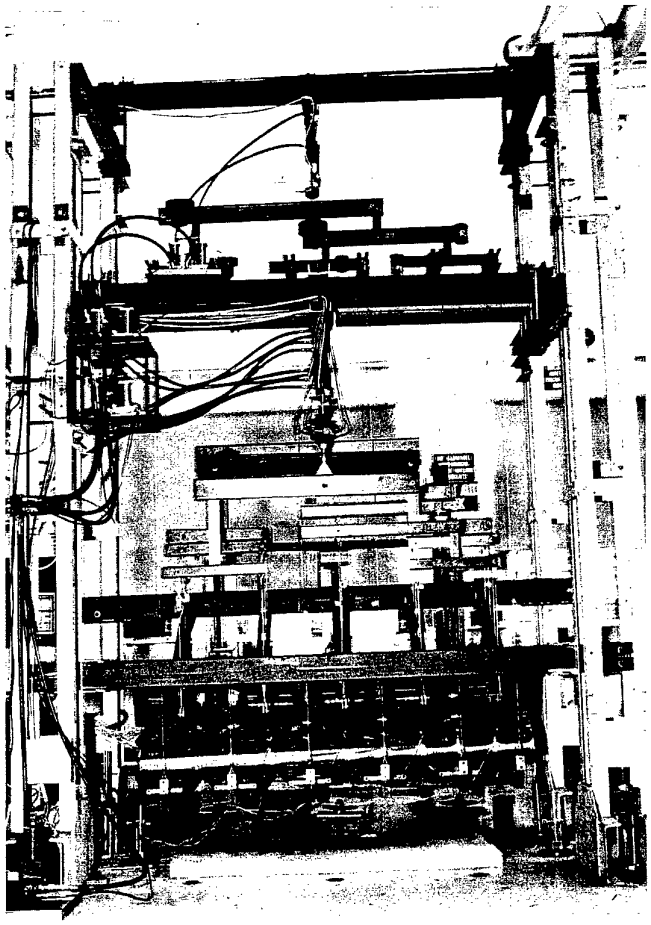

Figure A4. Front view of test article mounted in test rig.

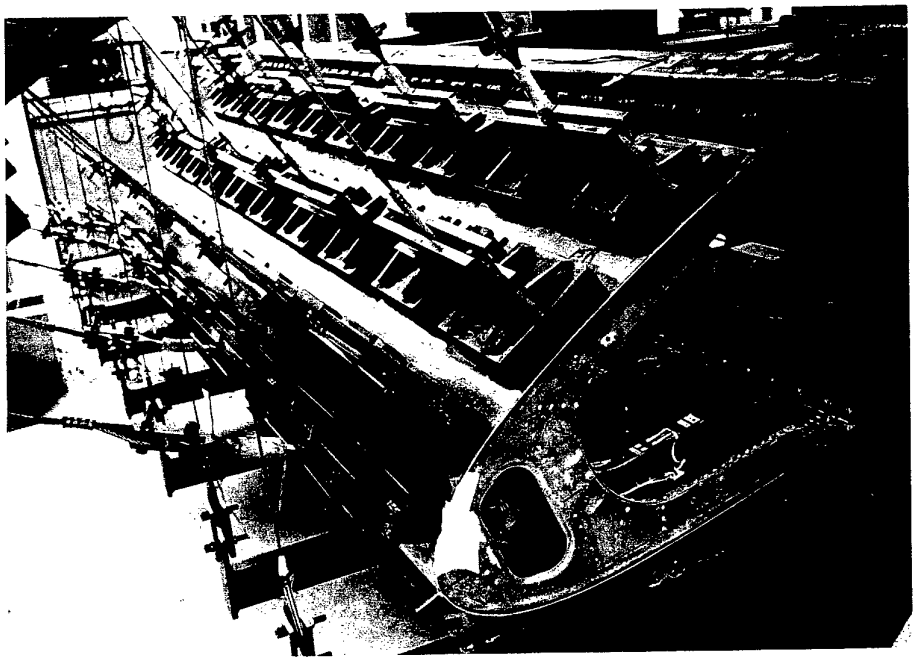

Figure A5. Test article in test rig showing tension pads.

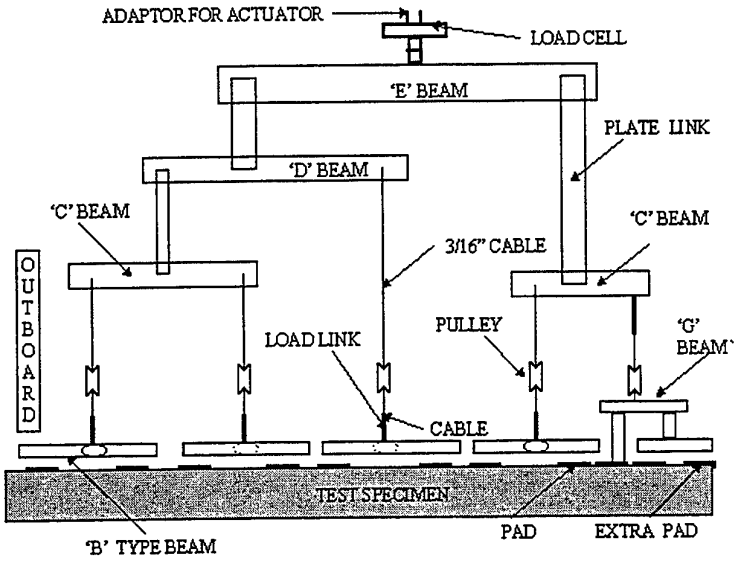

Figure A6. Upper whiffle tree configuration (looking forwards from rear of test article).

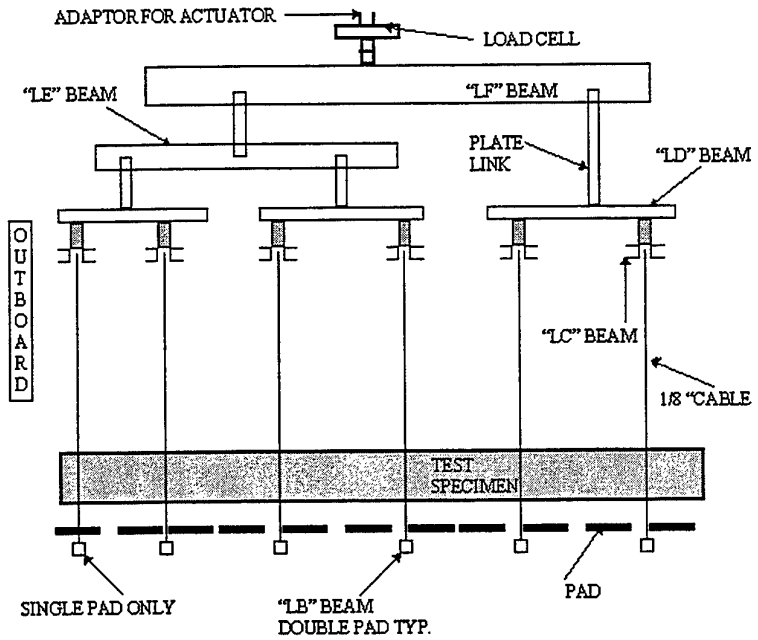

Figure A7. Lower surface whiffle tree configuration (looking forwards from rear of test article).

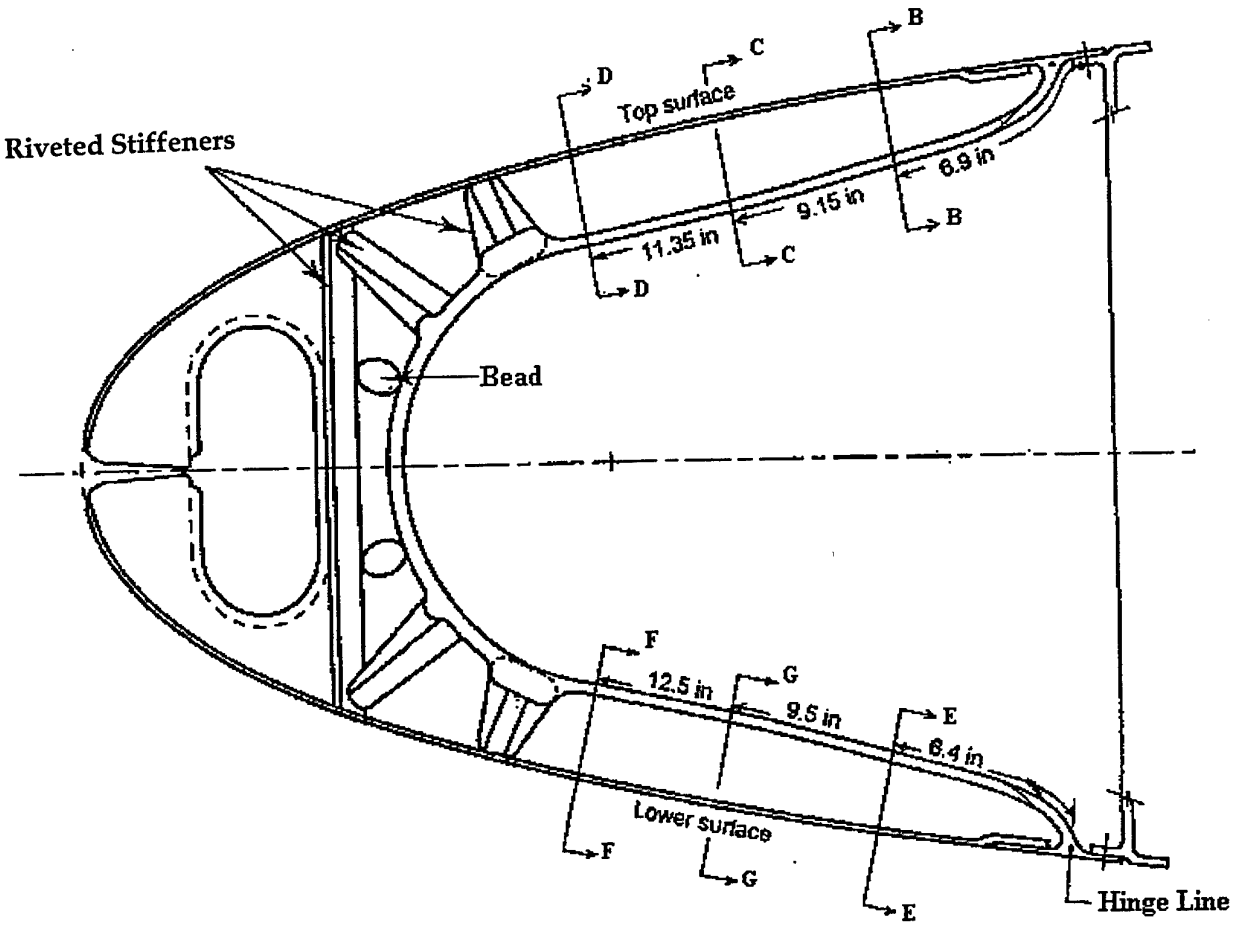

Figure A8. Side view of WS228 showing various sections where strain gauges were attached.

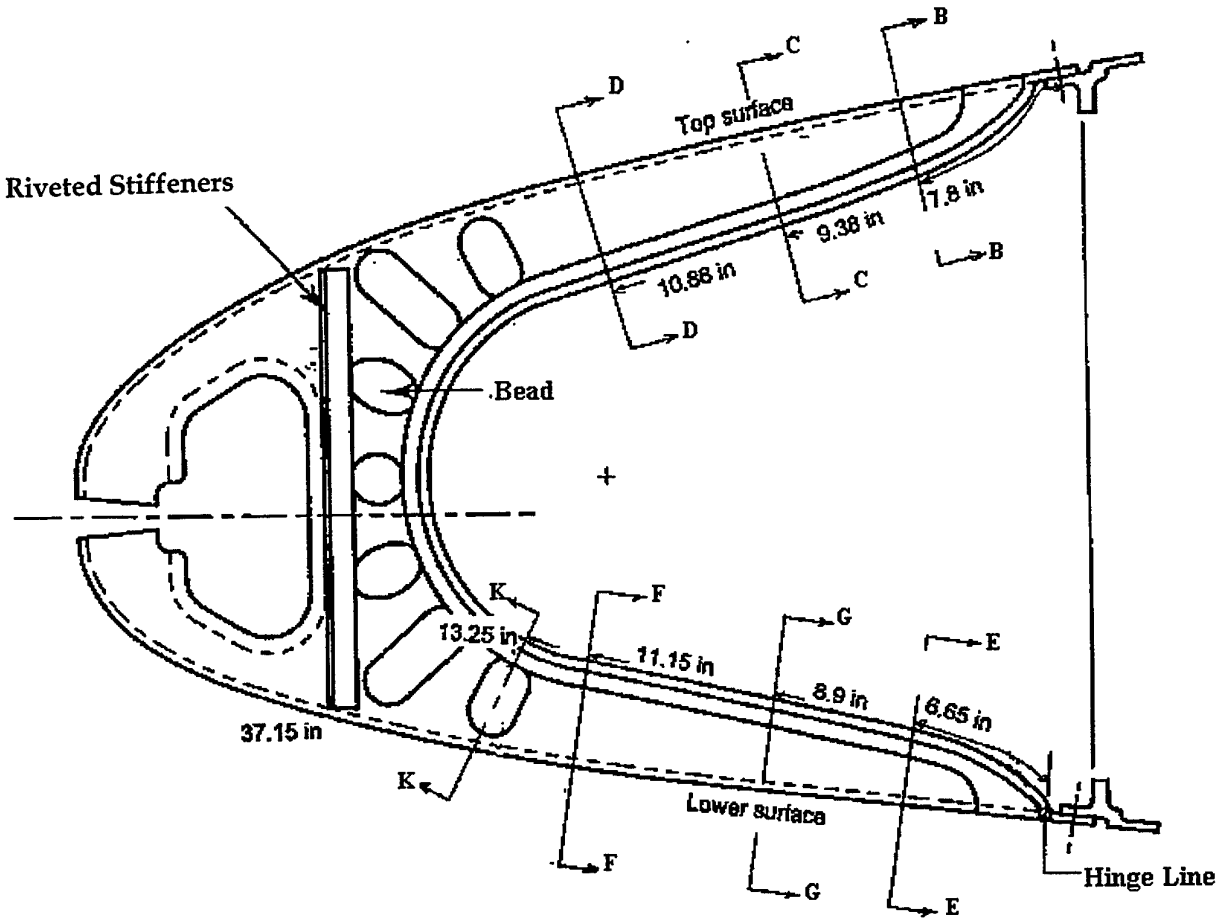

Figure A9. Side view of WS273 showing various sections where strain gauges were attached.

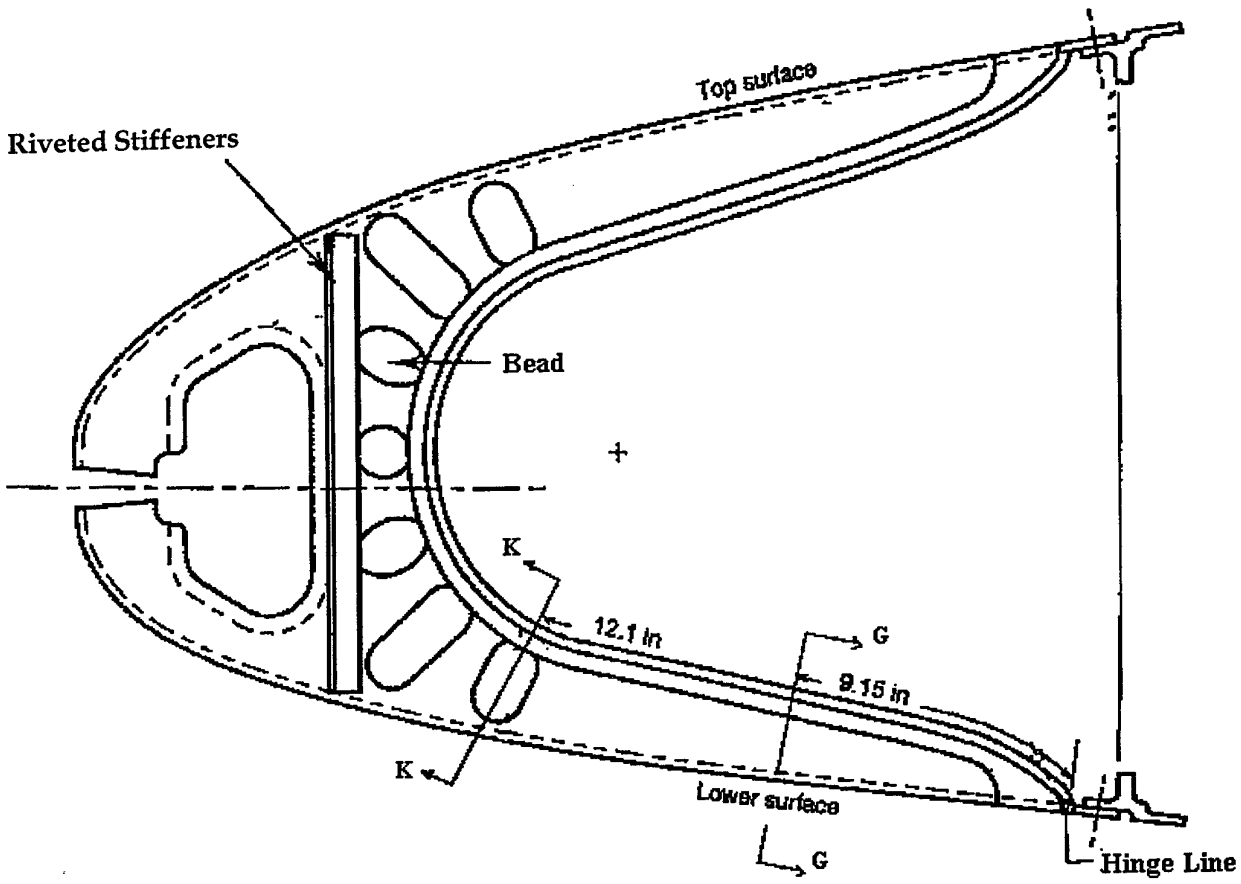

Figure A10. Side view of WS317 showing various sections where strain gauges were attached.

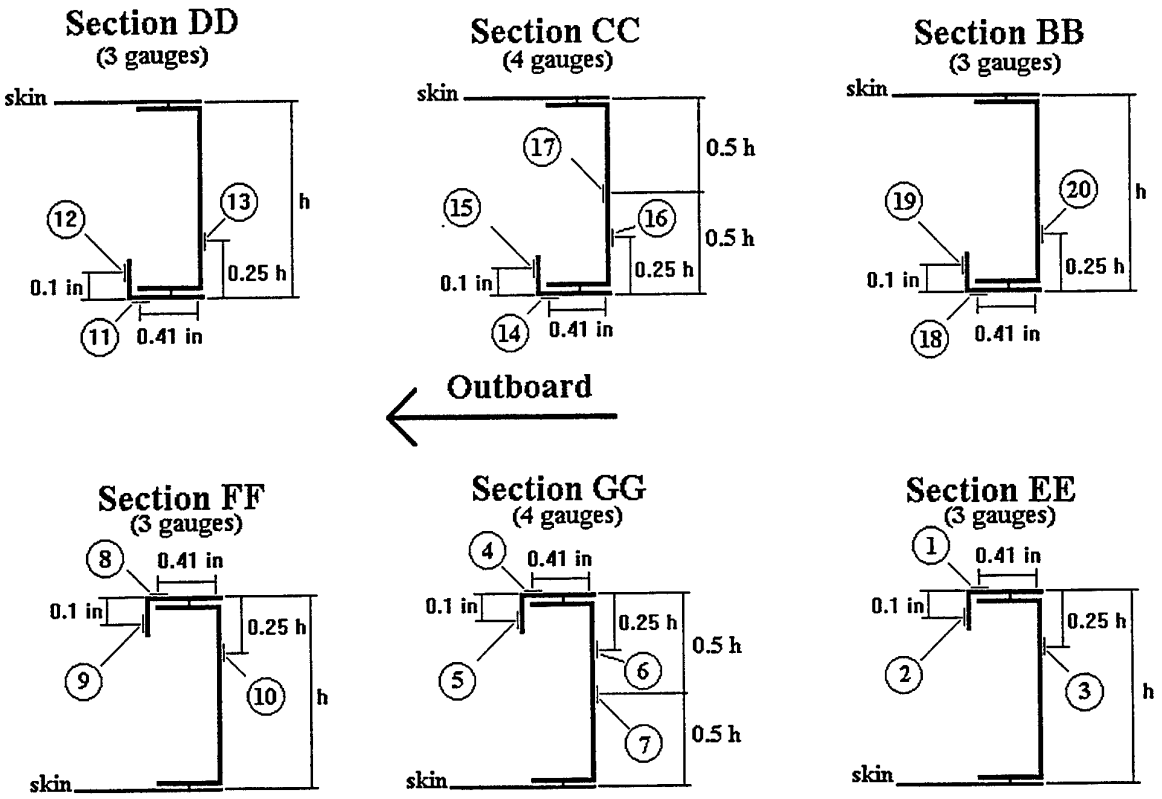

Figure A11. Cross Sectional diagrams for WS228 showing strain gauge locations (the strain gauge numbers are shown in circles).

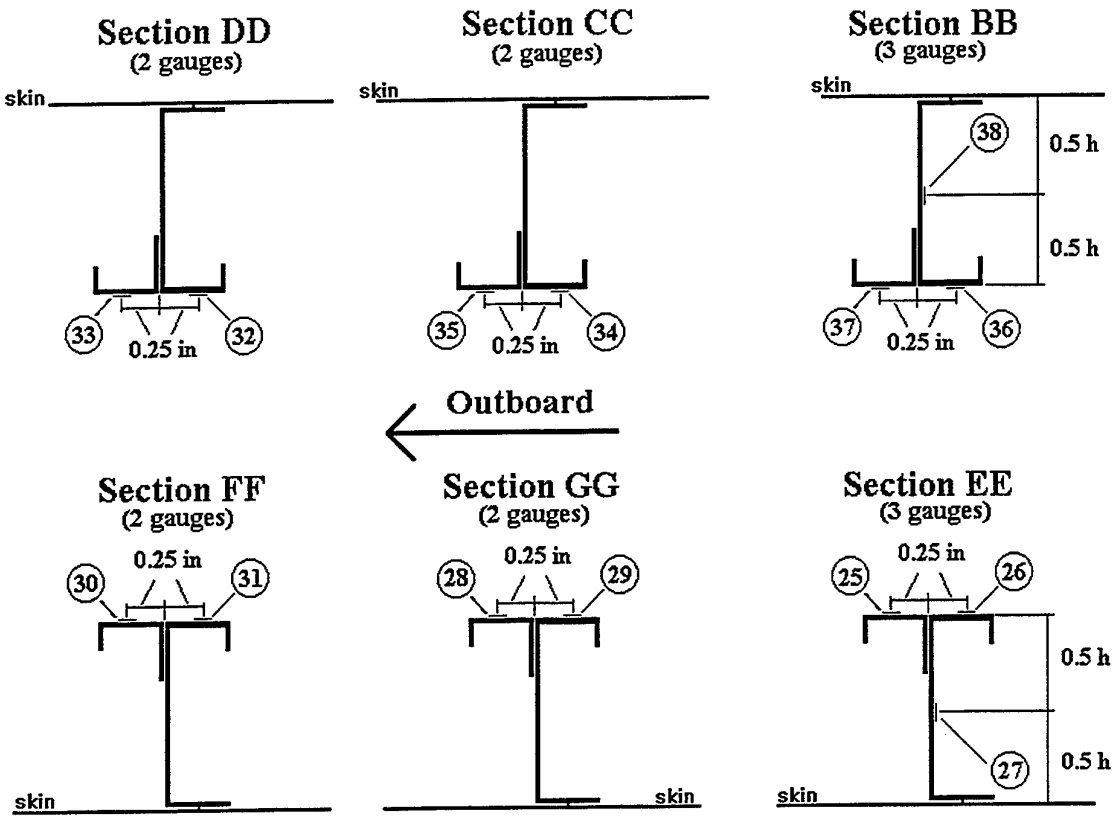

Figure A12. Cross Sectional diagrams for WS273 showing strain gauge locations (the strain gauge numbers are shown in circles).

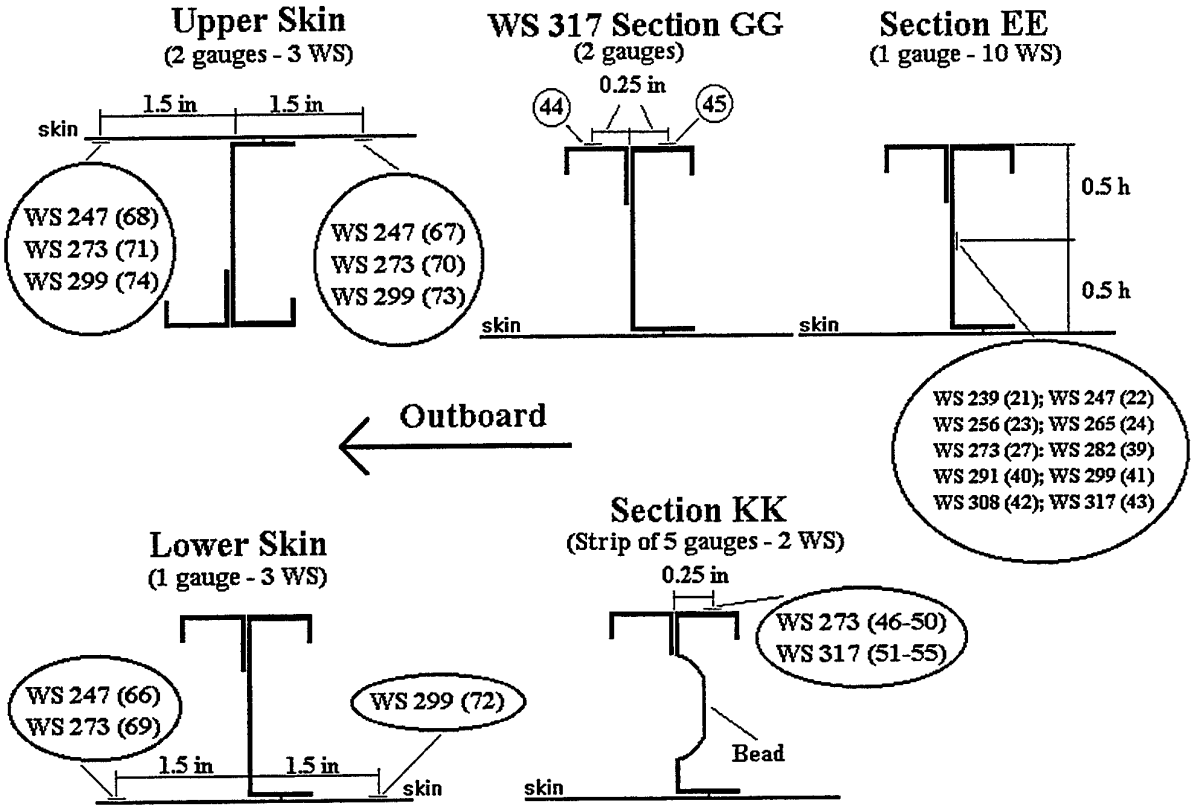

Figure A13. Cross Sectional diagrams showing various other strain gauge locations (the strain gauge numbers are shown in parentheses); the upper surface skin gauges (67, 68, 70, 71, 73 and 74) were located approx. 65mm from the trailing edge, and the lower surface skin gauges (66, 69, 72) were located approx. 75mm from the hinge trailing edge.

Table A1. Test pressure profiles and non-dimensional WLE profile coordinates (x: horizontal distance, y: vertical distance, c: chord length of wing section)

Lower Surface						Upper Surface					
x/c	y/c	PHAA (DLL) kPA	PHAA (DUL) kPA	PLAA (3g) kPA	PLAA (4.5g) kPA	x/c	y/c	PHAA (DLL) kPA	PHAA (DUL) kPA	PLAA (3g) kPA	PLAA (4.5g) kPA
0.142	0.0009	7.1	10.7	-0.1	5.6	0.000	0.0445	-56.2	-84.3	15.5	4.3
0.124	0.0029	7.3	11.0	0.2	6.2	0.001	0.0507	-57.8	-86.7	12.9	0.5
0.113	0.0043	7.4	11.2	0.5	6.7	0.003	0.0563	-64.8	-97.2	1.7	-16.6
0.099	0.0057	7.6	11.3	1.1	7.5	0.008	0.0618	-67.9	-101.9	-13.4	-38.7
0.094	0.0063	7.7	11.5	1.3	7.9	0.014	0.0665	-56.2	-84.3	-21.6	-48.8
0.090	0.0069	7.8	11.6	1.5	8.2	0.020	0.0704	-45.3	-67.9	-29.4	-58.6
0.085	0.0076	7.9	11.8	1.7	8.5	0.025	0.0729	-40.9	-61.3	-29.8	-60.0
0.081	0.0084	8.0	11.9	2.0	8.9	0.030	0.0753	-38.3	-57.4	-30.1	-61.3
0.076	0.0092	8.1	12.1	2.3	9.3	0.035	0.0775	-36.5	-54.7	-30.5	-62.7
0.069	0.0102	8.2	12.3	2.7	10.0	0.041	0.0797	-34.5	-51.7	-30.2	-63.1
0.062	0.0115	8.3	12.5	3.2	10.7	0.046	0.0814	-33.3	-49.9	-30.0	-63.3
0.055	0.0128	8.4	12.6	3.8	11.5	0.051	0.0830	-32.1	-48.2	-29.7	-63.5
0.048	0.0144	8.5	12.7	4.8	12.7	0.056	0.0845	-30.9	-46.3	-29.4	-63.8
0.041	0.0162	8.4	12.6	5.8	13.8	0.061	0.0859	-29.7	-44.6	-28.8	-64.5
0.035	0.0176	8.4	12.6	7.2	15.1	0.066	0.0872	-28.9	-43.3	-28.3	-65.2
0.030	0.0190	8.3	12.5	8.8	16.5	0.071	0.0884	-28.0	-42.0	-27.9	-66.0
0.026	0.0207	8.1	12.2	10.3	17.8	0.076	0.0894	-27.2	-40.8	-27.3	-66.6
0.021	0.0226	7.9	11.9	11.9	19.0	0.082	0.0905	-26.3	-39.5	-26.0	-66.6
0.015	0.0257	7.6	11.3	15.0	20.1	0.088	0.0916	-25.6	-38.4	-24.8	-66.6
0.009	0.0298	7.1	10.6	17.9	21.1	0.093	0.0927	-24.9	-37.4	-23.6	-66.6
0.004	0.0349	6.1	9.1	17.1	13.0	0.099	0.0938	-24.1	-36.2	-22.5	-66.4
0.001	0.0399	5.2	7.8	15.9	6.7	0.105	0.0952	-23.7	-35.6	-22.1	-62.9
0.000	0.0455	4.9	7.3	15.5	4.3	0.110	0.0960	-23.2	-34.8	-21.7	-59.3
						0.116	0.0971	-22.7	-34.0	-21.3	-55.5
						0.122	0.0980	-22.2	-33.3	-21.0	-51.5
						0.129	0.0992	-21.6	-32.4	-20.6	-46.8
						0.149	0.1023	-20.6	-30.8	-21.8	-30.5

Table A2. Spanwise pressure profile correction factors.

Wing Station	228	232	239	247	256	265	273	282	291	299	308	317	320
Scaling Factor	1.014	1.014	1.014	1.000	1.000	1.000	1.000	1.000	1.007	1.021	1.032	1.046	1.052

Table A3. Upper surface pad locations and applied loads.

					PHAA (DLL)			PLAA (4.5g Case)			PLAA (4g Case)		
PAD	x	y	C	S	Fx	Fz	F	Fx	Fz	F	Fx	Fz	F
I,J	mm	mm	mm	mm	N	N	N	N	N	N	N	N	N
1,1	32	102	60	150	-1422	1215	1871	-296	296	419	-105	119	158
1,2	32	330	60	150	-1572	1343	2068	-328	327	463	-116	131	175
1,3	32	533	60	150	-1559	1332	2051	-325	325	459	-115	130	173
1,4	33	762	60	150	-1569	1341	2064	-327	327	462	-116	131	174
1,5	33	991	60	150	-1580	1350	2078	-329	329	465	-116	132	176
1,6	34	1194	60	150	-1595	1363	2099	-332	332	470	-117	133	177
1,7	34	1422	60	150	-1615	1380	2124	-336	336	476	-119	135	180
1,8	34	1651	60	150	-1630	1393	2144	-340	339	480	-120	136	181
1,9	35	1854	60	150	-1664	1422	2189	-347	346	490	-123	139	185
1,10	35	2083	60	200	-1717	1467	2258	-358	357	506	-126	143	191
1,11	35	2243	60	100	-672	574	884	-140	140	198	-50	56	75
2,1	118	102	60	150	-114	255	279	-826	1845	2021	-823	1757	1940
2,2	119	330	60	150	-126	282	309	-913	2039	2234	-909	1942	2144
2,3	121	533	60	150	-125	280	306	-906	2022	2216	-902	1926	2127
2,4	122	762	60	150	-126	281	308	-911	2035	2230	-907	1938	2140
2,5	124	991	60	150	-127	283	310	-918	2049	2245	-914	1952	2155
2,6	125	1194	60	150	-128	286	313	-927	2069	2268	-923	1971	2176
2,7	127	1422	60	150	-129	289	317	-938	2094	2295	-934	1995	2202
2,8	128	1651	60	150	-131	292	320	-947	2114	2316	-943	2014	2223
2,9	130	1854	60	150	-133	298	327	-967	2158	2365	-962	2056	2270
2,10	131	2083	60	200	-138	308	337	-997	2227	2440	-993	2121	2342
2,11	132	2243	60	100	-54	120	132	-390	871	955	-389	830	916
3,1	260	102	150	150	-454	1718	1777	-619	2490	2565	-431	1752	1804
3,2	263	330	150	150	-502	1899	1964	-684	2752	2835	-476	1936	1994
3,3	266	533	150	150	-498	1884	1949	-678	2729	2812	-472	1920	1977
3,4	269	762	150	150	-501	1895	1961	-682	2746	2830	-475	1932	1990
3,5	273	991	150	150	-505	1909	1975	-687	2766	2850	-479	1946	2004
3,6	276	1194	150	150	-510	1928	1994	-694	2793	2878	-483	1965	2023
3,7	279	1422	150	150	-516	1951	2018	-702	2826	2912	-489	1988	2048
3,8	283	1651	150	150	-521	1969	2037	-709	2853	2940	-494	2007	2067
3,9	286	1854	150	150	-531	2010	2080	-724	2913	3001	-504	2049	2110
3,10	289	2083	150	200	-548	2074	2146	-747	3005	3097	-520	2114	2177
3,11	292	2243	120	90	-215	812	840	-292	1176	1212	-204	827	852
4,1	461	102	150	150	-135	832	843	-519	2899	2945	-413	2315	2351
4,2	467	330	150	150	-149	919	931	-573	3204	3255	-457	2558	2599
4,3	473	533	150	150	-148	912	924	-569	3178	3229	-453	2537	2578
4,4	479	762	150	150	-149	918	930	-572	3198	3249	-456	2553	2593
4,5	485	991	150	150	-150	924	936	-576	3220	3272	-459	2571	2612
4,6	491	1194	150	150	-151	933	945	-582	3252	3304	-463	2596	2637
4,7	497	1422	150	150	-153	944	957	-589	3291	3343	-469	2628	2669
4,8	502	1651	150	150	-155	953	966	-594	3322	3375	-473	2653	2694
4,9	508	1854	150	150	-158	973	986	-607	3392	3446	-483	2708	2751
4,10	514	2083	150	200	-163	1004	1017	-626	3500	3555	-499	2794	2838
4,11	518	2243	120	90	-64	393	398	-245	1369	1391	-195	1093	1111

Table A4. Lower surface pad locations and applied loads (Load shown are all compressive, and $\Delta\phi$ represents the error in the angle of the load vector between the ideal case and what was being applied.)

PHAA PLAA						PHAA (DLL)						PLAA (4.5g Case)						PLAA (4g Case)					
						IDEAL			ACTUAL			IDEAL			ACTUAL			IDEAL			ACTUAL		
PAD	x	x	y	C	S	Fx	Fy	F	Fx	Fy	$\Delta\phi$	Fx	Fy	F	Fx	Fy	$\Delta\phi$	Fx	Fy	F	Fx	Fy	$\Delta\phi$
I,J	mm	mm	mm	mm	mm	N	N	N	N	N	deg	N	N	N	N	N	deg	N	N	N	N	N	deg
5,1	57	57	102	150	150	172	238	294	152	251	4.8	368	536	650	337	556	3.2	387	543	667	345	570	3.2
5,2	58	58	330	150	150	164	226	280	145	239	4.8	350	511	619	321	530	3.2	369	517	635	329	543	3.2
5,3	59	59	533	150	150	163	225	278	144	238	4.8	348	507	615	319	526	3.2	366	514	631	327	540	3.2
5,4	59	59	762	150	150	163	225	278	144	238	4.8	348	508	615	319	526	3.2	367	514	631	327	540	3.2
5,5	60	60	991	150	150	165	228	281	146	240	4.8	352	513	622	322	532	3.2	371	520	638	331	546	3.2
5,6	61	61	1194	150	150	167	230	284	147	243	4.8	356	519	630	326	539	3.2	375	526	646	335	553	3.2
5,7	61	61	1422	150	150	168	231	286	148	245	4.8	358	522	633	328	541	3.2	377	529	649	336	555	3.2
5,8	62	62	1651	150	150	170	234	289	150	247	4.8	362	528	640	332	548	3.2	381	535	657	340	562	3.2
5,9	63	63	1854	150	150	174	239	295	153	253	4.8	370	539	654	339	560	3.2	390	546	671	348	574	3.2
5,10	64	64	2083	150	150	187	258	319	165	273	4.8	399	582	705	365	603	3.2	420	589	724	375	619	3.2
5,11	65	65	2266	150	150	101	139	172	89	147	4.8	216	314	381	197	326	3.2	227	318	391	203	334	3.2
6,1	336	304	102	150	150	130	807	817	125	808	0.4	166	945	960	160	946	0.4	116	674	684	114	675	0.4
6,2	340	308	330	150	150	124	769	779	119	770	0.4	158	901	915	153	902	0.4	111	642	652	109	643	0.4
6,3	345	312	533	150	150	123	764	774	118	765	0.4	157	895	908	152	896	0.4	110	638	648	108	639	0.4
6,4	349	316	762	150	150	123	764	774	118	765	0.4	157	895	909	152	896	0.4	110	639	648	108	639	0.4
6,5	353	320	991	150	150	125	773	783	120	773	0.4	159	905	919	153	906	0.4	111	645	655	109	646	0.4
6,6	358	324	1194	150	150	126	782	792	121	783	0.4	161	916	930	155	917	0.4	113	653	663	111	654	0.4
6,7	362	328	1422	150	150	127	786	796	122	787	0.4	162	921	935	156	922	0.4	113	657	666	111	657	0.4
6,8	366	332	1651	150	150	128	795	805	123	796	0.4	164	931	946	158	932	0.4	115	664	674	112	665	0.4
6,9	370	335	1854	150	150	131	812	823	126	813	0.4	167	951	966	161	952	0.4	117	679	689	115	679	0.4
6,10	375	339	2083	150	150	141	876	887	136	877	0.4	180	1026	1042	174	1027	0.4	126	732	743	124	732	0.4
6,11	380	344	2266	150	150	76	473	479	73	474	0.4	97	554	563	94	555	0.4	68	395	401	67	395	0.4

Table A5. Summary of strain gauge locations (continued next page).

Gauge #	Wing station	Section	Leg	Location Description	Ref. Fig.
1	228	EE	lower	horiz. part of flange near corner	A11
2	228	EE	lower	vertical part of flange near lip	A11
3	228	EE	lower	web, quarter depth from flange	A11
4	228	GG	lower	horiz. part of flange near corner	A11
5	228	GG	lower	vertical part of flange near lip	A11
6	228	GG	lower	web, quarter depth from flange	A11
7	228	GG	lower	web, half depth	A11
8	228	FF	lower	horiz. part of flange near corner	A11
9	228	FF	lower	vertical part of flange near lip	A11
10	228	FF	lower	web, quarter depth from flange	A11
11	228	DD	upper	horiz. part of flange near corner	A11
12	228	DD	upper	vertical part of flange near lip	A11
13	228	DD	upper	web, quarter depth from flange	A11
14	228	CC	upper	horiz. part of flange near corner	A11
15	228	CC	upper	vertical part of flange near lip	A11
16	228	CC	upper	web, quarter depth from flange	A11
17	228	CC	upper	web, half depth	A11
18	228	BB	upper	horiz. part of flange near corner	A11
19	228	BB	upper	vertical part of flange near lip	A11
20	228	BB	upper	web, quarter depth from flange	A11
21	239	EE	lower	web, half depth	A13
22	247	EE	lower	web, half depth	A13
23	256	EE	lower	web, half depth	A13
24	265	EE	lower	web, half depth	A13
25	273	EE	lower	horiz. part of outboard flange	A12
26	273	EE	lower	horiz. part of inboard flange	A12
27	273	EE	lower	web, half depth	A12
28	273	GG	lower	horiz. part of outboard flange	A12
29	273	GG	lower	horiz. part of inboard flange	A12
30	273	FF	lower	horiz. part of outboard flange	A12
31	273	FF	lower	horiz. part of inboard flange	A12
32	273	DD	upper	horiz. part of inboard flange	A12
33	273	DD	upper	horiz. part of outboard flange	A12
34	273	CC	upper	horiz. part of inboard flange	A12
35	273	CC	upper	horiz. part of outboard flange	A12
36	273	BB	upper	horiz. part of inboard flange	A12
37	273	BB	upper	horiz. part of outboard flange	A12

Table A5 (cont). Summary of strain gauge locations

Gauge #	Wing station	Section	Leg	Location Description	Ref. Fig.
38	273	BB	upper	web, half depth	A12
39	282	EE	lower	web, half depth	A13
40	291	EE	lower	web, half depth	A13
41	299	EE	lower	web, half depth	A13
42	308	EE	lower	web, half depth	A13
43	317	EE	lower	web, half depth	A13
44	317	GG	lower	horiz. part of outboard flange	A13
45	317	GG	lower	horiz. part of inboard flange	A13
46	273	KK	lower	horiz. part of inboard flange	A13
47	273	KK	lower	horiz. part of inboard flange	A13
48	273	KK	lower	horiz. part of inboard flange	A13
49	273	KK	lower	horiz. part of inboard flange	A13
50	273	KK	lower	horiz. part of inboard flange	A13
51	317	KK	lower	horiz. part of inboard flange	A13
52	317	KK	lower	horiz. part of inboard flange	A13
53	317	KK	lower	horiz. part of inboard flange	A13
54	317	KK	lower	horiz. part of inboard flange	A13
55	317	KK	lower	horiz. part of inboard flange	A13
56				load link 1	
57				load link 2	
58				load link 3	
59				load link 4	
60				load link 5	
61				load link 6	
62				load link 7	
63				load link 8	
64				load link 9	
65				load link 10	
66	247	skin	lower	outboard of rib	A13
67	247	skin	upper	inboard of rib	A13
68	247	skin	upper	outboard of rib	A13
69	273	skin	lower	outboard of rib	A13
70	273	skin	upper	inboard of rib	A13
71	273	skin	upper	outboard of rib	A13
72	299	skin	lower	inboard of rib	A13
73	299	skin	upper	inboard of rib	A13
74	299	skin	upper	outboard of rib	A13

Table A6. Recorded strain data for the PHAA Test (Gauges G1 to G24), all strain values in microstrains (continued next page).

% DLL	G1	G2	G3	G4	G5	G6	G7	G8	G9	G10	G11	G12
0	0	0	0	0	0	0	0	0	0	0	0	0
10	111	29	97	114	10	131	87	82	-33	186	-161	-104
20	228	51	202	239	17	275	180	172	-71	388	-348	-223
30	352	77	308	372	34	423	274	269	-103	595	-542	-342
40	475	107	411	506	59	566	364	373	-124	793	-722	-447
50	595	139	510	639	95	705	451	480	-133	984	-891	-536
60	720	186	609	777	150	849	540	594	-128	1180	-1057	-616
70	837	231	699	907	206	981	621	704	-116	1361	-1210	-683
80	956	280	791	1043	272	1114	702	822	-96	1543	-1359	-739
90	1075	331	884	1183	344	1247	784	945	-71	1727	-1506	-784
100	1196	385	979	1326	424	1381	865	1076	-36	1910	-1643	-814
20	266	50	240	270	10	332	219	195	-98	457	-389	-237
100	1196	386	978	1324	423	1379	864	1074	-36	1906	-1634	-809
105	1256	411	1026	1398	466	1447	905	1142	-17	2002	-1705	-816
110	1323	440	1080	1479	514	1519	949	1219	9	2108	-1772	-815
115	1393	474	1136	1565	569	1595	996	1301	39	2216	-1832	-806
120	1470	511	1199	1658	632	1680	1049	1392	74	2338	-1890	-785
125	1546	545	1260	1754	696	1762	1099	1488	110	2462	-1954	-764
130	1632	588	1330	1861	772	1854	1155	1596	156	2599	-2003	-718
135	1730	636	1410	1984	863	1959	1219	1725	215	2759	-2044	-645
140	1829	683	1492	2115	962	2068	1284	1868	281	2930	-2068	-538
145	1953	745	1596	2277	1092	2201	1365	2052	377	3140	-1995	-240
150	2299	918	1900	2760	1523	2582	1587	2664	743	3765	-1157	2422
100	1722	615	1431	1999	953	1977	1228	1911	303	2940	-1107	1767
50	956	246	823	1057	335	1139	720	999	-72	1765	-723	1019
20	474	68	437	512	83	583	375	519	-137	981	-289	806
0	171	7	166	180	30	209	133	254	-68	445	57	773

% DLL	G13	G14	G15	G16	G17	G18	G19	G20	G21	G22	G23	G24
0	0	0	0	0	0	0	0	0	0	0	0	0
10	-148	-143	-58	-138	-78	-108	-43	-125	65	54	75	80
20	-326	-311	-125	-301	-171	-237	-96	-272	144	93	148	142
30	-516	-489	-192	-474	-271	-374	-151	-427	240	131	197	196
40	-702	-658	-248	-640	-366	-505	-200	-575	339	177	245	249
50	-886	-818	-294	-802	-457	-631	-242	-716	434	236	302	306
60	-1078	-978	-331	-969	-550	-757	-280	-860	524	305	369	370
70	-1265	-1128	-360	-1129	-639	-878	-314	-997	604	370	437	433
80	-1459	-1276	-380	-1294	-731	-999	-343	-1136	683	437	505	499
90	-1664	-1425	-391	-1463	-826	-1123	-368	-1278	760	504	575	568
100	-1873	-1571	-391	-1632	-919	-1245	-388	-1418	837	573	645	638
20	-393	-362	-140	-351	-200	-274	-116	-309	181	102	166	155
100	-1865	-1563	-388	-1625	-915	-1239	-385	-1411	838	575	648	638
105	-1985	-1640	-383	-1720	-968	-1305	-395	-1489	876	610	682	674
110	-2109	-1716	-372	-1816	-1021	-1373	-400	-1566	918	648	720	714
115	-2232	-1787	-354	-1908	-1070	-1437	-402	-1640	962	689	760	757
120	-2364	-1861	-328	-2007	-1125	-1505	-399	-1718	1008	736	803	804
125	-2509	-1942	-301	-2114	-1187	-1583	-399	-1803	1052	778	844	849
130	-2653	-2016	-259	-2217	-1251	-1658	-390	-1883	1100	825	889	899
135	-2816	-2094	-198	-2328	-1328	-1741	-374	-1969	1153	876	938	948
140	-2986	-2166	-118	-2436	-1418	-1828	-353	-2052	1204	924	985	996
145	-3200	-2190	81	-2541	-1541	-1909	-278	-2118	1264	982	1041	1049
150	-3881	-1810	1535	-2620	-2020	-2000	303	-2008	1392	1113	1168	1157
100	-2846	-1382	928	-2009	-1380	-1455	52	-1453	1059	805	850	828
50	-1599	-779	410	-1066	-705	-794	-99	-732	578	381	415	393
20	-868	-304	305	-470	-328	-364	-51	-266	228	175	204	173
0	-400	48	319	-81	-87	-68	34	47	38	60	34	12

Table A6 (cont). Recorded strain data for the PHAA Test (Gauges G25 to G48), all strain values in microstrains (continued next page).

% DLL	G25	G26	G27	G28	G29	G30	G31	G32	G33	G34	G35	G36
0	0	0	0	0	0	0	0	0	0	0	0	0
10	159	152	78	186	174	244	183	-200	-221	-188	-206	-185
20	312	284	141	373	337	471	374	-401	-450	-377	-419	-373
30	439	388	184	516	464	647	523	-583	-657	-549	-613	-544
40	581	505	233	672	608	840	692	-759	-865	-719	-806	-713
50	744	649	303	855	779	1065	890	-943	-1090	-897	-1012	-890
60	914	803	379	1047	962	1298	1099	-1128	-1326	-1077	-1227	-1071
70	1073	951	449	1228	1137	1518	1294	-1299	-1555	-1249	-1433	-1244
80	1234	1102	522	1412	1315	1740	1495	-1465	-1790	-1418	-1642	-1415
90	1394	1254	594	1596	1495	1962	1698	-1619	-2021	-1579	-1844	-1578
100	1558	1411	667	1783	1678	2190	1906	-1769	-2264	-1742	-2051	-1744
20	355	318	148	417	380	531	429	-465	-530	-433	-496	-435
100	1558	1412	670	1783	1679	2190	1909	-1766	-2259	-1738	-2048	-1741
105	1647	1497	708	1884	1778	2316	2023	-1830	-2389	-1815	-2156	-1822
110	1742	1589	749	1993	1885	2451	2142	-1881	-2514	-1886	-2254	-1896
115	1840	1684	791	2104	1992	2588	2263	-1913	-2619	-1943	-2330	-1955
120	1949	1788	839	2226	2112	2739	2399	-1928	-2708	-1989	-2386	-2002
125	2051	1885	880	2344	2225	2887	2522	-1923	-2777	-2019	-2421	-2031
130	2164	1993	928	2473	2350	3043	2659	-1888	-2832	-2024	-2443	-2036
135	2293	2118	981	2621	2494	3222	2819	-1819	-2895	-2001	-2471	-2018
140	2421	2245	1032	2770	2642	3397	2979	-1715	-2977	-1947	-2522	-1973
145	2560	2390	1093	2931	2806	3574	3160	-1515	-3085	-1788	-2638	-1838
150	2899	2785	1218	3319	3266	3899	3698	-567	-3141	-741	-3583	-802
100	2167	2031	896	2463	2396	2887	2712	-400	-2526	-520	-2918	-588
50	1143	1003	443	1290	1195	1498	1336	-142	-1502	-180	-1774	-241
20	538	449	200	613	536	685	567	127	-821	118	-1034	73
0	156	117	49	182	142	124	106	383	-297	383	-487	351

% DLL	G37	G38	G39	G40	G41	G42	G43	G44	G45	G46	G47	G48
0	0	0	0	0	0	0	0	0	0	0	0	0
10	-191	-91	72	61	40	57	55	140	142	313	260	231
20	-386	-182	124	121	104	116	113	285	295	610	505	449
30	-566	-264	168	197	178	184	169	431	452	845	701	622
40	-745	-344	227	278	247	254	223	579	609	1100	915	814
50	-935	-426	297	357	310	323	278	729	767	1404	1168	1038
60	-1133	-511	371	433	372	391	334	877	923	1724	1434	1277
70	-1324	-592	441	503	427	453	384	1018	1071	2030	1688	1505
80	-1517	-675	512	572	483	513	434	1158	1220	2343	1950	1741
90	-1706	-753	583	642	538	575	486	1299	1373	2663	2216	1981
100	-1896	-832	657	713	594	635	534	1434	1519	2996	2490	2231
20	-451	-196	143	146	131	149	136	351	369	740	580	520
100	-1893	-829	658	712	592	633	533	1432	1517	2992	2482	2227
105	-1991	-871	696	748	621	664	557	1504	1595	3178	2637	2367
110	-2081	-909	738	787	651	698	584	1579	1678	3380	2803	2518
115	-2150	-939	782	828	682	732	611	1656	1761	3582	2969	2669
120	-2204	-965	830	871	715	767	642	1740	1852	3842	3182	2863
125	-2240	-988	875	912	747	801	669	1820	1940	4168	3446	3099
130	-2263	-1001	925	958	780	837	698	1901	2029	4549	3749	3370
135	-2290	-1011	982	1009	818	878	732	1995	2131	5058	4149	3725
140	-2334	-1020	1037	1057	854	918	762	2087	2232	5708	4650	4170
145	-2415	-1010	1100	1114	898	967	801	2196	2352	6533	5270	4742
150	-2929	-783	1238	1241	1004	1104	912	2566	2767	10064	7804	7334
100	-2312	-629	898	908	734	834	683	1923	2081	8915	6697	6273
50	-1359	-364	433	464	371	463	381	1078	1161	6675	4752	4418
20	-743	-160	177	180	136	222	189	556	592	5176	3507	3272
0	-283	9	35	29	9	68	44	168	178	3984	2551	2417

Table A6 (cont). Recorded strain data for the PHAA Test (Gauges G49 to G72), all strain values in microstrains (continued next page).

% DLL	G49	G50	G51	G52	G53	G54	G55	G56	G57	G58	G59	G60
0	0	0	0	0	0	0	0	0	0	0	0	0
10	214	218	193	187	178	170	163	48	18	-4	14	14
20	414	419	396	384	362	346	332	86	36	9	30	27
30	573	579	600	581	547	522	501	119	54	40	47	35
40	751	760	807	779	732	696	666	148	73	73	64	42
50	957	968	1006	971	912	867	828	176	95	109	86	49
60	1178	1191	1204	1162	1090	1035	986	200	118	140	108	52
70	1389	1403	1390	1342	1259	1194	1138	224	146	169	133	53
80	1609	1624	1580	1524	1429	1355	1290	246	172	199	158	53
90	1832	1846	1766	1704	1599	1518	1445	269	201	229	185	56
100	2066	2081	1944	1878	1765	1677	1596	292	230	262	213	58
20	478	485	504	486	457	434	417	71	35	8	23	46
100	2063	2079	1941	1875	1762	1674	1593	265	238	248	225	50
105	2196	2213	2039	1971	1853	1762	1676	277	253	269	240	52
110	2337	2355	2139	2070	1949	1855	1763	288	268	289	253	51
115	2481	2501	2240	2169	2043	1946	1850	300	284	310	269	52
120	2662	2678	2352	2277	2145	2044	1943	310	300	332	286	54
125	2882	2893	2466	2388	2251	2149	2043	322	321	357	304	53
130	3138	3145	2579	2498	2357	2251	2138	332	341	382	320	53
135	3478	3480	2715	2631	2484	2374	2253	343	365	410	339	50
140	3910	3907	2861	2776	2623	2510	2381	353	394	442	362	46
145	4493	4492	3029	2940	2781	2666	2527	363	425	476	389	40
150	7607	7427	3751	3653	3477	3359	3179	372	458	541	419	22
100	6662	6458	2945	2859	2717	2626	2476	263	277	356	251	63
50	4854	4646	1796	1734	1644	1593	1489	141	88	141	75	63
20	3743	3535	1049	1006	957	936	865	62	30	26	18	37
0	2911	2706	468	445	430	435	390	-2	2	-1	3	1

% DLL	G61	G62	G63	G64	G65	G66	G67	G68	G69	G70	G71	G72
0	0	0	0	0	0	0	0	0	0	0	0	0
10	35	20	37	18	24	-1	31	39	-29	9	9	-2
20	66	38	56	32	44	21	58	65	-3	21	18	-19
30	91	54	73	48	65	87	80	83	-3	31	23	-49
40	111	69	87	64	86	133	98	97	12	40	26	-82
50	135	84	103	82	106	160	118	112	41	50	28	-107
60	161	98	120	102	129	174	134	123	64	56	27	-112
70	190	112	134	123	151	183	148	133	77	60	22	-119
80	218	125	150	146	172	191	159	141	84	62	16	-127
90	248	139	166	168	193	197	168	152	90	66	11	-136
100	275	152	180	188	212	202	179	162	95	69	4	-152
20	70	59	59	30	44	36	67	69	-11	38	39	-54
100	274	160	175	197	222	197	176	157	92	69	6	-154
105	288	165	184	207	231	201	183	164	95	70	1	-166
110	301	171	194	219	243	199	184	166	92	70	-2	-175
115	315	175	201	228	252	201	191	172	91	70	-8	-191
120	331	182	210	241	264	200	194	176	89	68	-15	-208
125	344	187	217	252	275	199	197	178	82	64	-23	-227
130	358	193	226	263	286	195	198	181	73	58	-33	-252
135	369	197	235	276	298	189	197	179	60	49	-47	-283
140	366	202	243	287	309	183	198	179	45	39	-62	-322
145	378	207	249	298	320	173	196	174	27	24	-80	-370
150	390	212	256	310	333	122	183	114	-72	-15	-108	-523
100	269	161	186	224	261	107	182	108	-29	43	-21	-372
50	152	97	95	101	142	72	141	73	-7	62	45	-215
20	72	58	49	34	51	-8	77	34	-33	50	49	-126
0	-1	-3	9	6	7	-16	21	-24	-17	33	21	-97

Table A6 (cont). Recorded strain data for the PHAA Test (Gauges G49 to G72), all strain values in microstrains (continued next page).

% DLL	G73	G74	LOADC1 (kN)	LOADC2 (kN)	LOADC3 (kN)	LOADC4 (kN)	LOADC5 (kN)	LVDT1 (mm)	LVDT2 (mm)	LVDT3 (mm)	LVDT4 (mm)
0	0	0	0.0	0.0	0.0	0.0	0.0	0.00	0.00	0.00	0.00
10	-13	-4	2.0	0.3	2.0	1.0	1.1	-0.60	-0.63	-0.11	0.01
20	-24	-5	4.1	0.6	3.9	1.9	2.2	-1.29	-1.36	-0.13	0.07
30	-35	-7	6.1	0.9	5.8	2.8	3.3	-2.02	-2.14	-0.16	0.11
40	-47	-10	8.1	1.2	7.8	3.7	4.4	-2.78	-2.91	-0.19	0.14
50	-66	-22	10.2	1.5	9.7	4.6	5.5	-3.59	-3.68	-0.22	0.17
60	-86	-36	12.2	1.8	11.7	5.6	6.6	-4.43	-4.48	-0.24	0.30
70	-107	-51	14.3	2.1	13.7	6.5	7.7	-5.22	-5.24	-0.26	0.30
80	-127	-66	16.4	2.4	15.6	7.4	8.7	-6.01	-6.01	-0.29	0.32
90	-146	-82	18.4	2.8	17.6	8.4	9.8	-6.82	-6.80	-0.33	0.39
100	-168	-103	20.4	3.1	19.6	9.3	10.9	-7.64	-7.61	-0.37	0.41
20	-17	7	4.1	0.6	3.8	1.9	2.2	-1.87	-1.89	-0.03	0.24
100	-166	-104	20.5	3.1	19.5	9.3	10.9	-7.67	-7.63	-0.35	0.42
105	-181	-118	21.5	3.2	20.5	9.7	11.4	-8.13	-8.09	-0.37	0.43
110	-191	-128	22.6	3.4	21.5	10.2	12.0	-8.61	-8.58	-0.39	0.43
115	-207	-143	23.6	3.5	22.5	10.7	12.5	-9.11	-9.09	-0.43	0.44
120	-219	-155	24.6	3.7	23.5	11.1	13.1	-9.71	-9.68	-0.47	0.44
125	-232	-167	25.6	3.8	24.5	11.6	13.6	-10.23	-10.25	-0.53	0.45
130	-247	-181	26.7	4.0	25.4	12.0	14.2	-10.81	-10.88	-0.58	0.46
135	-262	-197	27.7	4.1	26.4	12.5	14.7	-11.46	-11.59	-0.65	0.46
140	-282	-217	28.7	4.3	27.4	13.0	15.2	-12.10	-12.33	-0.72	0.46
145	-303	-239	29.7	4.4	28.4	13.4	15.8	-12.83	-13.20	-0.94	0.30
150	-359	-301	30.8	4.6	29.4	13.9	16.3	-14.37	-15.47	-2.51	-2.10
100	-244	-189	20.5	3.0	19.5	9.3	10.9	-11.59	-12.45	-2.10	-2.07
50	-88	-41	10.2	1.5	9.7	4.6	5.5	-6.95	-7.69	-1.42	-1.55
20	-15	11	4.1	0.5	3.8	1.9	2.2	-3.74	-4.47	-1.05	-1.29
0	23	17	0.0	0.0	0.0	0.0	0.0	-1.59	-2.31	-0.85	-1.27

Table A7. Recorded strain data for the PLAA Test, 4g case (Gauges G1 to G24), all strain values in microstrains (continued next page).

%Max Load	G1	G2	G3	G4	G5	G6	G7	G8	G9	G10	G11	G12
0	0	0	0	0	0	0	0	0	0	0	0	0
5	63	13	53	71	6	79	49	53	-20	117	-101	-24
10	122	18	106	142	5	158	96	106	-47	237	-215	-54
15	215	51	187	247	33	268	169	191	-52	392	-311	-57
20	289	70	249	335	52	357	222	262	-64	524	-422	-71
25	367	87	312	427	73	448	276	337	-75	660	-535	-82
30	458	122	385	530	116	551	339	425	-66	807	-636	-76
35	549	157	455	634	161	653	400	514	-56	952	-739	-66
40	639	192	525	737	211	753	460	605	-41	1096	-836	-45
45	727	228	592	839	263	851	518	697	-20	1235	-925	-12
50	814	265	660	942	320	947	575	791	4	1372	-1006	34
55	902	304	729	1047	380	1044	632	889	34	1511	-1082	91
60	992	344	799	1156	445	1142	691	992	69	1652	-1153	160
65	1062	367	851	1247	496	1223	733	1080	91	1777	-1231	224
70	1172	428	940	1377	587	1339	808	1206	151	1933	-1272	333
75	1268	475	1017	1496	668	1442	870	1322	204	2081	-1315	445
80	1360	519	1089	1612	748	1542	928	1439	258	2224	-1354	567
85	1459	570	1168	1739	839	1649	992	1567	322	2378	-1378	711
90	1558	621	1248	1866	935	1756	1056	1697	390	2531	-1388	871
95	1663	675	1331	2001	1038	1867	1122	1837	467	2692	-1380	1057
100	1768	731	1415	2137	1145	1979	1188	1980	547	2851	-1356	1258
50	950	320	777	1090	422	1113	679	946	44	1618	-974	398
0	24	-12	28	9	-21	38	17	6	-33	42	-7	16

%Max Load	G13	G14	G15	G16	G17	G18	G19	G20	G21	G22	G23	G24
0	0	0	0	0	0	0	0	0	0	0	0	0
5	-115	-97	-17	-108	-67	-76	-28	-100	34	29	35	39
10	-247	-208	-38	-231	-146	-165	-63	-212	66	44	68	73
15	-367	-303	-36	-343	-210	-239	-78	-312	124	80	123	121
20	-504	-412	-45	-468	-288	-327	-104	-425	174	105	158	150
25	-646	-525	-53	-598	-370	-420	-131	-541	228	130	186	184
30	-782	-627	-47	-720	-444	-504	-147	-649	291	164	223	224
35	-926	-733	-38	-849	-525	-593	-163	-762	355	197	259	262
40	-1071	-835	-23	-978	-605	-681	-176	-873	416	232	296	299
45	-1215	-931	1	-1105	-685	-766	-183	-983	476	271	334	338
50	-1359	-1022	34	-1230	-764	-847	-184	-1089	532	313	374	378
55	-1508	-1110	75	-1358	-845	-930	-181	-1197	588	356	416	421
60	-1661	-1197	125	-1488	-929	-1011	-172	-1305	644	401	460	465
65	-1828	-1292	169	-1630	-1028	-1105	-171	-1425	685	434	493	498
70	-1974	-1356	252	-1748	-1105	-1173	-138	-1524	750	492	551	555
75	-2133	-1427	335	-1877	-1196	-1249	-107	-1629	805	541	601	604
80	-2301	-1499	427	-2009	-1298	-1332	-74	-1741	857	587	648	651
85	-2471	-1566	537	-2137	-1405	-1412	-28	-1853	914	640	701	704
90	-2644	-1630	662	-2259	-1524	-1494	26	-1966	968	690	753	754
95	-2819	-1690	810	-2373	-1656	-1576	93	-2079	1026	745	809	809
100	-2989	-1749	972	-2469	-1799	-1656	168	-2190	1083	799	865	863
50	-1577	-1053	250	-1389	-883	-907	-87	-1194	616	389	444	434
0	-11	-6	6	-8	-4	1	0	-7	8	4	2	1

Table A7 (cont). Recorded strain data for the PLAA Test, 4g case (Gauges G1 to G24), all strain values in microstrains (continued next page).

%Max Load	G25	G26	G27	G28	G29	G30	G31	G32	G33	G34	G35	G36
0	0	0	0	0	0	0	0	0	0	0	0	0
5	91	84	40	109	103	154	114	-105	-146	-109	-146	-111
10	179	166	75	213	204	310	233	-213	-302	-222	-301	-227
15	274	253	117	322	308	458	354	-294	-435	-310	-437	-318
20	353	320	143	413	394	584	454	-381	-574	-403	-578	-413
25	437	393	169	510	487	713	563	-463	-712	-493	-718	-507
30	534	482	205	621	595	857	686	-537	-845	-577	-852	-592
35	635	577	244	738	710	1007	818	-607	-982	-658	-989	-676
40	742	679	288	859	832	1162	957	-675	-1119	-739	-1127	-758
45	852	784	335	987	959	1321	1103	-738	-1258	-815	-1264	-836
50	964	891	383	1115	1087	1478	1250	-795	-1393	-885	-1403	-908
55	1077	1002	432	1246	1220	1639	1404	-847	-1531	-954	-1544	-979
60	1192	1116	483	1380	1357	1803	1561	-894	-1670	-1017	-1690	-1046
65	1294	1219	522	1502	1483	1953	1707	-943	-1811	-1081	-1839	-1113
70	1421	1348	582	1649	1634	2129	1880	-968	-1934	-1124	-1973	-1159
75	1540	1470	635	1788	1778	2296	2047	-994	-2059	-1166	-2115	-1203
80	1658	1591	684	1928	1923	2464	2216	-1020	-2191	-1209	-2266	-1249
85	1783	1722	739	2076	2078	2641	2397	-1036	-2315	-1240	-2417	-1282
90	1908	1852	791	2223	2233	2817	2579	-1050	-2438	-1268	-2573	-1312
95	2039	1990	847	2378	2397	2999	2771	-1054	-2553	-1284	-2730	-1330
100	2169	2126	902	2532	2559	3180	2960	-1055	-2663	-1295	-2888	-1343
50	1151	1073	456	1323	1308	1708	1534	-737	-1591	-844	-1703	-887
0	18	14	3	18	14	17	18	12	-17	9	-28	4

%Max Load	G37	G38	G39	G40	G41	G42	G43	G44	G45	G46	G47	G48
0	0	0	0	0	0	0	0	0	0	0	0	0
5	-142	-65	38	31	17	26	32	90	93	209	193	171
10	-295	-134	72	58	32	44	63	179	186	422	389	346
15	-426	-183	103	100	66	87	108	287	302	609	562	501
20	-563	-238	131	144	103	123	141	374	397	785	724	645
25	-701	-293	165	189	141	159	171	464	495	969	895	799
30	-833	-341	208	242	184	200	206	558	597	1171	1080	963
35	-968	-390	254	297	227	241	241	654	702	1386	1278	1140
40	-1102	-439	302	350	267	281	273	748	806	1617	1490	1330
45	-1238	-486	353	402	305	321	306	846	914	1859	1710	1525
50	-1373	-531	403	451	343	359	338	942	1020	2107	1935	1725
55	-1510	-576	454	501	381	400	370	1040	1129	2364	2166	1931
60	-1646	-619	508	554	422	442	404	1142	1241	2631	2406	2147
65	-1788	-669	550	594	451	473	427	1232	1342	2897	2645	2361
70	-1913	-698	613	655	500	524	468	1342	1463	3181	2897	2588
75	-2043	-732	670	708	543	568	503	1447	1579	3470	3155	2820
80	-2181	-768	723	759	582	610	535	1550	1693	3781	3431	3067
85	-2317	-797	782	814	626	655	571	1658	1813	4105	3720	3328
90	-2457	-826	840	868	668	700	605	1766	1931	4449	4024	3602
95	-2600	-849	902	926	715	748	644	1882	2060	4824	4357	3899
100	-2739	-869	962	983	760	795	680	1994	2183	5212	4700	4207
50	-1580	-547	491	525	403	438	381	1104	1206	3006	2627	2316
0	-17	3	2	-2	-5	-3	-1	2	2	186	130	107

Table A7 (cont). Recorded strain data for the PLAA Test, 4g case (Gauges G1 to G24), all strain values in microstrains (continued next page).

%Max Load	G49	G50	G51	G52	G53	G54	G55	G56	G57	G58	G59	G60
0	0	0	0	0	0	0	0	0	0	0	0	0
5	162	163	127	124	119	115	112	58	26	1	22	14
10	330	333	261	255	243	234	225	108	50	36	44	27
15	478	482	405	394	375	360	347	145	75	84	70	42
20	614	617	528	514	490	472	454	181	106	125	101	51
25	761	763	661	643	611	588	566	212	140	163	131	59
30	917	920	792	770	732	704	678	243	178	204	165	66
35	1087	1091	932	907	861	827	794	273	217	246	201	69
40	1268	1270	1066	1036	983	944	907	302	258	290	241	73
45	1455	1458	1205	1172	1112	1068	1025	331	299	334	280	75
50	1645	1646	1337	1301	1237	1188	1141	360	341	383	324	80
55	1843	1845	1477	1439	1367	1313	1259	385	382	431	365	83
60	2053	2055	1620	1578	1498	1439	1379	410	419	481	401	88
65	2259	2261	1760	1715	1630	1566	1501	432	450	530	434	95
70	2478	2482	1907	1859	1767	1699	1628	454	483	581	467	101
75	2704	2708	2055	2004	1906	1833	1757	478	514	630	500	107
80	2944	2947	2205	2150	2047	1971	1891	504	546	681	534	113
85	3202	3206	2364	2305	2194	2113	2027	529	577	729	567	117
90	3471	3476	2524	2465	2348	2262	2169	556	608	777	597	119
95	3762	3766	2694	2632	2510	2420	2322	585	641	828	631	123
100	4068	4074	2865	2800	2671	2576	2471	613	673	874	661	126
50	2241	2247	1627	1584	1504	1445	1384	341	271	447	252	136
0	110	106	23	20	18	17	15	-10	4	-3	3	-1

%Max Load	G61	G62	G63	G64	G65	G66	G67	G68	G69	G70	G71	G72
0	0	0	0	0	0	0	0	0	0	0	0	0
5	-2	-3	7	0	-2	-3	27	43	5	13	7	19
10	-1	-5	8	2	0	-9	56	70	10	21	9	28
15	1	-5	8	3	2	-8	85	93	18	30	9	33
20	2	-4	8	4	4	9	108	107	18	36	5	25
25	5	-2	11	6	5	34	127	119	19	43	3	17
30	6	-2	13	6	6	55	141	128	18	45	-3	9
35	7	-2	15	7	7	72	151	134	21	46	-10	0
40	10	0	17	7	7	85	163	142	28	48	-17	-10
45	11	-1	19	8	9	92	170	144	38	44	-30	-16
50	13	0	21	7	8	100	180	151	50	44	-39	-18
55	15	1	23	9	10	103	185	152	52	39	-54	-17
60	17	3	25	10	11	106	193	156	54	29	-67	-15
65	19	2	26	9	11	112	202	161	57	17	-80	-16
70	21	3	27	9	12	114	209	162	56	2	-95	-16
75	23	5	30	11	14	113	212	161	51	-16	-112	-19
80	25	6	31	11	13	116	218	163	48	-29	-126	-21
85	27	6	32	12	15	117	222	163	41	-46	-143	-26
90	27	6	33	12	16	117	225	160	31	-67	-165	-36
95	29	6	33	12	16	118	230	160	23	-87	-185	-44
100	30	6	34	12	18	117	231	156	10	-110	-207	-54
50	14	8	32	9	11	83	192	149	44	24	-43	-17
0	1	0	11	7	7	0	0	11	-1	7	15	-3

Table A7 (cont). Recorded strain data for the PLAA Test, 4g case (Gauges G1 to G24), all strain values in microstrains (continued next page).

%Max Load	G73	G74	LOADC1 (kN)	LOADC2 (kN)	LOADC3 (kN)	LOADC4 (kN)	LOADC5 (kN)	LVDT1 (mm)	LVDT2 (mm)	LVDT3 (mm)	LVDT4 (mm)
0	0	0	0.0	0.0	0.0	0.0	0.0	0.00	0.00	0.00	0.00
5	-18	-2	0.1	1.1	0.9	1.3	0.7	-0.44	-0.46	-0.04	0.03
10	-34	-4	0.2	2.2	1.9	2.6	1.3	-0.94	-0.97	-0.09	0.04
15	-51	-8	0.3	3.2	2.9	3.9	2.0	-1.51	-1.54	-0.12	0.06
20	-70	-15	0.3	4.3	3.9	5.2	2.6	-2.03	-2.08	-0.17	0.07
25	-85	-22	0.4	5.3	4.9	6.5	3.2	-2.63	-2.65	-0.21	0.09
30	-102	-31	0.5	6.4	5.9	7.8	3.9	-3.26	-3.24	-0.26	0.11
35	-120	-46	0.6	7.5	6.9	9.1	4.5	-3.91	-3.84	-0.31	0.12
40	-139	-64	0.7	8.5	7.9	10.3	5.1	-4.56	-4.45	-0.36	0.14
45	-159	-81	0.8	9.6	8.9	11.7	5.8	-5.22	-5.04	-0.41	0.15
50	-178	-99	0.8	10.7	9.9	12.9	6.4	-5.86	-5.63	-0.46	0.15
55	-195	-116	0.9	11.8	10.9	14.2	7.1	-6.50	-6.22	-0.53	0.15
60	-215	-136	1.0	12.8	11.9	15.5	7.7	-7.14	-6.83	-0.59	0.11
65	-235	-158	1.1	13.9	12.9	16.8	8.3	-7.75	-7.42	-0.66	0.07
70	-254	-178	1.2	15.0	13.9	18.1	9.0	-8.36	-8.03	-0.73	-0.01
75	-272	-197	1.3	16.1	14.9	19.4	9.6	-8.98	-8.64	-0.80	-0.09
80	-293	-220	1.4	17.1	15.9	20.7	10.3	-9.61	-9.26	-0.87	-0.18
85	-314	-242	1.4	18.2	16.9	22.0	10.9	-10.25	-9.90	-0.97	-0.29
90	-340	-267	1.5	19.3	17.9	23.3	11.5	-10.90	-10.54	-1.08	-0.40
95	-362	-291	1.6	20.4	18.9	24.6	12.2	-11.62	-11.18	-1.21	-0.56
100	-386	-315	1.7	21.4	19.9	25.9	12.8	-12.33	-11.84	-1.34	-0.69
50	-204	-128	0.9	10.7	9.9	12.9	6.5	-7.50	-6.86	-0.64	-0.47
0	-7	7	0.0	-0.1	0.0	0.0	0.0	-0.32	-0.22	0.06	-0.11

Table A8. Recorded strain data for the PLAA Test, 4.5g case (Gauges G1 to G24), all strain values in microstrains (continued next page).

% Max Load	G1	G2	G3	G4	G5	G6	G7	G8	G9	G10	G11	G12
0	0	0	0	0	0	0	0	0	0	0	0	0
5	75	14	66	90	6	97	60	67	-25	146	-133	-34
10	169	37	148	196	24	212	134	150	-44	311	-262	-56
15	267	64	232	310	53	328	207	242	-54	480	-397	-72
20	376	100	321	436	94	452	284	348	-53	661	-530	-75
25	473	136	396	551	143	562	351	445	-45	824	-660	-73
30	584	181	480	679	204	686	425	558	-25	1003	-785	-54
35	693	227	565	807	270	807	499	672	0	1177	-897	-17
40	801	272	648	934	339	925	568	787	30	1347	-1003	34
45	912	323	735	1068	418	1047	642	913	70	1521	-1094	110
50	1022	373	821	1202	500	1167	714	1040	115	1694	-1178	201
55	1136	426	910	1341	590	1292	787	1175	169	1871	-1251	312
60	1251	482	1000	1485	687	1416	861	1316	230	2050	-1310	445
65	1369	541	1095	1634	792	1544	937	1466	301	2233	-1353	602
70	1487	600	1188	1785	902	1671	1012	1620	378	2416	-1378	776
75	1616	669	1291	1950	1027	1809	1095	1790	471	2612	-1374	992
80	1742	736	1392	2115	1155	1944	1175	1962	566	2806	-1352	1227
85	1879	810	1501	2294	1301	2088	1260	2152	678	3015	-1296	1527
90	2045	901	1634	2513	1486	2260	1361	2393	827	3269	-1198	2002
95	2508	1192	1957	3128	2171	2679	1601	3275	1470	3927	-2488	1371
0	-93	61	-88	-182	216	112	-13	-1.85E+07	-1.89E+07	3232	-405	-1466
0	-104	50	-92	-192	204	109	-17	-1.85E+07	-1.89E+07	3224	-409	-1461

% Max Load	G13	G14	G15	G16	G17	G18	G19	G20	G21	G22	G23	G24
0	0	0	0	0	0	0	0	0	0	0	0	0
5	-153	-129	-24	-143	-91	-101	-39	-132	42	31	44	48
10	-305	-253	-36	7-285.3	-177	-199	-68	-261	98	61	97	100
15	-472	-386	-45	-440	-274	-306	-97	-401	161	95	149	139
20	-647	-520	-44	-601	-372	-415	-122	-543	235	136	190	185
25	-821	-651	-42	-759	-473	-525	-147	-684	304	169	226	227
30	-1003	-781	-26	-922	-574	-635	-164	-825	384	213	272	275
35	-1182	-902	2	-1080	-674	-741	-173	-963	458	259	319	321
40	-1365	-1019	39	-1240	-775	-846	-177	-1100	529	310	368	370
45	-1549	-1127	95	-1399	-878	-947	-168	-1234	600	366	423	425
50	-1741	-1232	162	-1562	-986	-1050	-155	-1371	667	420	477	479
55	-1939	-1332	245	-1726	-1099	-1152	-130	-1509	735	478	536	537
60	-2142	-1426	344	-1891	-1218	-1253	-95	-1647	802	537	595	596
65	-2350	-1514	466	-2052	-1347	-1354	-46	-1787	869	599	658	658
70	-2561	-1598	604	-2206	-1487	-1456	11	-1927	936	660	720	720
75	-2773	-1674	776	-2345	-1647	-1556	89	-2065	1008	728	789	788
80	-2987	-1754	971	-2467	-1832	-1662	176	-2207	1076	792	856	853
85	-3200	-1823	1220	-2561	-2046	-1765	300	-2353	1149	863	930	924
90	-3432	-1891	1567	-2582	-2315	-1879	466	-2478	1229	943	1017	1002
95	-2144	-2364	336	-1861	-1671	-1855	-607	-1808	1352	1063	1154	1110
0	429	-741	-1067	833	321	-607	-1115	776	-62	25	20	66
0	420	-744	-1065	824	314	-612	-1116	768	-66	22	15	63

Table A8 (cont). Recorded strain data for the PLAA Test, 4.5g case (Gauges G1 to G24), all strain values in microstrains (continued next page).

% Max Load	G25	G26	G27	G28	G29	G30	G31	G32	G33	G34	G35	G36
0	0	0	0	0	0	0	0	0	0	0	0	0
5	116	108	50	139	132	198	149	-138	-191	-145	-188	-145
10	228	214	100	270	260	388	297	-257	-371	-272	-368	-275
15	326	297	132	382	365	543	422	-366	-544	-389	-543	-394
20	445	397	169	517	492	718	575	-467	-723	-500	-724	-510
25	557	501	210	647	620	890	723	-562	-893	-607	-897	-620
30	689	625	263	798	770	1083	896	-650	-1068	-710	-1071	-725
35	825	754	320	954	925	1278	1076	-733	-1244	-810	-1247	-827
40	961	885	378	1112	1084	1473	1258	-807	-1417	-901	-1421	-921
45	1105	1027	442	1278	1253	1675	1452	-871	-1589	-987	-1596	-1009
50	1245	1167	502	1441	1421	1875	1647	-929	-1764	-1067	-1779	-1093
55	1390	1314	565	1611	1596	2081	1849	-976	-1935	-1136	-1962	-1167
60	1536	1463	628	1783	1776	2289	2056	-1015	-2104	-1196	-2149	-1232
65	1686	1619	692	1960	1961	2502	2273	-1045	-2269	-1247	-2339	-1287
70	1836	1776	755	2137	2148	2715	2490	-1071	-2429	-1292	-2528	-1336
75	1997	1945	825	2327	2348	2940	2726	-1081	-2580	-1319	-2722	-1366
80	2154	2112	891	2515	2547	3162	2960	-1088	-2725	-1342	-2919	-1390
85	2321	2290	961	2714	2759	3393	3210	-1079	-2852	-1344	-3123	-1390
90	2513	2495	1038	2942	3005	3650	3497	-1028	-2946	-1298	-3368	-1333
95	2840	2851	1156	3313	3428	3919	3982	-684	-2790	-1074	-3904	-910
0	67	130	76	53	127	-157	174	1361	-1051	1179	-1686	1596
0	62	125	72	48	123	-163	170	1348	-1050	1169	-1683	1585

% Max Load	G37	G38	G39	G40	G41	G42	G43	G44	G45	G46	G47	G48
0	0	0	0	0	0	0	0	0	0	0	0	0
5	-186	-85	47	37	19	29	40	115	118	270	248	219
10	-362	-160	88	80	51	66	87	231	242	519	478	423
15	-532	-229	123	134	96	116	132	350	369	729	673	599
20	-707	-295	170	198	148	169	177	471	502	970	891	793
25	-875	-360	220	261	197	215	216	582	624	1217	1122	997
30	-1046	-421	280	331	251	267	259	702	755	1495	1379	1225
35	-1219	-482	341	394	298	315	299	821	886	1792	1653	1466
40	-1389	-540	403	455	345	365	339	942	1020	2098	1935	1715
45	-1559	-594	470	520	395	417	381	1067	1158	2419	2229	1975
50	-1731	-649	534	581	443	468	419	1190	1294	2751	2528	2240
55	-1902	-699	601	646	493	521	461	1317	1435	3099	2845	2521
60	-2072	-745	669	711	545	575	503	1446	1578	3459	3169	2810
65	-2245	-787	739	777	597	630	545	1576	1721	3843	3516	3117
70	-2418	-827	809	842	648	684	587	1706	1865	4243	3878	3439
75	-2592	-857	886	914	706	745	635	1849	2022	4673	4267	3784
80	-2768	-886	959	981	760	800	678	1985	2173	5132	4683	4154
85	-2946	-902	1038	1056	820	862	728	2135	2337	5673	5166	4581
90	-3149	-899	1126	1140	890	933	785	2315	2533	6505	5904	5242
95	-3476	-750	1261	1273	1008	1069	916	2769	3018	11571	10946	9932
0	-411	42	94	25	-5	-15	-41	-289	-161	10455	12055	13591
0	-412	37	90	22	-9	-20	-45	-291	-167	10430	12037	13579

Table A8 (cont). Recorded strain data for the PLAA Test, 4.5g case (Gauges G1 to G24), all strain values in microstrains (continued next page).

% Max Load	G49	G50	G51	G52	G53	G54	G55	G56	G57	G58	G59	G60
0	0	0	0	0	0	0	0	0	0	0	0	0
5	208	209	164	161	154	149	144	64	32	7	27	23
10	405	409	327	319	304	292	282	115	63	52	53	41
15	575	581	498	484	459	440	423	154	96	101	86	58
20	760	767	671	653	620	595	572	191	133	152	122	70
25	954	959	829	806	766	737	709	228	177	208	170	76
30	1173	1181	1004	976	925	888	853	263	219	262	212	79
35	1404	1411	1174	1142	1083	1040	998	300	263	316	259	83
40	1641	1647	1343	1306	1239	1191	1143	336	307	372	311	89
45	1893	1899	1519	1477	1401	1346	1291	372	356	427	361	92
50	2148	2156	1697	1651	1568	1507	1444	409	405	482	412	94
55	2421	2428	1877	1827	1735	1668	1600	444	456	539	466	97
60	2704	2714	2065	2012	1912	1838	1762	478	506	594	516	97
65	3003	3014	2252	2196	2090	2012	1930	511	561	652	568	98
70	3319	3331	2447	2388	2274	2190	2101	545	614	708	612	97
75	3659	3673	2653	2590	2469	2379	2282	579	666	769	657	99
80	4025	4038	2862	2795	2666	2571	2466	615	709	831	701	105
85	4455	4471	3094	3022	2882	2779	2664	651	746	885	746	112
90	5147	5158	3395	3322	3174	3067	2940	689	791	942	797	115
95	10566	10305	4699	4605	4494	4462	4316	725	895	1037	885	105
0	19641	16030	7624	10111	16777	31761	8340	-3	9	15	13	-15
0	19633	15898	7597	10082	16752	31733	8191	-4	8	15	13	-12

% Max Load	G61	G62	G63	G64	G65	G66	G67	G68	G69	G70	G71	G72
0	0	0	0	0	0	0	0	0	0	0	0	0
5	4	-2	3	1	1	-4	35	53	7	13	11	22
10	9	-3	7	4	6	-11	72	81	12	20	5	33
15	14	1	16	7	9	-7	101	101	14	27	1	32
20	19	3	21	8	12	25	129	117	29	31	-8	18
25	26	6	25	9	13	53	150	131	34	36	-13	12
30	30	8	28	11	16	70	163	139	41	37	-22	1
35	35	9	31	12	18	82	174	144	57	35	-35	-8
40	40	11	33	13	19	91	187	154	75	36	-47	-8
45	45	13	36	15	22	95	195	157	79	31	-63	-5
50	49	13	37	15	24	102	204	160	81	16	-81	-6
55	55	15	39	17	26	107	213	164	82	2	-99	-5
60	58	15	39	19	31	108	217	162	77	-17	-119	-7
65	63	16	40	19	32	113	224	165	75	-31	-135	-9
70	66	16	42	22	36	113	228	162	65	-52	-158	-17
75	70	16	43	25	40	114	232	161	54	-72	-181	-26
80	74	17	44	26	43	115	236	160	44	-91	-202	-32
85	78	18	46	31	48	110	235	153	26	-118	-228	-42
90	81	17	46	34	55	102	230	139	-6	-154	-263	-60
95	85	16	44	39	61	78	211	89	-103	-213	-320	-109
0	-6	-12	-29	35	38	-58	6	-36	-25	-64	-37	-14
0	-6	-11	-29	33	37	-57	4	-36	-23	-65	-39	-13

Table A8 (cont). Recorded strain data for the PLAA Test, 4.5g case (Gauges G1 to G24), all strain values in microstrains (continued next page).

% Max Load	G73	G74	LOADC1 (kN)	LOADC2 (kN)	LOADC3 (kN)	LOADC4 (kN)	LOADC5 (kN)	LVDT1 (mm)	LVDT2 (mm)	LVDT3 (mm)	LVDT4 (mm)
0	0	0	0.0	0.0	0.0	0.0	0.0	0.00	0.00	0.00	0.00
5	-18	-4	0.2	1.1	1.4	1.6	0.7	-0.58	-0.59	-0.08	0.02
10	-39	-11	0.4	2.2	2.8	3.2	1.5	-1.20	-1.23	-0.13	0.03
15	-56	-16	0.7	3.3	4.2	4.8	2.3	-1.89	-1.94	-0.18	0.05
20	-78	-28	0.9	4.4	5.6	6.5	3.1	-2.69	-2.72	-0.25	0.08
25	-98	-42	1.1	5.5	7.1	8.1	3.9	-3.44	-3.42	-0.30	0.10
30	-117	-58	1.3	6.6	8.5	9.7	4.6	-4.26	-4.18	-0.36	0.12
35	-140	-78	1.5	7.8	9.9	11.3	5.4	-5.08	-4.92	-0.42	0.14
40	-163	-99	1.8	8.9	11.3	13.0	6.2	-5.90	-5.65	-0.49	0.15
45	-186	-120	2.0	10.0	12.8	14.6	6.9	-6.70	-6.40	-0.58	0.15
50	-214	-147	2.2	11.1	14.2	16.2	7.7	-7.50	-7.13	-0.66	0.12
55	-239	-172	2.5	12.3	15.6	17.8	8.5	-8.30	-7.88	-0.75	0.06
60	-262	-197	2.7	13.4	17.0	19.5	9.3	-9.08	-8.64	-0.84	-0.05
65	-286	-223	2.9	14.5	18.4	21.1	10.0	-9.86	-9.40	-0.93	-0.16
70	-311	-249	3.1	15.6	19.8	22.7	10.8	-10.64	-10.19	-1.05	-0.29
75	-336	-276	3.4	16.7	21.3	24.3	11.6	-11.45	-10.97	-1.20	-0.44
80	-358	-301	3.6	17.8	22.7	25.9	12.3	-12.27	-11.78	-1.35	-0.61
85	-386	-331	3.8	19.0	24.1	27.6	13.1	-13.17	-12.65	-1.54	-0.86
90	-424	-371	4.0	20.1	25.5	29.2	13.9	-14.26	-13.69	-1.81	-1.23
95	-502	-452	4.3	21.2	27.0	30.8	14.7	-16.26	-16.47	-2.63	-2.56
0	-204	-20	-0.1	-0.1	0.0	-0.2	-0.8	-4.49	-6.75	60.75	-14.62
0	-204	-22	-0.1	-0.1	0.0	-0.2	-0.8	-4.27	-6.37	60.75	-14.61

DISTRIBUTION LIST

The Static Testing of a Lockheed P-3 Orion Wing Leading Edge Centre Section

Albert K. Wong and Glenn Luke

AUSTRALIA

DEFENCE ORGANISATION

Task Sponsor DGLOGCOM
Chief Engineer, MPLM, RAAF Edinburgh

S&T Program
Chief Defence Scientist
FAS Science Policy } shared copy
AS Science Corporate Management
Counsellor Defence Science, London (Doc Data Sheet)
Counsellor Defence Science, Washington (Doc Data Sheet)
Scientific Adviser to MRDC Thailand (Doc Data Sheet)
Director General Scientific Advisers and Trials/Scientific Adviser Policy and Command (shared copy)
Navy Scientific Adviser (3 copies Doc Data Sheet and 1 copy distribution list)
Scientific Adviser - Army (Doc Data Sheet and distribution list only)
Air Force Scientific Adviser
Director Trials

Aeronautical and Maritime Research Laboratory
Director

Electronics and Surveillance Research Laboratory
Director

Chief of Airframes and Engines Division
Chief of Air Operations Division
F. Rose, Research Leader
A. Wong
L. Molent
M.G. Stimson
S.A. Barter
T. van Blaricum

DSTO Library
Library Fishermens Bend
Library Maribyrnong
Library DSTOS (2 copies)
Australian Archives
Library, MOD, Pyrmont (Doc Data sheet only)

Forces Executive

Director General Force Development (Sea) (Doc Data Sheet only)
Director General Force Development (Land) (Doc Data Sheet only)
Director General Force Development (Air)

Army

ABCA Office, G-1-34, Russell Offices, Canberra (4 copies)

Air Force

CENG
MPLM Squadron, RAAF Base Edinburgh (5 copies)

OC
92 Wing, RAAF Base Edinburgh

LASC REP
492 Squadron, RAAF Base Edinburgh

DFS
DFS-AF
Russell Offices E03048, Canberra

DTA/LSA
HQLC
RAAF Williams, VIC

OICASI-LSA
OICATS-LSA
HQLC
RAAF Williams, VIC

S&I Program

Defence Intelligence Organisation
Library, Defence Signals Directorate (Doc Data Sheet only)

B&M Program (libraries)

OIC TRS, Defence Central Library
Officer in Charge, Document Exchange Centre (DEC), 1 copy
*US Defence Technical Information Centre, 2 copies
*UK Defence Research Information Center, 2 copies
*Canada Defence Scientific Information Service, 1 copy
*NZ Defence Information Centre, 1 copy
National Library of Australia, 1 copy

UNIVERSITIES AND COLLEGES

Australian Defence Force Academy
Library
Head of Aerospace and Mechanical Engineering
Deakin University, Serials Section (M list), Deakin University Library, Geelong, 3217
Senior Librarian, Hargrave Library, Monash University
Librarian, Flinders University

DEFENCE SCIENCE AND TECHNOLOGY ORGANISATION
DOCUMENT CONTROL DATA

1. PRIVACY MARKING/CAVEAT (OF DOCUMENT)

2. TITLE

The Static Testing of a Lockheed P-3 Orion Wing Leading Edge Centre Section

3. SECURITY CLASSIFICATION (FOR UNCLASSIFIED REPORTS THAT ARE LIMITED RELEASE USE (L) NEXT TO DOCUMENT CLASSIFICATION)

Document	(U)
Title	(U)
Abstract	(U)

4. AUTHOR(S)

Albert K. Wong and Glenn Luke

5. CORPORATE AUTHOR

Aeronautical and Maritime Research Laboratory
PO Box 4331
Melbourne Vic 3001

6a. DSTO NUMBER	6b. AR NUMBER	6c. TYPE OF REPORT	7. DOCUMENT DATE
DSTO-TR-0423	AR-009-899	Technical Report	November 1996

8. FILE NUMBER	9. TASK NUMBER	10. TASK SPONSOR	11. NO. OF PAGES	12. NO. OF REFERENCES
M1/9/181	93/169	DGLOGCOM	68	6

13. DOWNGRADING/DELIMITING INSTRUCTIONS

None

14. RELEASE AUTHORITY

Chief, Airframes and Engines Division

15. SECONDARY RELEASE STATEMENT OF THIS DOCUMENT

Approved for public release

OVERSEAS ENQUIRIES OUTSIDE STATED LIMITATIONS SHOULD BE REFERRED THROUGH DOCUMENT EXCHANGE CENTRE, DIS NETWORK OFFICE, DEPT OF DEFENCE, CAMPBELL PARK OFFICES, CANBERRA ACT 2600

16. DELIBERATE ANNOUNCEMENT

No limitations

17. CASUAL ANNOUNCEMENT Yes

18. DEFTEST DESCRIPTORS

Orion aircraft, Leading edges, Static tests, Structural failures

19. ABSTRACT

This report documents the design of the test rig and the results of the static test of the Lockheed P-3 Orion Wing Leading Edge centre section structure. The test comprised of two parts, viz., the validation of the structural integrity of the structure under design load conditions, and the determination of the static strength of the structure for the local transonic flight regime within which the RAAF Orion A9-754 had evidently failed. The test clearly showed that the structure meets its design specifications and had an adequate margin of safety even for the high speed regime. However, it is pointed out that this margin can be quickly eroded if the material thickness is below specification, as was reported for the case of Orion A9-754, and it is recommended that this aspect be investigated for the RAAF Orion fleet.

OTHER ORGANISATIONS

NASA (Canberra)
AGPS

OUTSIDE AUSTRALIA

ABSTRACTING AND INFORMATION ORGANISATIONS

INSPEC: Acquisitions Section Institution of Electrical Engineers
Library, Chemical Abstracts Reference Service
Engineering Societies Library, US
American Society for Metals
Documents Librarian, The Center for Research Libraries, US

INFORMATION EXCHANGE AGREEMENT PARTNERS

Acquisitions Unit, Science Reference and Information Service, UK
Library - Exchange Desk, National Institute of Standards and Technology, US

PROGRAM PARTNERS

COMNAV AIRSYSCOM
AIR 4.3.3.1 (N. Phan)
1421 Jefferson Davis Highway
Arlington, VA 22243-5300
USA

P-3 Engineering Manager
Dept 70-E1
LMASC
86 South Cobb Drive
Marrietta, GA 30063
USA

SPARES (10 copies)

Total number of copies: 71